Computational Fluid Dynamics of Intracranial Aneurysms: Eulerian and Lagrangian Analysis of the Effect of Endovascular Treatment on Hemodynamics

Laurel Morgan Miller Marsh

A dissertation
submitted in partial fulfillment of the
requirements for the degree of

Doctor of Philosophy

University of Washington

2023

Reading Committee:

Alberto Aliseda, Chair

James Riley

Fanette Chassagne

Program Authorized to Offer Degree:
Department of Mechanical Engineering

University of Washington

Abstract

Computational Fluid Dynamics of Intracranial Aneurysms: Eulerian and Lagrangian Analysis of the Effect of Endovascular Treatment on Hemodynamics

Laurel Marsh

Chair of the Supervisory Committee:
Alberto Aliseda
Mechanical Engineering

Intracranial aneurysms are dilated portions of an artery that supplies bllod to the brain. These abnormal dilatations of the arterial wall carry the risk of rupture, which represents a leading cause of subarachnoid hemorrhage and have very high mortatility and morbidity. Endovascular therapies are deployed by neurointerventionalists to treat intracranial aneurysms, reducing further growth and the risk of rupture. The success of these therapies involves the cessation of blood flow into the aneurysmal cavity, because of a clot fully occluding the aneurysm, allowing reendothelialization of the parent vessel. If there is any remnant flow, the treatment is considered unsuccessful and may warrant retreatment.

While both coil embolization devices and flow-diverting stents (FDS) are proven endovascular therapies, there is no way to predict the treatment outcome in either of two treatment modalities, whether using pre- or post-operative information. The patient is therefore required to return for medical imaging to determine the outcome, which increases the burden on the healthcare system, as well as the procedural and rupture risk of the patient. The inability to predict treatment outcome can be addressed with the use of computational fluid dynamics (CFD). While many studies have been conducted with small patient populations, the use of CFD to understand the evolution of intracranial aneurysm has yet to identify thresholds for hemodynamics metrics to predict treatment outcomes, or even which metrics are physiologically relevant. Standard image-based patient-specific

CFD simulations rely on a variety of models to account for the effect of treatment on hemodynamics. Unfortunately, a lack of standardization and automation, coupled with the uncertainty associated with many of the models used historically for their simplicity without a rigorous validation of their accuracy, has led to a lack of consensus on which hemodynamics metrics should be studied for their predictive potential.

This dissertation investigates two main forms of endovascular therapy of cerebral aneurysms: coils and FDS, via a computational simulation framework that introduces novel models and validates them against gold-standard, experimentally-derived coil- and stent-resolved simulations. The overall goal is to contribute to the state-of-the-art simulation framework to move CFD towards becoming a clinical standard of care tool. The first question addressed is whether the two devices can be considered analogous when seeking metrics that are predictive of outcomes. The follow-up question is whether a new framework for studying the hemodynamics of intraaneurysmal flow and potential thrombosis, Lagrangian particle tracking, can shed light on the physiological processes that determine aneurysm embolization, and success post-treatment. As a side project, during my Fullbright stay at the Otto Von Guericke University in Magdeburg, Germany, I considered the differences between saccular and fusiform aneurysms and how the hemodynamics and FDS deployment differ for these two phenotypes. Finally, my last contribution is the evaluation of a new porous media model, used to model the coil mass comparing it to coil-resolved simulations to determine its efficacy in predicting Eulerian and Lagrangian metrics.

TABLE OF CONTENTS

LIST OF FIGURES

LIST OF TABLES

ACKNOWLEDGMENTS

I am immensely grateful to my advisor, Prof. Alberto Aliseda, for his invaluable guidance and support throughout my PhD journey. Without his unwavering dedication and encouragement, I would not have been able to complete this challenging yet rewarding experience. You've offered me not only your expertise and knowledge in the field, but also a genuine interest in my well-being academically and personally. Thank you for your unwavering belief in me as a researcher. I also want to extend my gratitude to my entire committee whose guidance and encouragement has been instrumental in my academic growth and success.

To the Multiphase and Cardiovascular Flow lab, I want to express my heartfelt appreciation for all of the late nights working in the office, constructive criticism at lab meetings where you have all already seen my presentation a few times, tea breaks, potluck dinners, and camping trips. I can always count on my lab mates for support and inspiration whether in regards to a research project, navigating the challenges of graduate school, or trying times in my life. Aarshana Parekh, thank you for all the late night talks, ice creams, and movie nights to help us both through grad school. To Maria Yang, thanks for all the giggles and walks around the farmer's market.

Many other University of Washington students and staff/faculty have also had a strong impact on my PhD. I want to thank Sari Emese Barczay, Fanette Chassagne, and Julia Romero Bhathal for bolstering my confidence as a researcher and sanity checks through frequent Zoom calls even throughout COVID. Those three along with Prasanna Rajagopal, Angela Straccia, Marissa Miramontes, and Ariana Mendible are all invaluable running buddies who helped keep me mentally and physically in check. Vijeth Rai, I will forever cherish the deep and meaningful conversations we have had. I will perhaps cherish the silly ones even more. Spending time with you, Benjamin Ferleger, and Patricia Jordan always provided relief along my PhD journey and is greatly appreciated as were all the chais along the way.

I would also like to express my deep gratitude to the community of Mechanical Engineering Students Against Racism. Talking with y'all helped me gain a better perspective on life and the world around us. I hope it helps many more navigate the complex and daunting terrain of academia.

I have also been supported by many other friends that I would like to thank like Dailey Jones: I have been truly grateful to have such a wonderful friend by my side. Jami Nettles, thank you for continuously inspiring me and being a kick-ass lady boss in STEM. To Jared Jones, you made me believe I could do graduate school or even become a teacher, thank you so much for that gift. DeAnna Brown, you have been making me laugh and inspiring me to succeed since our youthful rocket building days - you are amazing. To the greatest friend of all time, Alex Calhoun, your unfaltering support, friendship, and belief in me have made all the difference. Thank you to you and your whole family, the Ducks, who are truly like my own family, for being an integral part of my life and for making this journey more enjoyable and rewarding. Finally, I want to send some love to Rachel Witbeck and the whole family, who again, were genuinely like family to me and whose impact on my life has been immeasurable. Thank you for the extremely strong foundation you provided, without which, I would not have completed this program.

My family has always been a source of comfort and support. Thanks to my grandparents for always being so proud and making me feel accomplished. I am also deeply grateful to Lindsay Stovall. Growing up my older sister instilled many values in me and with her constant inspiration and guidance, I have become who I am today. Thank you for being with me every step of the way. Thanks to you and the kids for always being available for video calls to lift my spirits. Finally, Leslie Hammons has been my confidant, sounding board, biggest cheerleader, and another inextinguishable source of support. Momma, your strength, resilience, compassion, and patience have inspired me to be a better person.

DEDICATION

To Leslie and Lindsay,

I did it!

Chapter 1

INTRODUCTION

1.1 Background and Motivation

Cerebral or intracranial aneurysms are diseased portions of the arteries that supply blood to the brain which have ballooned out, and can rupture causing subarachnoid hemorrhage, a life-threatening type of stroke that carries a mortality rate higher than 40% [10]. Because of the lack of understanding of the causes that control their origin and continuous growth, and the uncertainty in the estimation of the probability of rupture, intracranial aneurysms are often recommended for treatment once detected. Endovascular approaches have become the preferred method of treatment because the procedures, aided by angiography, are minimally invasive and carry a much lower complication rate [72].

1.1.1 Angiographic Imaging Data

These endovascular therapies are deployed in an angiography suite by neurointerventionalists as shown in Figure 1.1. Here, 3-dimensional rotational angiography (3DRA) can be taken for diagnostics or during the procedure itself. This form of imaging is commonly used to create patient-specific image-based computational fluid dynamics (CFD) models of blood flow in aneurysms [125]. The raw images must be segmented in order to create a surface for meshing, see Fig. 1.2. Finally, 2-dimensional radiopaque images, seen on the display screens, can be captured to show the position of the catheter, endovascular device deployment, and any other devices used during the procedure. Figure 1.3 shows radiographic imaging of an aneurysm before and after coil deployment.

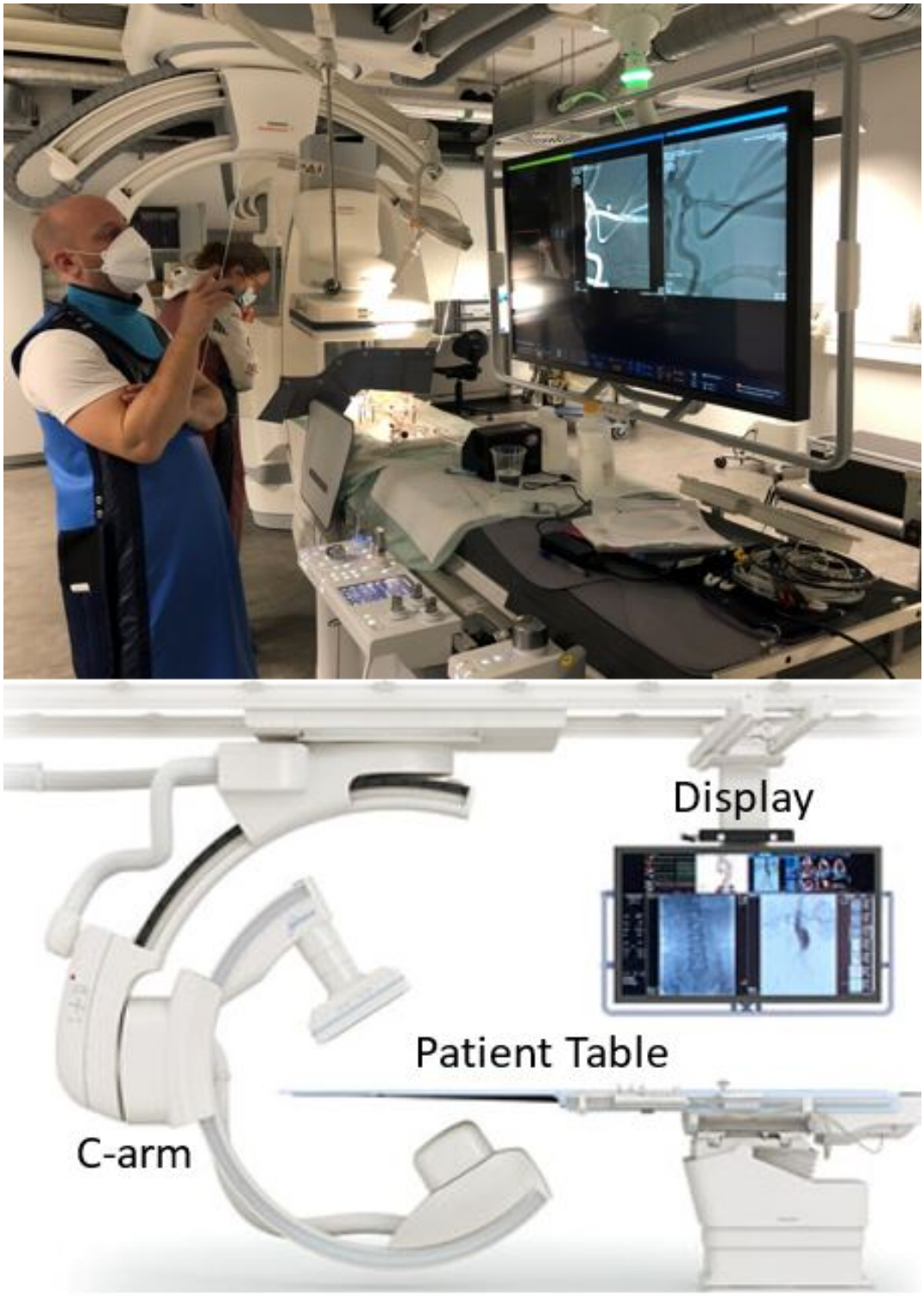

Figure 1.1: An angiography suite with a cardiovascular flow model illustrating the radiopaque imaging capabilities on the display screen of a C-arm x-ray system. Below shows the setup of a Toshiba Medical System C-arm.

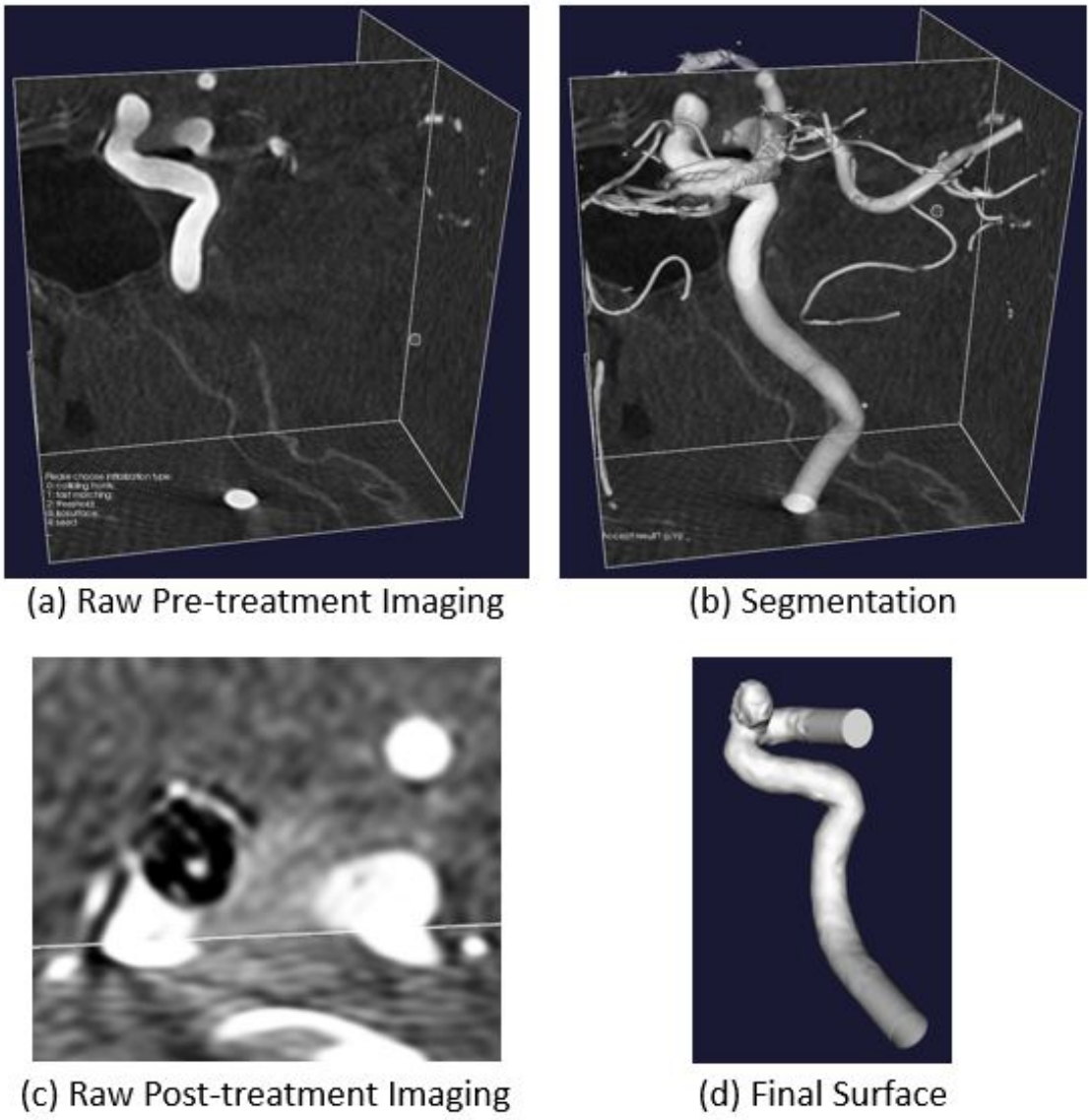

Figure 1.2: The raw 3D imaging taken before (a) and after (c) coil deployment can be segmented (b) before being converted into a surface (d) used for CFD simulations.

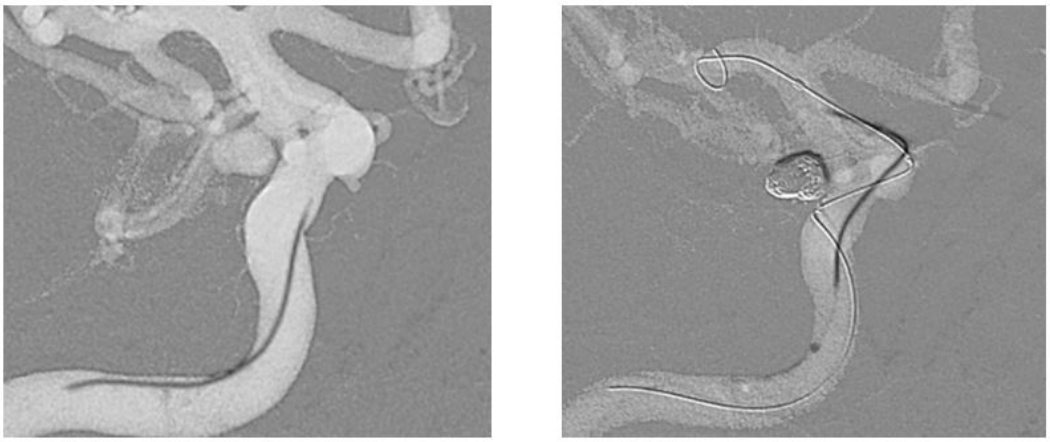

Figure 1.3: Radiopaque 2D imaging captured before (a) and after (b) coil deployment shows the catheter, device (in (b) only), and Doppler ComboWire.

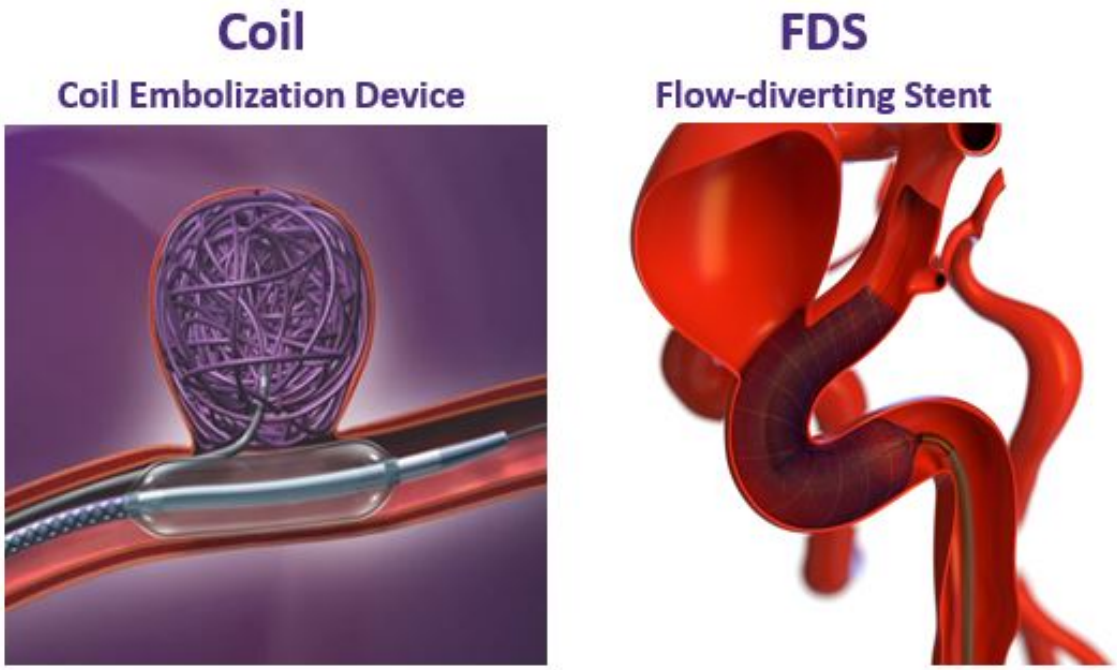

Figure 1.4: The coil embolization device on the left [35] is being deployed with a catheter within the aneurysm and aided by a balloon, while the flow diverting stent on the right [87] is deployed along the parent vessel.

1.1.2 Coil Embolization Device

A preferred strategy for treating cerebral aneurysms is to fill the aneurysm with platinum coils, promoting blood stasis, thrombosis within the aneurysm, and re-endothelialization of the parent vessel [90]. These platinum shape-memory alloy wires have been wound into a sheath such that they coil as they are delivered through an endovascular catheter, which is navigated into the aneurysmal sac under radiological surveillance during the procedure. As the coils fill a relatively high percentage of the aneurysmal sac volume (15-30%), they represent an obstacle to flow in the aneurysm, not unlike a porous material, that slows down the velocity of blood in the aneurysm [120]. If the treatment is successful, the increased stasis that the coils impose on the blood inside the aneurysm result in a stable thrombus filling the entire aneurysmal sac. If there are regions of the aneurysmal sac still patent to blood flow several weeks or months after the procedure, as evidenced by radio-opaque contrast injected in the vasculature filling any portion of the aneurysmal sac, the treatment is considered unsuccessful. A radiological follow-up examination showing any remnants of radiopaque contrast flow into the sac indicates the need for retreatment, due to risk of rupture. Periodic exams are required because there is no reliable way to predict the outcomes of aneurysms treated endovascularly, during or after placement, leading to a burdensome schedule of follow-ups and a higher risk for patients.

1.1.3 Flow Diverting Stents

The other preferred endovascular treatment strategy is to divert flow away from the aneurysm without deploying a device within the aneurysm itself [52, 90]. To achieve this, a flow-diverting stent (FDS) is deployed in the parent vessel harboring the aneurysm, with the stent covering the entire neck area. The neck is the surface that, along with the actual aneurysm dome wall, defines the aneurysmal volume. For FDS patients, this could be thought of as the surface where the parent vessel existed before the aneurysm originated. The combination of aneurysmal thrombosis and stent placement is thought to provide scaffolding upon which the endothelium regrows along the parent blood vessel and "heals" over the neck, preventing the aneurysm from being exposed to the mechanical stresses associated with blood flow [22, 52]. Even after endovascular treatment, aneurysms can rupture if blood flow persists inside part of the aneurysmal sac and the mechanical

stresses acting on the aneurysmal dome contribute to continued wall remodeling and deterioration of its structural integrity. Without a stable embolization to completely occlude the aneurysm and allow for full reendothelialization along the aneurysmal neck, the aneurysmal sac would be open to blood flow, as observed in angiography during follow-up, which constitutes a failed treatment. Aneurysms that rupture after FDS placement have an even higher mortality or morbidity than untreated ones [72], and so treatment failures always merit retreatment, with significant associated economic and human costs [94].

1.2 Hemodynamics of Cerebral Aneurysms

1.2.1 Untreated

Flow in saccular cerebral aneurysms can often be modeled as pulsatile flow in a cavity on the side wall of a circular vessel (exceptions are aneurysms lying between a bifurcation such as basilar tip aneurysms). The most basic flow in a cavity located on the side of a curved vessel develops counter-rotating flow, with strength dependent on the curvature, flowrate, and flow pulsatility [24]. For more complicated patient-specific aneurysms, the flow becomes increasingly complicated as inflow jets, impingement regions, vortices, and recirculation zones are created by the combination of anatomy and high inertia (Reynolds and Womersley numbers) [56]. From both experimental and computational investigations, many relevant hemodynamics parameters have been calculated, starting with velocity, dissipation rate, wall shear stress, and many others borrowed from the ample literature on atherosclerosis and plaque growth and remodeling [71, 105]. A strong coherent vortex created inside the aneurysmal sac can greatly increase the velocity in the cavity, while broken down patches of a slow recirculation zone will reduce the average velocity within the aneurysm; slow recirculation in the aneurysm can also lead to low wall shear stress areas, while inlet jet impinging on the distal wall produce high wall shear stresses on the aneurysmal dome [18].

1.2.2 Coil Embolization Device

A coil mass slows and diverts the flow entering the aneurysm. For the flow that does enter the aneurysmal sac, the coil mass adds resistance and slows down the persistent flow as it traverses the coiled aneurysm sac [117]. This post-treatment reduction of the inflow is strongly dependent

on the porosity, a variable dependent on the ratio of coil volume to aneurysm volume [39]. The aneurysmal dome WSS is similarly reduced by coils [27, 117]. While porosity has been shown to minimally affect pressure[17], wall shear stress (WSS) has been noted to decrease significantly with porosity [6]. Both in vitro and coil-resolved simulations show that narrow-necked and wide-necked aneurysms are affected differently by coiling [7, 6]. In particular, a narrow-necked aneurysm produces larger reductions in aneurysmal inflow and in the velocity in the aneurysmal sac than wide-necked aneurysm [6].

1.2.3 Flow Diverting Stents

Deploying a flow diverting stent has been shown to reduce inflow, velocity, and wall shear stress while inducing minor changes to pressure [19, 47, 93]. The curvature of the parent vessel has a definite effect on not only inflow into the aneurysm and resulting flow patterns [9], but also on the porosity of the stent, and therefore has a double effect on the flow resulting from treatment[128]. Studies comparing different stents (flow diverters versus supporting stents) [121], stents of different sizes [76], and stents of different porosities [47] have proven that the effects of treatment on the hemodynamics are strongly dependent on the specifics of the stent treatment. At low curvature of the parent vessel, flow in an idealized aneurysm treated with an FDS was found to be co-rotating, which was not observed in the untreated aneurysm for any conditions studied. As the curvature increases, the flow detaches from the wall and eventually becomes fully counter-rotating as in the untreated case [9].

1.3 State-of-the-Art in Endovascularly-treated Cerebral Aneurysm Simulations

CFD simulations of blood flow in intracranial aneurysms have been carried out for at least two decades [104, 110], with the applications ranging from initiation, growth, and rupture [15, 74, 106] to other clinical uses such as investigating recanalization in coiled aneurysms and the efficacy of both forms of endovascular treatment [28, 58, 86, 101, 117]. Further simulation studies seek to identify which hemodynamics metrics can best characterize the effect of the endovascular treatment in an effort to create thresholds that could predict treatment outcome (whether or not the aneurysm successfully occludes due to a stable blood clot fully filling the aneurysmal sac) for both

FDS [12, 14, 25, 63, 83] and coils [27, 32, 123]. Such numerical studies have investigated hemodynamics metrics like inflow, velocity, WSS, WSS gradient, oscillatory shear index (OSI), vorticity, energy (kinetic energy or energy dissipation), and relative residence time. Unfortunately, there is currently no consensus on which metrics are most physiologically relevant and more precisely which hemodynamics are predictive of treatment outcomes [102]; this is true even when considering studies combining morphological parameters [32] or machine learning [84] which have failed to produce certainty in the search for predictive metrics.

The current inability of patient-specific image-based CFD to provide a predictive hemodynamics metric of endovascular treatment outcome is due in part to two key issues: i) lack of standardization and automation and ii) inaccuracies of current models [15]. The reproducibility and comparability of CFD studies must be improved by the community as we seek to move towards clinical applicability. There are many steps that can be taken to remedy these issues, but the changes must be widely accepted throughout the community. If a common methodology that allows for comparison between differing studies is not readily adopted, the discrepancy in the results and uncertainty of predictive metrics will persist.

The lack of reproducibility springs primarily from the absence of standards and automation within cerebral aneurysm CFD studies. For comparable results, having a clear definition of the surface or volume on which the metric was extracted is imperative. However, the aneurysm neck or ostium can be defined in many different ways, with some methods preferred by engineers and others by clinicians. This creates a problem for not only neck metrics but the aneurysm volume and surface metrics as well, since both will be affected by where the neck is defined. Saalfeld [97] proposed an automatic neck detection and generation that, if adopted widely by the community, could contribute significantly to the automation of this process and to the repeatability of CFD studies of aneurysms. Despite this and other work in this direction, there has not been community consensus of the definition or generation of the aneurysmal neck, to date. Unfortunately, an accurate neck definition is not possible without a quality segmentation of the vasculature. A valid patient-specific image-based simulation relies upon precise segmentation. Many researchers echo the call for validation and standardization of this process [15, 20, 74, 102]. Furthermore, Gambaruto [38] found that variations in segmentation can impact CFD outcomes more than other fluid mechanics parameters used in modeling blood flow in aneurysms. Finally, with an accurate domain defined

for the simulation, boundary conditions must be considered. Babiker and Rayz found a strong influence of the parent vessel inflow rate on the hemodynamics [6, 92]. While not feasible in every case, Berg recommends using patient-specific data for inflow (as does Saqr [101]) and explains that a zero-pressure condition should not be used, but rather a flow-splitting method for multiple outlets [15, 99]. McGah showed not only the importance of using patient-specific data [67], but furthermore, the feasibility of implementing this method clinically[68].

Simulations require assumptions and models to predict the neurovascular flow field, including inside the aneurysm. Each assumption and model introduces some uncertainty into the CFD results. Understanding the limitations and error of each model is important before implementing it in a study. Saqr [101] reports that 90% of CFD cerebral aneurysm studies employ a Newtonian model for blood viscosity. While studies have shown inaccuracies in WSS magnitude prediction [62, 101], others show that the differences are insignificant [21, 38, 73]. Particularly because the data required to finetune a patient-specific non-Newtonian model are rarely available and there is a lack of consensus on which model is correct in general, a constant-viscosity Newtonian model is used in this dissertation. Another modeling assumption that is hotly debated is the distensibility of the vessel and aneurysm walls. Berg [15] pointed out that wall modeling is only as accurate as the patient-specific data that is informing the parameter selection. However, cerebral aneurysms are more rigid than other non-intracranial aneurysms or the parent vessel [36], and Steinman proved in his seminal study[109] that rigid walls introduce less uncertainty in cerebral neurovascular flow CFD than any other of the many parameters and modeling choices (anatomy segmentation, inflow conditions, spatial and temporal resolution and numerical convergence thresholds, etc.).

1.3.1 Modeling Endovascular Treatment

Simulating blood flow of endovascularly-treated cerebral aneurysms can either have the treatment resolved within the mesh or modeled. While the direct inclusion of treatment is desirable for certain research purposes, models that can be created with clinically available data and the reduction of computational time that comes with modeling the treatment are imperative for CFD to be clinically relevant. Porous medium models, a porous surface for FDS and a porous volume for coils, are frequently used to mimic endovascular treatment as an isotropic, homogeneous medium [1, 59].

Because these models can oversimplify the effects of treatment on aneurysmal flow, work has been done on improving the models for both coils [96] and FDS [1].

In 2008, the isotropic, homogenous porous media model was first applied to CFD of a cerebral aneurysm treated with embolic coils [70]. Since then, using a porous volume to model a coil mass has become the standard for cerebral aneurysm CFD [30, 44, 116, 123]. This includes studies seeking to find hemodynamic metrics predictive of endovascular treatment outcome [61, 117]. Recently, new porous medium models have been created that take into account the heterogeneity of the deployed coil embolization device [96, 116, 130]. The coil-resolved simulations are a costly yet useful research tool and can be employed to compare against porous media models as a ground-truth [27, 49, 96].

Similarly, a porous medium to model the stent surface has been extensively used in research and pilot clinical applications[30]. Augsburger investigated the pressure drop across an FDS at multiple flowrates and generated the inertial and viscous coefficient required to define a porous pressure jump [5]. Raschi followed a similar analysis to find coefficients for a different type of FDS [89]. This modeling of FDS has also been used in studies seeking to find predictive hemodynamics metrics [40, 132].

1.4 Successful Endovascular Treatment

In order for an aneurysm to be healed, it must become completely isolated from the parent vessel flow, without any blood entering the dome. In a surgical clipping procedure, the aneurysm is immediately rendered non-patent by a clip placed around the neck of the aneurysm. However, for endovascular devices, the aneurysm remains at risk of rupture until a thrombus (blood clot) has fully embolized the aneurysm dome. This process could take months since the patient is almost always on anti-platelet therapy to prevent blood clots in the parent vessel and detached in the general circulation, by platelets being in contact with the treatment devices.

For this healing process to proceed and to achieve total aneurysm occlusion in endovascular device treatment of intracranial aneurysms, the coagulation cascade needs to be triggered and platelets need to be activated. Platelets are one of three types of cells in blood and are the ones responsible for thrombus formation, and can be triggered by physiological changes and biomechanical stimuli [78, 91]. A widely accepted mechanism for activation is prolonged time spent in a given region, commonly referred to as residence time (RT) [48, 131]. Work has been done experimentally

to set absolute thresholds of platelet RT sufficient for thrombus formation [41]. Activated platelets occur in the cardiovascular system in the recirculation zone after a stenosis[115] or a left ventricular assist device (LVAD) [3], similarly they can be found in the recirculation of an aneurysm dome. Increased RT would be expected after endovascular device deployment, ideally leading to a stable thrombus.

While increased RT alone may lead to platelet activation [48, 131], shear exposure of the platelets can initiate thrombosis [42, 80, 115]. With LVADs, unphysiologically high shear stresses are experienced by platelets leading to activation [3]; however, these levels of shear rate are not present in the cerebrovascular system even when a treated aneurysm is present [33, 77]. At these magnitudes, very low shear has been shown to activate platelets as well [78, 82, 91]. Furthermore, there have been studies that demonstrated platelet activation from shear stress changes seen at these lower levels, and a model has been proposed, based on that mechanism [78, 122].

1.5 Specific Aims of this Thesis

The main aim of this dissertation is to improve the understanding of how endovascular therapies affect the flow in cerebral aneurysms, through CFD simulations. This involves not only gaining deeper insight into the flow modifications, but also improving the models and frameworks used in the simulations, so that an accurate flow field can be produced for both pre-treatment and, more importantly, post-treatment. Furthermore, the methods need to be clearly described to be standardized and, where possible, incorporate automated steps to aid in the goal of standardization of aneurysm CFD simulations.

Specific Aims proposed to reach this overall goal are: the comparison of endovascular treatments (coils versus stents), the introduction of Lagrangian tracking to understand the biomechanics environment experienced by platelets in the aneurysmal domain, the comparison of fusiform and saccular aneurysms, and the comparison of a novel coil modeling approach.

1.5.1 Organization of the Thesis

This dissertation is divided into six chapters:

Chapter 2

This chapter reviews CFD-derived hemodynamics data of a large cohort of cerebral aneurysms to determine if the two endovascular therapies, coils and FDS, modify the intra-aneurysmal flow in a similar manner. The aim of this study is to determine if flow modifications due to endovascular treatment are similar enough to produce a single predictive set of metrics that work for both endovascular devices. If the two therapies do produce similar changes in the hemodynamics in order to achieve the same goal of fully filling the aneurysm with a blood clot, then the mechanism for thrombosis and embolization of intracranial aneurysms could be studied under a single study, and the metrics to predict treatment outcomes could be defined with the ensemble of cases treated with either device. If the mechanism for flow modification is proven to be different, then endovascular therapies must be studied separately and the metrics to predict outcomes should be tailored to the treatment type.

Chapter 3

This chapter introduces Lagrangian tracer particles into the aneurysmal flow to provide information on the biomechanical environment that platelets are experiencing before and after treatment. The aim of this study is to investigate novel Lagrangian hemodynamics metrics that might be predictive of endovascular treatment outcomes. A new Lagrangian approach is established for cerebral aneurysms and applied for each of the endovascular treatments, to explore new metrics that could be clinically predictive of treatment success, since there currently is no agreement on which Eulerian metrics are predictive of outcomes.

Chapter 4

This chapter compares two types of cerebral aneurysms, fusiform and saccular, by examining both hemodynamics metrics and FDS deployment characteristics. The aim of this study is to quantify the changes post-FDS deployment of the flow, in order to see if fusiform aneurysms can be combined with saccular aneurysms in a single cohort for a study on predicting FDS outcomes. Because of their circumferential dilation, fusiform aneurysms cannot be coiled and only FDS treatment is considered in this study.

Chapter 5

This chapter quantifies the improvement introduced by a new bilinear porous media model, comparing this novel model for coiling against the standard homogeneous, isotropic porous medium model. The error of both models is computed by qualitatively comparing their results against the gold-standard coil-resolved simulations. The aim of this chapter is to assess the level of improvement introduced by the bilinear model in the accuracy of different metrics. The study in Chapter 3 illuminates the inability of the standard porous medium model to compute Lagrangian metrics accurately, and the overdampening of the flow in general. Therefore, both Eulerian and Lagrangian metrics are compared.

Chapter 6

The concluding chapter presents a summary of the conclusions reached in each chapter along with recommendations for future work.

Chapter 2

DISTINGUISHING HEMODYNAMICS EFFECTS BETWEEN TWO FORMS OF ENDOVASCULAR THERAPY

Aneurysms treated with flow diverting stents (FDS) and coil embolization devices are compared using computational fluid dynamics to determine if they effect of the flow in a similar manner. The aim of this section is to determine if the two devices can be considered together in the same cohort for a study seeking to identify hemodynamic metrics that can predict the outcome of the treatment.

2.1 Background and Motivation

Although the overall goal of the two main forms of endovascular devices, FDS and coils, remains the same, the healing process differs between the two therapies: complete occlusion of the aneurysm such that no blood flow can enter from the parent vessel. The flow-diverting stent redirects a majority of parent vessel flow away from the aneurysmal neck and sac, while providing scaffolding over which healthy endothelial cells can regrow. An embolic coil mass is meant to fill the entire aneurysmal sac and initiates a thrombus soon after deployment. While the end goal of fully filling the aneurysm is the same for both devices, the hemodynamic alterations have not been directly compared to determine if the two treatment types can be studied together. Hence, this study uses image- and data-based patient-specific CFD simulations of aneurysms treated with either endovascular device to investigate how similar the hemodynamic changes are between the two types of therapies.

2.2 Method and Materials

Enhanced description of patient inclusion criteria, application of the Womersley inlet flow and Windkessel model for pressure outlet, and porous media approximation can be found in previous work done in the Multiphase and Cardiovascular Flow Lab at UW [8].

2.2.1 Patient Population and Data Collection

Consenting patients were enrolled in this IRB-approved study through the University of Washington Medical Center. Only unruptured aneurysms treated with either a coil embolization device, Target coils (Stryker Endovascular, Kalamazoo, Michigan, USA), or flow-diverting stents, Pipeline Embolization Device (PED, Medtronic, Dublin, Irelend), are included. Data was collected for each patient by neurointerventionalists in the angiography suite directly before and after treatment. Data collection does not disturb the established workflow of the procedure. Three-dimensional rotational imaging of the aneurysm and surrounding vasculature is obtained using a biplane angiographic unit. A dual-sensor pressure and Doppler velocity endovascular guidewire (ComboWire, Volcano Philips, Rancho Cordova, CA) provides the blood flow velocity and pressure every 5ms at specified locations. The wire is removed after flow data has been collected for at least 10 cardiac cycles at each location. A post-treatment contrast-enhanced flat-panel CT scan is obtained to guide post-treatment simulations, see Fig 1.3. This angiographic and hemodynamic data allow for creation of patient-specific models.

2.2.2 Determination of Endovascular Treatment Outcome

Treatment outcome for an endovascular deployment is determined by the treating neurointerventionalist. To determine if the aneurysm is fully patent, with no flow entering, contrast-enhanced medical imaging is required. The first step to a successful treatment, redirection, is immediately achieved to some degree by both devices. This provides an environment favorable to platelet activation, assuming enough of the flow has slowed. Then once enough of the blood has slowed, a thrombus, which is a blood clot, can form. If there's full occlusion or filling, then we consider this a successful outcome. However, even an aneurysm, partially occluded by a large thrombus, is at risk of rupture due to the remaining exposed wall.

A successful case requires that no contrast be filling the aneurysm at a angiography follow up visit, as soon as 6 months after treatment. If full occlusion is not achieved, patients will have to come back for follow-ups and possibly retreatment. These visits are required because there's no other way to determine the outcome.

2.2.3 Computational Model

Image Segmentation

Pre-treatment three-dimensional rotational angiography (3DRA) is used to reconstruct a surface of the vessel and aneurysm using the Vascular Modeling Toolkit (VMTK, `http://www.vmtk.org`). The post-treatment 3DRA is also segmented using VTMK. Both are shown in Fig. 1.2. The coil surface that is open to the parent vessel, and therefore blood flow, is used as the boundary to delineate the coil mass, see Fig. 2.1. This surface is transformed to match the centerlines of the pre-treatment vessel then intersected to create the coil volume. Due to the nature of the stent geometry, accurate centerlines cannot be created from the post-treatment imaging of the vessel. The post-treatment 3DRA guides the semi-automated reconstruction of the stent based on the pre-treatment centerline. The reconstructed vessel surface intersected by the treatment surface is meshed (StarCCM+, V13.06, Siemens PLM Software Inc., Plano, TX, USA). A tetrahedral mesh is created in the two volumes, the treated aneurysmal sac and the parent vessel. A global element size of 0.2 mm and 4 prismatic layers along walls are used. Prismatic layers are also grown in the direction normal to the treatment interface. This level of spatial discretization has been shown to be sufficient to resolve the flow and produce accurate hemodynamic metrics in the cerebral vasculature [66].

Aneurysmal Domain Definition

Saalfeld's method for semiautomatic neck detection is applied to define the aneurysm's ostium for every patient [97]. This provides a new delineation for the aneurysm sac which can be applied to both treatment cohorts.

For analysis of the coil cohort, the aneurysm, as defined by the intersection of the planar ostium, is used for the dome WSS, ostium shear stress, viscous dissipation, and average velocity measurements. A plane is fitted through the outermost points of the ostium (MATLAB, R2020a, The MathWorks Inc., Natick, Massachusetts, USA) so that the undulation of the ostium does not disturb the analysis of shear stress. The increase in shear stress of the coil surface itself is excessively large when the surface exhibits complex curvature simply due to the geometry; this can be seen in Fig. 2.1. Furthermore, the measurement of aneurysm inflow is highly sensitivity to the location

of the surface if the plane intersects or lies below the coil surface (with respect to the aneurysm dome). Therefore for robustness, a second plane (Q ostium), offset to be fully submerged in the coil mass, is used to measure aneurysmal flowrate for coil patients.

For analysis of the stent cohort, the aneurysm, as delimited from the parent vessel by the ostium and the stent, is used for the flowrate, dome WSS, viscous dissipation, and velocity measurements. This means that if the stent does intersect the ostium as in Fig. 2.1, the highest surface of the intersection, which will include both the ostium and stent, is used to define the aneurysm; if there is no intersection, the ostium is used without modification. Since the stent provides a scaffold over which healthy endothelial cells can regrow, the stent is the optimal surface to quantify the change of shear stress due to treatment. Hence, ostium shear stress is calculated over the actual treatment surface for FDS patients.

2.2.4 Computational Simulations

A finite-volume solver (ANSYS FLUENT, ANSYS Inc., V16.2, Canonsburg, PA, USA) is used to solve the incompressible Navier-Stokes equations. A second-order-in-time, implicit, flux-splitting scheme is selected, with a PISO correction algorithm. The time step is set to 1x10^{-3} s. Blood is modeled as Newtonian in this high-shear-rate flow [50] with a constant dynamic viscosity of 3.5 cP and a density of 1050 kg/m^3. Three cardiac cycles are simulated, with the first two cycles discarded to exclude transient effects from simulation start-up. The flow field is stored throughout the third cardiac cycle, peak systole and a time-average of the flowfields are evaluated to calculate the 5 hemodynamics metrics of interest.

Boundary Conditions

A domain consists of 3 types of boundaries: inlet, outlet, and wall. Aneurysms treated endovascularly are typically accessed through the internal carotid artery (ICA), and all aneurysms in this study are on the ICA or basilar artery which serve as the inlet. At the termination of these two arteries, a major bifurcation occurs: the middle cerebral artery and anterior cerebral artery for the ICA bifurcation and the right and left posterior cerebral arteries for the basilar. Certain aneurysms may form directly on a bifurcation, whether a major branch split or a minor branch originating

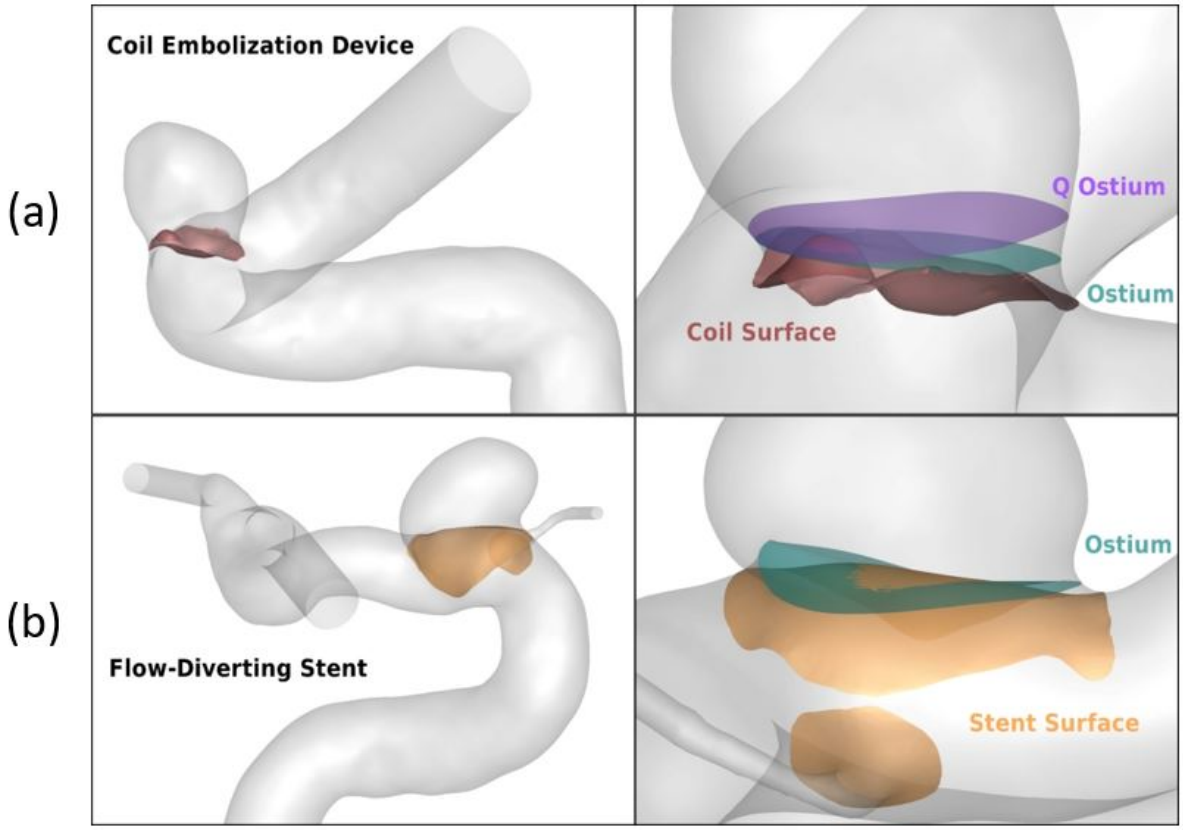

Figure 2.1: (a) A coil case with only one outlet on the ICA (top left): The coil surface defines the boundary of the porous medium; the planar ostium is used to extract all variables except flowrate which is calculated through Q ostium. (b) FDS distal to the ICA bifurcation and covering the post communicating artery (bottom left): Shear stress will be calculated for the stent surface across the aneurysm only. The surface closet to the apex of the aneurysm for this case is composed of two parts: the exterior portion of the ostium and the stent that intersects the ostium.

from the parent vessel such as the posterior communicating artery (see Fig.2.1).

Inlet: At the inlet of the domain, a Womersley velocity profile is prescribed [124]. The inlet of the domain is ≈ 5mm proximal to the wire measurements' most proximal location, and the time-resolved Doppler velocity measurements at this location are used as the centerline (maximum) axial velocity. To accurately compare the change in hemodynamics caused purely by treatment, the inlet flowrate is constant in pre- and post-treatment simulations. Measurements for 8-20 cardiac cycles are phase-averaged to generate the centerline velocity waveform.

Employing the equation for the Womersley profile, $w(r,t)$, provides a time-varying pulsatile waveform, and has the analytical solution of:

$$w(r,t) = A_0(1-(\frac{r}{R})^2) + \sum_{n=1}^{N} \tilde{A_n}[1 - \frac{J_0(\frac{r}{R} \cdot i^{3/2} \cdot Wo_n)}{J_0(i^{3/2})}]e^{i\omega_n t} \tag{2.1}$$

where A are the Fourier coefficients, r is the radius of interest, R is the vessel radius, and J_0 is the 0^{th}-order Bessel functions of the first kind. Finally, the Womersley number, α, is calculated as:

$$Wo_n = R\sqrt{\frac{2\pi n}{T\nu}} \tag{2.2}$$

Two validation studies have been run assessing the accuracy of ComboWire data and the feasibility of applying it to patient-specific simulations. ComboWire data is taken at multiple locations distal to the inlet measurement. To verify the ComboWire data, velocity and pressure fields were simulated and compared at these locations [67]. Later, PIV experiments measured by an ultrasonic flow-meter showed no detectable bias from the derived ComboWire flowrates [68]. With both *in-silico* and *in-vitro* validation studies, ComboWire data is confidently applied to the boundary conditions in this study.

Outlet: If a simulation has more than one outlet, which is the case for most of this cohort, a two-element Windkessel model is used for each branch based on their respective radii. Resistance (R) is defined by the estimated flow split into the branches and the pressure waveform of the inlet. Capacitance (C), the second of the two elements, is based on the pressure waveform and the respective radius of each branch. Each outlet then has its own RC values based on the inflow

and respective radius. A one-vessel outflow is employed only when the aneurysm does not occur at a bifurcation and is more than 5 parent-vessel-diameters proximal to a major flow split. A zero-pressure condition is used in these cases.

Wall: The vessel lumen is treated as a rigid wall [65] with a no-slip boundary condition where the flow velocity is set to zero: $\mathbf{u}|_{wall} = 0$.

Treatment Implementation

The endovascular treatments are modeled using a porous media approach [5, 89]. The treatment is approximated as a momentum sink, since the clinical imaging does not allow for a precise, physical reconstruction of the endovascular device.

Coil Embolization

The coil mass is not directly resolved, but modeled to simulate the resistance the blood flow would see in a coiled aneurysm sac. To do this, the porosity must be determined from the packing density, a function of the coil volume and aneurysm volume $PD = \frac{V_{coil}}{V_{aneurysm}}$. Coil volume is dictated by the treatment, since each coil has a known diameter and length. Aneurysm volume, when calculating packing density for coil patients, is the volume of the aneurysm as defined by the coil surface.

The entire volume of the aneurysm, as defined by the coil surface from post-treatment 3DRA, is affected by the porous medium [51, 60, 61, 75]. The Darcy-Brinkman equation is used to estimate the viscous and inertial loss coefficients, used for the porous media model, based on the porosity of the coil mass inside the aneurysmal sac:

$$S_i = \frac{\mu}{K} u_i + \frac{1}{2} \rho C_2 |u| u_i \tag{2.3}$$

where i represents the ith component, μ the viscosity, ρ is the density, u is velocity, K and C_2 are the permeability and form factor coefficients (geometric parameters that depend on the porosity of the medium), and S_i is the source term for momentum.

Permeability, K, the inverse of the viscous resistance coefficient applied in simulations and the inertial resistance coefficient, C_2, are estimated using the same method described by Barbour [8]. In short, the capillary theory of Kozeny [55] provides an equation for permeability based on the

volumes of the coils and aneurysm as well as the cylindrical shape of the coil which determines the Kozeny coefficient.

The viscous resistance is defined as:

$$\frac{1}{K} = \frac{c(\frac{V_{aneurysm}}{R*V_{coil}})^2}{(1-\frac{V_{coil}}{V_{aneurysm}})^3} \tag{2.4}$$

where c is the Kozeny coefficient which is 2 for when the resistive structures have a cylindrical cross-section, V_{coil} and $V_{aneurysm}$ and the volumes of the deployed coils and the aneurysm, and R is the radius of the coils.

The inertial resistance, C_2, is simply the product of the packing density and an empirical coefficient set by studies from Muscheborn [75].

Flow-Diverting Stent

Unlike a coil mass, FDS are modeled only over a surface or interface. The porous approximation used here is modeled as a pressure jump applied to the the momentum equations at the stent interface using Eq. 2.3. The viscous and inertial resistance coefficients, K^{-1}= 7.1x10$^{-10}m^{-2}$ and $C_2 = 1.4\text{x}10^{-4}m^{-1}$, are computed following a previously published study [5] and remain constant for all patients. Currently, the curvature of the parent vessel and sizing of the stent are not accounted for in treatment modeling [45]. The thickness of the specific FDS is set as the thickness over which the pressure drop is approximated within the CFD porous jump model; within the given patient cohort, this ranged from 61 to 67.3 nm.

Hemodynamic Metrics of Interest

Five hemodynamic variables are measured for each patient in the pre- and post-treatment simulations to determine the effect the treatment has on the blood flow and anuerysmal environment. They are as follows: 1) flowrate into the aneurysm integrated across the ostium, Aneurysm Flow Rate (mL/min); 2) WSS magnitude area-averaged across the aneurysmal dome, Aneurysm Dome WSS (Pa); 3) shear stress magnitude area-averaged across the ostium, Neck Plane Shear (Pa); 4) viscous dissipation integrated throughout the anuerysmal sac, Viscous Dissipation (mW); 5) velocity averaged throughout the anuerysmal sac, Aneurysm Average Velocity (m/s). The aneurysmal dome and sac are defined by the ostium for all hemodynamic parameters. As mentioned, flowrate

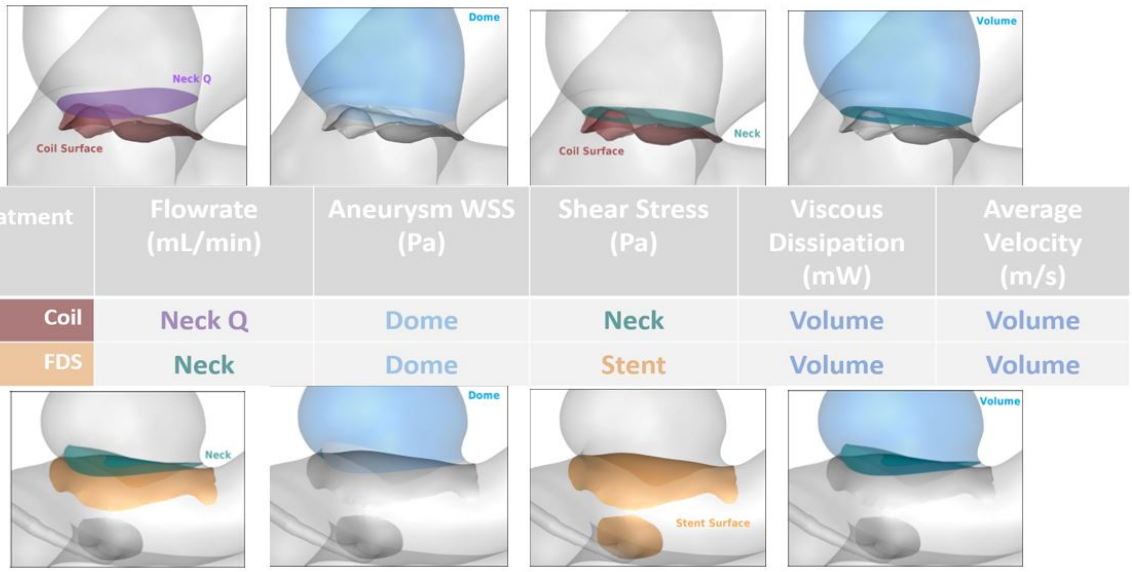

Treatment	Flowrate (mL/min)	Aneurysm WSS (Pa)	Shear Stress (Pa)	Viscous Dissipation (mW)	Average Velocity (m/s)
Coil	Neck Q	Dome	Neck	Volume	Volume
FDS	Neck	Dome	Stent	Volume	Volume

Figure 2.2: The 5 hemodynamic metrics of interest and the location on which each was extracted.

for coil patients is defined by a separate plane, and shear stress of the aneurysm neck for FDS patients is defined by the stent treatment surface. Figure 2.2 provides a visual table of the metrics and location of extraction. Each variable is calculated at 20 times steps, one of which is peak systolic inflow rate, within the final cardiac cycle. The maximum and time-averaged values of each metric are used to calculate change scores.

$$\Delta\beta = \frac{\beta_{Post} - \beta_{Pre}}{\beta_{Pre}} \cdot 100 \tag{2.5}$$

Statistical Analysis

The relevance of hemodynamic variables are compared using statistical analysis. Our cohort can be split by treatment type, FDS and coil. The entire cohort, or simply each treatment type, can be further split by treatment outcome: success or failure. The hemodynamics can be split by pre- and post-treatment cases. A paired t-test could be employed when comparing pre- and post-treatment metrics because this constituted matching pairs of metrics. For the other unpaired two-sample tests, the data must be further characterized in order to chose the correct independent t-test. Whether

comparing treatment type or treatment outcome, how many tails the data has must be determined. Flowrate, WSS, viscous dissipation, and average velocity are all expected to decrease and the data confirms this. However, aneurysm volume, neck area, and ostium shear stress would be considered two-tailed as they have a more symmetric spread that can increase or decrease. For each group, the variance must also be checked to determine if the two groups have similar values. When comparing FDS and coil, five groups had heteroscedasticity: aneurysm volume, neck area, flowrate, WSS, and viscous dissipation. The remaining are homoscedastic because of the similar variance between the two treatment type's data set: ostium shear stress and average velocity. For this study, a pair of data was labeled homoscedastic if the ratio of variance was below 1.5.

2.3 Results

2.3.1 Cohort-wide Morphological Parameters and Hemodynamic Changes

Pre- and post-treatment patient-specific simulations, employing a porous media approach and using ComboWire Doppler measurements as inlet/outlet boundary conditions, were performed for 42 patients. A summary of the inlet flowrate, Reynolds number, and diameter, as well as aneurysm volume are all presented in Table 2.1. The Doppler-derived inlet flowrates are all within normal physiological range; however, the flowrate variability is large within the cohort. The standard deviation is almost half of the mean flowrate for systolic (231 $\pm$ 108 mL/min) and time-average (132 $\pm$ 59 mL/min) values.

Table 2.2 give the population average of the hemodynamics changes for all metrics of interest. As expected and shown by numerous studies [8, 13, 32, 113], endovascular treatments are effective in reducing the blood flow into the aneurysm. The result is evident from the reduction in velocity at the perimeter of the aneurysm and by investigating the flow field inside the dome through energy dissipation, velocity, and even dome WSS, which can indicate reduction of inflow aneurysmal jet impingement.

2.3.2 Endovascular-grouping of Cohort: Coil vs FDS

The two endovascular therapies not only have separate mechanisms for healing, but each affect the flow differently. Separating the cohort by treatment type splits the group into 17 aneurysms treated

Table 2.1: Summary of patient inlet flowrate, Reynolds number, diameter, and aneurysm volume, averaged across patients. Standard deviation is shown in parenthesis.

		Pre-treatment
Inlet Flowrate	Peak	230.7 (108.2)
(mL/min)	Time-averaged	131.6 (58.6)
Reynolds Number	Peak	317.5 (119.4)
	Time-Averaged	182.7 (67.8)
Inlet Diameter (mm)		4.50 (0.62)
Aneurysm Volume (mm^3)		425 (937)

Table 2.2: Overall effect of endovascular treatment, coils and FDS, on hemodynamic metrics before and after treatment, and % change from pre- to post-treatment.

		Pre	Post	% Change	p-value
Aneurysm Flowrate (mL/min)	Peak	68.1	33.7	-50.9	<0.001
	Time-Averaged	38.3	15.5	-59.7	<0.001
Aneurysm Dome WSS (Pa)	Peak	1.47	0.474	-67.6	<0.001
	Time-Averaged	2.38	0.97	-57.6	<0.001
Ostium Shear Stress (Pa)	Peak	0.825	0.855	6.40	0.090
	Time-Averaged	0.442	0.465	8.35	0.051
Viscous Dissipation (mW)	Peak	0.094	0.022	-74.0	<0.001
	Time-Averaged	0.028	0.006	-76.5	<0.001
Aneurysm Average Velocity (m/s)	Peak	0.152	0.058	-63.6	<0.001
	Time-Averaged	0.080	0.026	-68.0	<0.001

with coils and 27 with FDS. For the coil group, even with a reduced population size, the treatment effect still shows statistical significance between the pre- and post-treatment hemodynamics for all metrics except ostium shear stress similar to Table 2.2. However, the FDS treatment effects, when separated from coils, show a statistical significance ($p<0.001$) for all metrics, including the shear stress on the stent surface across the aneurysmal neck.

Table 2.3 compares the hemodynamic changes introduced by the two different treatments, highlighting the distinction between hemodynamic changes caused by each. First, a larger decrease in shear rate averaged across the ostium following treatment is observed in FDS patients compared to patients who received coil embolization treatment, both at peak systole and time-averaged ($p=0.001$). The reduction in volume-averaged velocity is larger in coil patients than FDS ($p<0.001$). There is a similar trend of coil patients exhibiting a larger reduction for dome WSS and viscous dissipation. It is interesting to note the reduction of flowrate into the aneurysm is closely related between the two treatment groups. As mentioned, hemodynamic changes measured in coiled patients are extremely sensitive to the location of the surface used to extract the data. Ostium shear stress, for instance, is greatly altered if computed at the complex-curvature coil surface versus a planar surface intersecting the coil surface. This causes a significantly larger increase in ostium shear stress for coiled patients. The change of flowrate into a coiled aneurysm is quite variable based on the surface location as well. Prior to using the more robust neck definition, the change in flowrate for any coil patient may exhibit strong inconsistencies from small variations in the choice of surface where it is computed. Because of these multiple definitions of the neck surface, the change in flowrate showed a strong, yet false, statistical significance the two treatment types.

2.3.3 Predicting Treatment Outcomes

The ultimate goal of this CFD is to create clinically realistic models for treatment planning and predictions of treatment outcome. A treatment is considered to be a failure if blood flow is present in any part of the aneurysm because it has not been fully occluded by a stable thrombus a few months after treatment. For the FDS group, 21 of 27 aneurysms treatments were successful, results can be seen in Table 2.4. Of the 17 coil patients, 11 were successful while 6 were considered to be failed treatments, results can be seen in Table 2.5. Unfortunately, the current results show no

Table 2.3: Differences in hemodynamic metrics across patients who were treated with Flow Diverting Stents vs coil embolization device.

		FDS	**Coil**	p-value
Δ Aneurysm Flowrate (%)	Peak	-50.8	-51.1	0.483
	Time-Averaged	-59.5	-60.0	0.467
Δ Aneurysm Dome WSS (%)	Peak	-58.9	-73.6	<0.001
	Time-Averaged	-63.8	-73.9	0.010
Δ Ostium Shear Stress (%)	Peak	17.2	-11.4	<0.001
	Time-Averaged	20.8	-12.1	0.001
Δ Viscous Dissipation (%)	Peak	-69.3	-81.8	0.005
	Time-Averaged	-72.9	-82.4	0.020
Δ Aneurysm Average	Peak	-55.1	-77.6	<0.001
Velocity (%)	Time-Averaged	-80.2	-60.6	<0.001

Table 2.4: The hemodynamic results of the FDS cohort split by treatment outcome.

FDS	**Success** (n = 21)	**Fail** (n = 7)	p-value
Δ Aneurysm Flowrate (%)	-52	-48	>0.05
Δ Dome WSS (%)	-59	-58	>0.05
Δ Neck Shear (%)	19	12	>0.05
Δ Viscous Dissipation (%)	-69	-69	>0.05
Δ Average Velocity (%)	-56	-52	>0.05

Table 2.5: The hemodynamic results of the coil cohort split by treatment outcome.

Coil	**Success** (n = 11)	**Fail** (n = 6)	p-value
Δ Aneurysm Flowrate (%)	-50	-53	>0.05
Δ Dome WSS (%)	-72	-77	>0.05
Δ Neck Shear (%)	-8	-19	>0.05
Δ Viscous Dissipation (%)	-81	-83	>0.05
Δ Average Velocity (%)	-78	-77	>0.05

statistical significance in predicting success from changes in the hemodynamic parameters studied between the successful and unsuccessful cases, for both treatment types.

2.4 Discussion

Change in Eulerian metrics alone, particularly with this sample size of less than 30 cases for each type of treatment, cannot accurately distinguish between successful and failed treatments, whether grouped together or by treatment type. However, it was determined as part of this study that the two techniques and devices clearly alter the blood flow in different ways and should be considered separately. The coil mass affects the entirety of the aneurysm, and thus it makes sense that this treatment method leads to higher reductions in volume-averaged bulk metrics for high packing densities seen in this study. Furthermore, the shear stress on the stent surface is an important metrics for the successful healing of FDS patients. Yet, this data cannot be directly compared to shear stress on the complex-curvature coil surface as the changes in hemodynamic metrics would be vastly higher. This large increase would, however, be mostly due to the surface shape rather than from flow redirection.

In order to improve the uncertainty surrounding the success of endovascular therapies, the reliability of CFD must be increased to move toward clinical applicability in terms of both predicting treatment outcome and treatment planning. To achieve this, Berg et al.[15] calls for standardizations and automations leading to greater reproducibility and reliability of the hemodynamic data

produced by CFD.Throughout this work, it was seen that small variability in the neck caused disproportionately large changes in the aneurysmal inflow and neck shear stress, particularly for the post-treatment coil patients due to the porous media aneurysmal region. The neck definition process is not standard and, in most cases, not automated. However, much care should be given to the procedure as it determines the aneurysm's boundaries and therefore, where metrics are calculated. Furthermore, the modeling of treatment may need to be improved, again for coil patients in particular.

Similar average hemodynamic decreases have been reported in a study by Damiano [31] where the effectiveness of coils vs FDS treatments were analyzed on a single aneurysm. Coil treatment was shown to reduce aneurysm-averaged velocity and WSS more than FDS. This study also reported that aneurysm inflow reduction is highest when treated with an FDS; however, the packing density was varied from 3-30% whereas our study was comprised of coil masses with realistic clinical densities, falling on the higher end of the range. When coil is the primary treatment, high packing densities of at least 20-25% are desirable [100]. Paliwal [83] demonstrated similar reductions for average velocity in FDS patients and slightly smaller reductions of flowrate with an average of -38% for 15 patients. Mut [76] also found similar results. The coil cohort has a similar reduction of flowrate to certain coil studies [32, 117].

Shear stress along the coiled aneurysm ostium or stent surface provide a more direct quantification for flow redirection. Increases in neck shear stress are expected as the treatment tends to realign flow with the parent vessel, making the flow at the aneurysmal neck more tangential to the arterial wall (reducing the normal component and therefore the net flow into the aneurysmal sac). The treatment effect is significant ($p<0.001$) for all metrics except ostium shear stress.

2.5 Conclusion

Coil embolization device and flow-diverting stent treatments must be considered separately as studies of the effectiveness of each treatment continue both *in-silico* and *in-vitro*. This study shows that even for a cohort of 27 FDS or 17 coil patients, predictive metrics cannot be established, at least not for these 5 hemodyanmic metrics. Therefore, more large-scale studies, using high-quality imaging and validated models, are required before hemodynamic studies on treatment outcome can become clinically applicable. Though without standardization and validation, cross-comparison of

studies is impossible.

Chapter 3

ANALYSIS OF PLATELET DYNAMICS IN CEREBRAL ANEURYSM TREATED ENDOVASCULARLY

In this section, two cohorts of patients treated with different endovascular therapies have pre- and post-treatment simulations performed with Lagrangian tracer particles integrated into the blood flow to aid in the analysis of hemodynamics within the aneurysm and the change in the flow caused by the treatment. The first cohort focuses on patients treated with flow-diverting stents. The simulations follow the same procedure as the previous study. This work was published in the Annals of Biomedical Engineering in 2020 [63]. The second cohort follows coil embolization patients and employs a new coil-resolved simulation as a ground truth to the porous media approximation of the coil treatment. This work was published in the Journal of Biomechanical Engineering in 2021 [27].

3.1 Background and Motivation

In vitro and *in silico* studies, including those presented in Chapter 2, have demonstrated the effectiveness of coils and FDS to limit blood flow into the aneurysm, which inherently reduces the mechanical stresses on the aneurysmal wall [8]. The end goal being complete isolation of the aneurysm from flow, and therefore stress, to mitigate any possibility of rupture. The analysis of CFD simulations of intra-aneurysmal hemodynamics have traditionally focused on Eulerian metrics that best represent the effect of treatments on the vascular endothelium [30]. Yet, similar to the efforts to predict rupture risk by the CFD community, studies regarding aneurysm embolization of any kind, and specifically recent pilot studies of flow-diverting stents, face issues of conflicting results regarding the effect of treatment on hemodynamic variables and their capability of predicting outcomes [8, 14, 32, 37, 83]. This may indicate that Eulerian metrics are imperfect predictors of treatment outcome. Investigating purely Eulerian flow variables cannot fully represent the progressive platelet activation, accumulation, aggregation, and intrasaccular thrombus formation that is thought to lead to aneurysm occlusion and successful treatment [79].

Lagrangian- tracking of platelets has been well established in computational modeling of cardiac disease and ventricular assist devices where extreme shear stress gradients and accumulation of platelets in regions of high residence times (RT) instigate thrombosis, which becomes a source of embolic stroke [3, 81]. This approach provides exact calculation of the length of time platelets spend in a particular region and the shear stress experienced along their trajectories. Having been successfully employed to model the risk of undesirable platelet activation in stenosed vessels [103] or in left ventricular assist device therapy [3], the technique is a prime candidate for detecting platelet activation necessary for the formation of a stable thrombus in intracranial aneurysms.

Based on the lack of consensus for predictive variables from traditional Eulerian CFD and the potential advantages of Lagrangian-metrics, particle-tracking is applied to high-fidelity simulations in an effort to understand the impact of aneurysm anatomy and physiology, and of endovascular FDS treatment on the trajectories and biomechanical environment of platelets as they flow in and out of the aneurysmal sac. Platelet activation, a necessary mechanism for thrombus formation, is known to be related to high RTs in regions of the vasculature and to respond to biomechanical stimuli, particularly to the platelets' shear stress exposure [3]. Laboratory experiments of platelet activation *ex vivo* have shown that platelet aggregation and thrombus formation can begin as early as 1s after exposure to slow or stagnate blood flow [41, 43]. More notably, particularly in the case of endovascular FDS treatment, platelets activate and accumulate when prolonged RT in the aneurysm is achieved from stent placement, especially when combined with exposure shear stresses gradients [91]. The high shear rates typically associated with stenosis or the even higher unphysilogical shears seen in a left ventricular assist devices (LVAD) are not experienced in the cerebrovascular system, even when an aneurysm is introduced. Rather, lower wall shear stresses have been the threshold for previous studies [33, 82, 91]. Hence, in this study, Lagrangian platelet trajectories are computed from the blood velocity field to characterize the mechanical environment experienced by platelets, allowing for a direct comparison of two metrics of platelet thrombogenicity, RT and shear history (SH), in the aneurysmal vasculature before and after endovascular treatment.

3.2 Methods and Materials

A subset of the patient cohort from the previous study is used here: 19 FDS for the first portion and 4 coiled patients for the latter. The basic computational setup remains consistent, while a

Lagrangian framework is introduced to evaluate the effect of treatment on platelet surrogates.

3.2.1 Lagrangian Platelet Model

To capture the trajectories of platelets, massless tracer particles are used as platelet surrogates. Each patient model is initially seeded with thousands of platelets throughout the domain. Platelets are also injected 10 times per cardiac cycle at the inlet boundary. Injections, where platelets are seeded at each point on the inlet, are spaced proportional to the flowrate integrated over time as opposed to with a constant time step between injections.

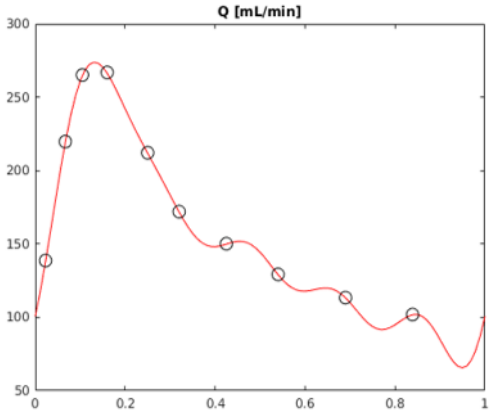

Figure 3.1: The inlet platelet injections, denoted by the black circles, are chosen based on the flowrate throughout the cardiac cycle which is 1s for this case.

An example of patient-specific flowrate and platelet injection times is displayed in Fig. 3.1. One platelet is released from each computational node during the inlet injection. Because of the distribution of nodes along the mesh, with prism layers along the vessel wall, a large proportion of platelets is injected closer to the outer edge of the vessel wall. This is consistent with the platelets' tendency to preferentially migrate away from the center of the vessel into the red blood cell-free layer near the vessel walls [119]. The number of platelets injected is scaled down from the actual concentration found in plasma by a factor of a thousand (typical platelet count is 150-400,000 per mm^3 [11]) due to the computational burden of tracking a physiological number of platelets. Thus, approximately 200 platelets are present in a 1 mm^3 volume of blood in the simulations. This density provides a sufficient number of platelets to obtain converged statistics past the typical first, second, third, and fourth moments of the probability distribution. The number of platelets is kept constant for each patient between the pre- and post-treatment analysis.

Position and shear stress data are stored for each platelet's trajectory within the reconstructed

vasculature. When a platelet enters or exits through the aneurysm neck, the simulation time and accumulated SH are recorded. Each platelet's RT (Eq. 3.1) is determined from the time it enters the aneurysmal sac crossing the neck from the parent vessel, to the time it exits the sac, crossing the aneurysmal neck in the opposite direction (towards the parent vessel). The SH is calculated as the integral of τ, the second invariant of the instantaneous shear stress tensor, accumulated throughout this same RT as shown in Eq. 3.2.

$$RT = T_i^{exit} - T_i^{enter} \tag{3.1}$$

$$SH = \int_{T_i^{enter}}^{T_i^{exit}} \tau(x, y, z)_i \, \mathrm{d}t \tag{3.2}$$

These two variables are introduced as the search for one or multiple metric(s) to predict endovascular treatment outcome continues. To begin quantifying the treatment effect, change scores (Eq. 2.5) are applied to the new metrics.

3.2.2 Treatment modeling

For the porous media simulations, the porous jump for the FDS simulations are enforced in the same manner as from Chapter 2. The coil study employs both the porous volume from Chapter 2 as well as simulations that do not use a model but rather directly include the mesh into the simulation geometry.

3.2.3 Coil Resolved Simulations

Silicon phantoms of patient-specific geometries [26], created from the segmented pre-treatment 3DRA, undergo the exact treatment in the angiography suit at the University of Washington Medical Center by one of two experienced neurointerventionalists who originally treated the patient. These models are then scanned at the European Radiation Facility (`http://www.esrf.eu/`) in Grenoble, France [59]. The resulting high-resolution microCT images are reconstructed with ImageJ (`https://imagej.nih.gov/ij/`) to produce a treatment surface. The treatment is registered in the computational domain of the aneurysm before meshing. Cells size near treatment is appropriately

small to capture the flow's reaction. Coil embolization devices used in this study have a large range of diameters, 0.24-0.36mm, and were resolved with cells as small as 20μm.

3.3 Initial Lagrangian Analysis of Flow-Diverting Stent

3.3.1 FDS Results

The reduction on the flow seen in Chapter 2 can be demonstrated from a Lagrangian framework by the increase in RT between the pre- and post-treatment cases. Figure 3.2 shows a subset of the platelets that have passed through the stent surface, color-coded based on time spent within the aneurysm. This figure visualizes another treatment effect: the FDS causes fewer particles to enter into the aneurysal sac.

Figure 3.3b, a histogram of all platelets that cross the neck, reveals the evolution of platelet RT. The post-treatment case displays a significant reduction in the percentage of platelets entering the aneurysm for short times (low RT values). The long tail of the treated case represents a significant increase in platelets recirculating inside the aneurysmal sac for an extended RT. As the box plot in Fig. 3.3a shows, this shift also occurs for the median RT.

The median RT, however, is not a good correlate of stable thrombus formation as it is triggered by long residence times. The outliers, however, are of the most interest as they represent the extreme cases of platelet quasi-stagnation. The prolongation of RT due to the FDS can be more clearly seen in Fig. 3.3c where only particles with RT $\geq$ 1s are considered. This threshold is chosen in part due to Hathcock's work showing thrombus formation initiating as early as 1 second [41]. Although calculating the tendency of platelets to clot inside the aneurysmal sac based on the platelets with RT $\geq$ 1s is ineffective, as multiple patients in our cohort demonstrate a median RT $>$ 1s in the aneurysm, even before treatment. The coagulation time is strongly dependent on patient blood and flow characteristics [79] but also depends on the individual platelet dynamics. Since blood does not spontaneously clot inside the aneurysmal sac before treatment, even for high RT platelet recirculation, the change score of the particles's RT in the aneurysmal sac can be employed, rather than an absolute cutoff of RT, which better characterizes the effects of the FDS placement on hemodynamics.

However, larger aneurysms provide platelets with a vast flow domain which allows for greater

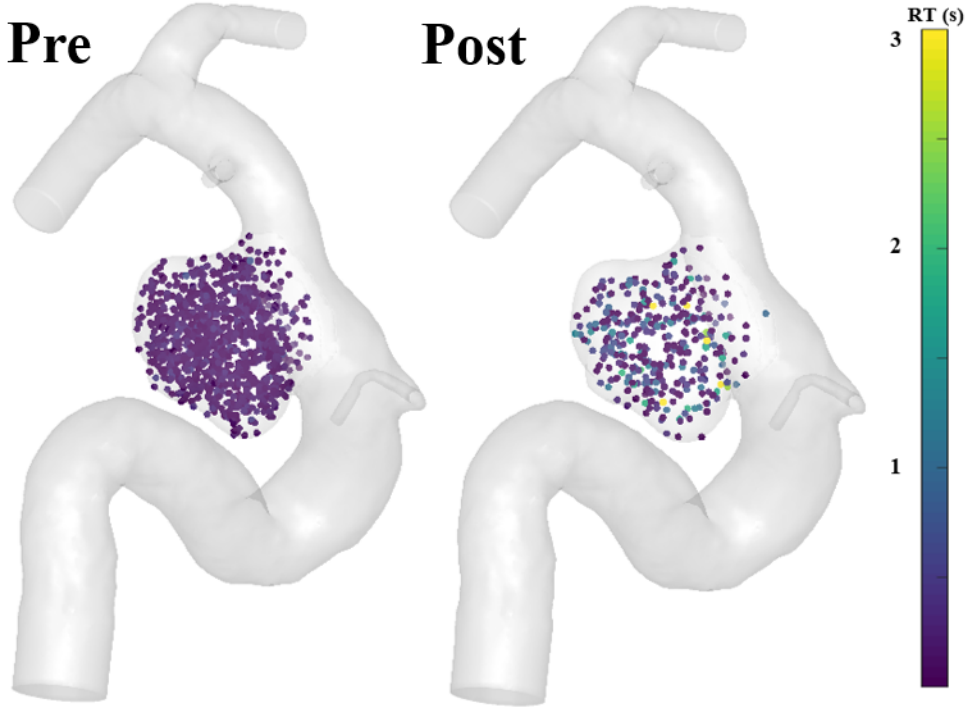

Figure 3.2: The FDS in the post-treatment case acts to slow the flow, increasing most platelets' residence time (RT).

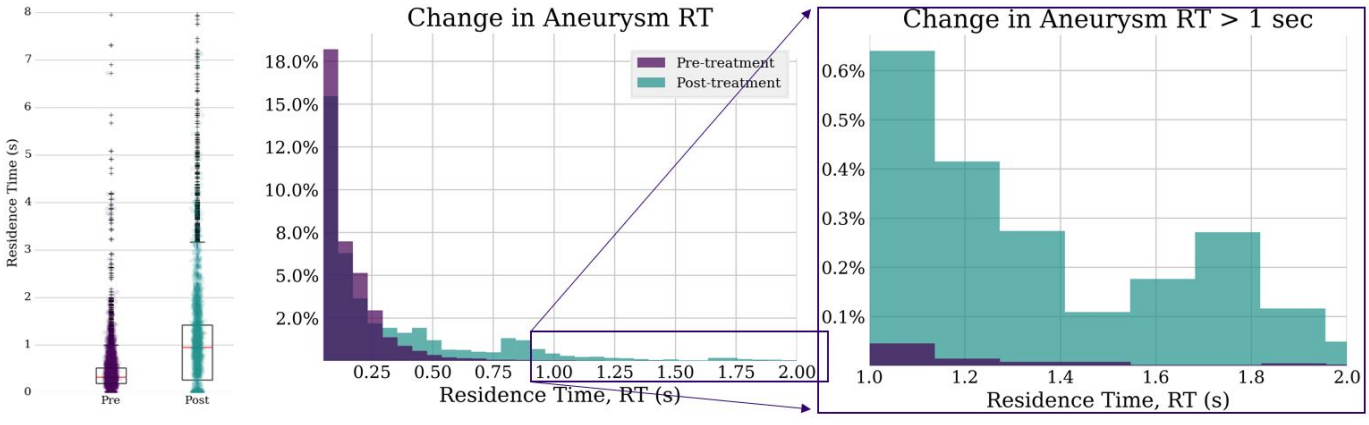

Figure 3.3: (a) Boxplot showing distribution of RT for all particles. (b) Histogram of RT. (c) Histogram emphasizing particles with RT > 1s.

recirculation zones. For example, in a large-volume aneurysm, unlike for the majority of aneurysms studied, the median RT and the percentage of platelets with RT greater than 1s decreases after the treatment; similarly, the aneurysmal flowrate does decrease once the stent is deployed. The large recirculation zone, allowing for high pre-treatment RTs, may still exist post-treatment. This is because the aneurysmal inflow has been partially redirected by the endovascular treatment, lessening the number of platelets entering, and could actually lead to a shorter RT of a majority of platelets that are only briefly enter the aneurysm dome after treatment. This disturbance to the flow simultaneously redirects and weakens the jet formed at the proximal stent region. Still, the FDS does increase the number of platelets that remain in the aneurysm dome for long RTs, as well as the maximum platelet RT found. Therefore, a comparison based on the increased probability of platelets after treatment having a RT larger than the 99^{th} percentile RT in the untreated case is performed. The same approach is followed for the probability of platelets after treatment experiencing a "high" SH, above the 99% value for the same patient in the untreated case. This is still quite low compared to the high shear that activates platelets in other medical devices [3]. The idea behind looking at high shear histories is that this may relate to steeper gradients which is the key factor cited by some researchers [91]. Using these "outlier" thresholds, the problem of aneurysms with large recirculation zones caused by complex flow or jet impingement are overcome and the impact of FDS placement on platelet activation can be readily quantified.

Stable intra-aneurysmal thrombus formation starts from activated platelets in areas of slow flow. Platelets in regions of lower blood velocity will accumulate lower shear stress exposure even as the RT increases. Therefore, a useful variable to compare the effect of treatment is the ratio of SH and RT. Activated platelets that linger in close proximity to other platelets can initiate activation and aggregation of the others triggering the coagulation cascade [64, 69]. Hence, the key to stable thrombus formation is again not what the majority of the platelets are experiencing, but the dynamic experience of the outliers within the aneurysmal dome. Therefore, to pinpoint one characteristic value of the SH to RT ratio, the 99^{th} percentile value in the pre-treatment case for each patient is used as a threshold. These values are used to calculate the increased probability of platelets experiencing a low SH:RT ratio (Eq.3.3), where the higher RT values after treatment decrease the metric. Inherently, $SH : RT_{pre}$ is always $\approx$1. The percentage of particles experiencing a higher RT, or SH, than that set by a certain percentile will be, by definition, the remainder of

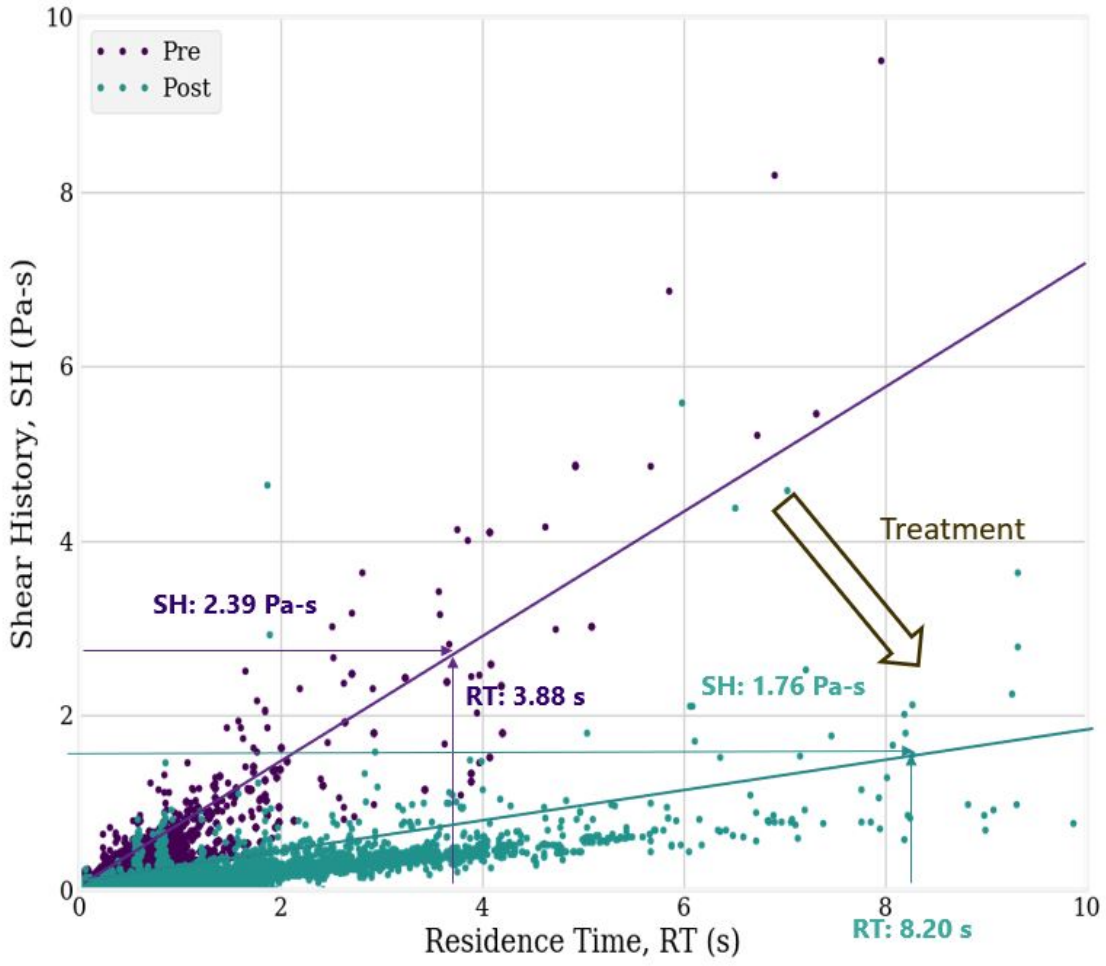

Figure 3.4: Platelet RT as a function of SH. The 99.9^{th} percentile of these two metrics designates the boundary of extreme platelet exposure. The decreasing slope represents the increased intensity of this exposure: prolonged time spent in the aneurysm combined with lower accumulation of shear stress.

the set.

$$SH : RT_{case} = \frac{\%(SH_{case} \geq SH_{Pre}^{\%tile})}{\%(RT_{case} \geq RT_{Pre}^{\%tile})} \tag{3.3}$$

To illustrate this treatment effect in another way, a more restrictive percentile (99.9th as opposed to the 99th) is chosen as the cutoff for thresholding RT and SH. All particles are graphed for this representative patient are shown in Fig. 3.4. The reduction of this biomechanical platelet exposure ratio can be seen by the lowered accumulation of shear stress even at high RTs after FDS deployment.

3.3.2 FDS Discussion

Assessing the degree of change in the hemodynamics experienced by the platelets within an intracranial aneurysm when it is treated with a FDS captures a range of mechanisms by which the flow diverting stent alters blood flow patterns in the parent vessel, in the aneurysmal sac, and at the aneurysmal neck. These are not fully characterized in fluid mechanics studies that rely on Eulerian metrics. Biochemical reactions are not simulated here, since the focus is on the analysis of the platelet dynamics to initiate thrombus formation rather than on the process of formation and growth; however, the ability to compute actual platelet RT statistical distributions is a first step to understand the role of hemodynamics on the complex kinetics of the clotting cascade and how platelets modulate the cascade in the presence of complex hemodynamics. Additionally, the ability to quantify the exposure of platelets to mechanical stresses, SH, before and after FDS treatment, allows for the quantification of FDS treatment on platelet exposure to stimuli that contribute to activation. Chapter 2 is based on 5 Eulerian variables: WSS on the dome, flow velocity and dissipation in the dome, flow rate and shear stress at the neck; most of which focus on the aneurysmal boundaries which fail to characterize the spatial variations in the aneurysmal sac. Eulerian analysis can only provide approximations of the "relative" residence time (RRT) based on the WSS on the endothelium in the area of interest [4, 57]. Figure 3.5 demonstrates the typical change scores of certain metrics. RRT involves compounding changes since it is an inverse function of time-averaged WSS and the oscillatory shear index (both defined on the aneurysm dome wall). When endovascular treatment is resolved in the simulation, the patient can exhibit a change in RRT on the scale of

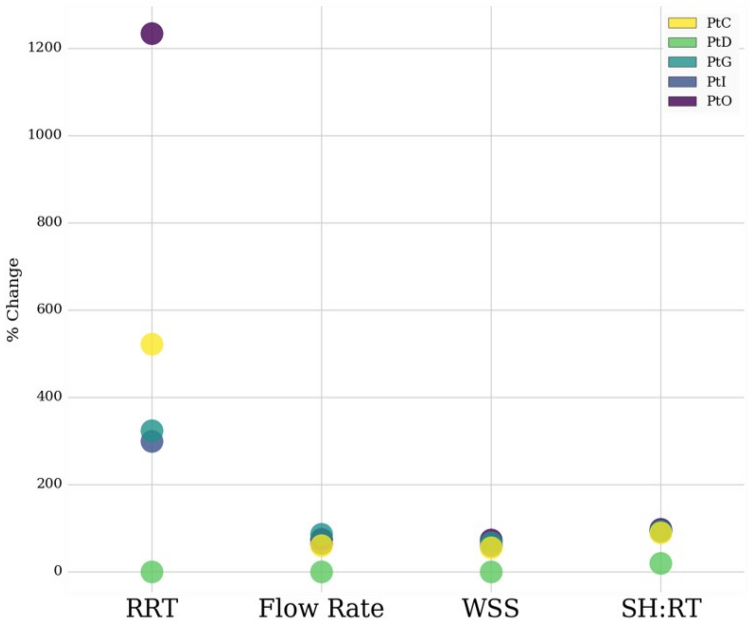

Figure 3.5: Change scores for Eulerian and Lagrangian variables. The relative residence time has the largest spread in the changes experienced between patients.

5 orders of magnitude simply because the WSS is reduced dramatically—increasing the RRT even more drastically. Flow rate into the aneurysm, time-average WSS of the dome, and the SH/RT ratio all appear within a more condensed, reasonable range.

The novel Lagrangian methodology applied to the study of the hemodynamics of FDS treatment of intracranial aneurysms focuses on the initial mechanism of healing of endovascular treatment: to induce the formation of a stable thrombus. Formation is directly related to the activation and agglomeration of platelets inside the aneurysmal sac. The analysis of the biomechanical stimuli and non-physiological flow patterns experienced by platelets before and after aneurysm treatment has the potential to enable the accurate prediction of treatment outcome. This methodology will enhance the understanding gained from Eulerian studies by complementing wall metrics, such as WSS, and opening this field to statistical analysis of the large number of blood-borne platelets in the flow inside aneurysms. Thrombogenesis is not a process initiated by mean or median behavior but rather one in which outliers and extreme cases trigger the clotting cascade in a highly non-

linear manner [69, 107], even when the bulk blood flow presents no changes or even counterintuitive behavior such as the observed decrease of the median RT of platelets in some treated aneurysms.

Lagrangian-tracking studies of thrombogenic potential of intra-ventricular flows of medical devices have focused predominantly on the exposure of platelets to unphysiologically high levels of shear stress, as well as long RTs. The values of shear stress and SH associated with hemolysis or platelet activation in cardiac devices (LVAD, artificial cardiac valves, extracorporeal membrane oxygenation, Impella, etc.) are not found anywhere in the aneurysmal or perianeurysmal circulation, before or after FDS treatment, again, this is why shear history is used to track the changing shear environment. However, studies have found a direct relationship between increasing RT and platelet activation, demonstrating that prolonged RT can lead to platelet activation regardless of accompanying shear stress magnitude [48, 131]. The successful outcome of a FDS requires both platelet activation and a region where platelets can linger for extended periods of time, signaling other platelets to aggregate and begin thrombus formation [69]. Furthermore, the lower shears seen here have been shown to activate platelets which has been the basis for modeling thrombosis of cerebral aneurysms [82]. The combination of increased RT and reduced SH of the platelets is, in this context, indicative of effective FDS treatment, since those are the conditions that will potentially lead to stable thrombus formation and subsequent aneurysm embolization. An activated platelet in hemodynamic stasis has the best chance of recruiting other platelets and adhering to the aneurysmal wall, which is the precursor of a successful treatment. Hence, the pre-/post-treatment ratio of SH and RT based on extrema of each variable is considered as the most promising metric for establishing a threshold to predict the effectiveness of FDS treatment.

3.4 Comparison of Lagrangian Analysis: Porous Media vs Coil-Resolved

3.4.1 Coil Introduction

The FDS-treatment is modeled as a pressure jump across a surface, meaning the platelet surrogate has limited interaction with this momentum sink. Lagrangian particles in a coil-treated simulation, which employs the porous media approximation, experience this modeled resistance their entire trajectory as opposed to when crossing the treatment boundary. This motivated a direct comparison between the gold-standard isotropic and homogenous porous media (PM) approach and the ground

truth of the coil geometry obtained via Synchrotron μCT.

3.4.2 Coil Results

The heterogeneity of a true coil mass is one of the pitfalls of a volume defined by a single isotropic and homogeneous PM. The approximation does capture the sharp redirection of flow caused by a coil mass, as seen in the bulk flow. However, past that the model fails to captures the pockets of blood within the coil and near the aneurysmal dome as seen in Fig. 3.6. The dynamic path of blood entering a coil mass may include wall and coil impingement, slow flow in tightly packed regions, and free flow in pouches found throughout.

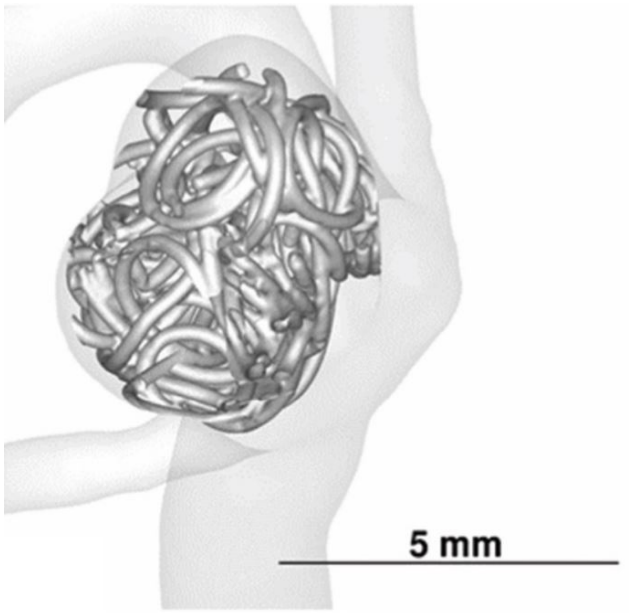

Figure 3.6: High-resolution Synchrotron X-ray microtomography of coils deployed in flow phantoms are segmented and meshed with the patient's vasculature [8].

The higher untreated aneurysmal inflow is matched by the very low RT the particles exhibit when being quickly swept out by the inflow. The smoothness of the PM is apparent by comparing the initial inflow to the greatly reduced, yet stable and coherent, inflow of the PM-treated simulation. The intra-aneurysmal flow, much less chaotic now filled with the PM, exhibits a good environment for platelet activation. In reality, the jet impingement on the coils of the resolved simulation indicates disturbed flow begins immediately upon entering the treatment volume, unlike the artificially smooth transition provided by the PM. The PM model slows and diverts the flow in such an exaggerated manner that it over-estimates the decrease in aneurysm flowrate for three of the four cases, with only one showing the same reduction for peak and time-average.

Eulerian metrics' inability to capture the experience of platelets is most pronounced in coil-

Table 3.1: The Eulerian and Lagrangian hemodynamic changes from pre- to post-treatment (all values are percentages) of coil patient 1.

	Porous Media	Coil-Resolved
RRT (s)	755.7	$55.5 \cdot 10^6$
Median RT	-75.0	-25.0
RT >3 s	224.0	3383.1

resolved cases. Relative residence time (RRT) shows an increase of 755% for PM and $55 \cdot 10^6$% for coil-resolved simulation of one patient in Table 3.1. The absurd increase is not representative of the actual change and furthermore does nothing to characterize the flow away from the aneurysm walls. This study echos the FDS study in that a decrease in median RT may be observed. Slower post-treatment flow, that is in some cases also less chaotic, may quickly carry particles outside the aneurysm which is now fully occupied.

Direct comparison of the two treatment models using Lagrangian metrics shows varying results. RT outliers and SH outliers are identified in this study as the percentage of particles exceeding the threshold of 3s and 3Pa-s respectively. The Median RT and SH along with other Eulerian metrics are described by Chivukula and Marsh et al.[27].

The PM performance in predicting the outliers of RT and SH are shown in Table 3.2 for all four patients. The PM over-estimated the reduction of RT outliers for three out of the four cases, which is expected since the PM tended to over-predict the reduction of flowrate. PM matched the SH outliers and Median SH change scores for the coil-resolved case of one patient. In another patient, PM over-predicted each metric. The PM model, however, failed to predict the magnitude or sign (increase/decrease) of these change scores for two patients.

Table 3.2: The Lagrangian outlier variables compared for all four patients. All metrics are percent changes between the pre- and post-treatment, either porous media (PM) or coil-resolved (CR).

	Pt1		Pt2		Pt3		Pt4	
	PM	CR	PM	CR	PM	CR	PM	CR
RT >3 s	224.0	3383.1	526.8	171.6	937.0	21.7	2014.6	112.3
SH >3 $Pa \cdot s$	−39.7	−8.1	−34.7	65.7	−59.5	−52.7	6138.1	−7.1

3.4.3 Coil Discussion

This study has demonstrated that the PM grossly overestimates the dampening affects of the coil embolization device when compared to the high-resolution coil-resolved simulations used as the ground truth. Because of the artificial resistance provided by the PM, Eulerian metrics such as flowrate into the aneurysm and relative residence time are predicted to be much higher than when predicted by CR. The Lagrangian metric of RT was similarly over-predicted by the PM; however, the homogeneous, isotropic PM was not even able to capture the direction of change (increase vs decrease) for the SH of two out of four patients.

3.5 Conclusion

A Lagrangian approach to studying the hemodynamics of intracranial aneurysms before and after treatment provides not only neck flow rate and shear on the vessel and aneurysmal walls, but also the trajectory of platelets. This enables direct calculation of biomechanical stimuli that can induce platelet activation. Two main variables, RT and SH, aid investigation into the probability that platelets will initiate thrombosis in the sac. Examining a new metric defined by the outliers of platelet RT and SH provides a simple, but powerful approximation of how much FDS treatment affects platelet trajectories within the aneurysm, impacting the likelihood of adequate thrombus formation for different patients' anatomies (aneurysmal location, volume, and shape) and physiology (flow rate and cardiac frequency).

The shear that platelets accumulate in a coiled aneurysm can vary greatly due to the complexity

of the flow. Less dense areas of the coil mass can induce acceleration and deceleration which exposes platelets to larger gradients of shear. The particles in a PM will experience a homogeneous resistance and can smoothly enter the momentum sink with no true obstruction or abrupt redirection. Therefore, the isotropic PM model cannot reproduce this flow caused by a gradient of porosities of the coil mass nor accurately predict the true level of shear history which particles experience on their intra-aneurysmal trajectories.

Chapter 4

DISTINGUISHING HEMODYNAMIC EFFECTS BETWEEN FUSIFORM AND SACCULAR ANEURYSMS TREATED WITH STENTS

In this chapter, saccular aneurysms, which are much more common in the intracranial vasculature, are compared to fusiform aneurysms which are characterized by circumferential dilation of the entire parent vessel. The aim is to determine if the anatomical differences are critical in determining the hemodynamics at the aneurysmal neck and inside the sac and, thus, if the two morphologies should be separated for study of the flow evolution, as was shown to be necessary with the two dominant endovascular treatment types (stents vs coils).

4.1 Background and Motivation

Many IAs can be classified as saccular IAs (SIA) based on the balloon-like shape of the aneurysmal dome, with an identifiable neck separating the aneurysm from the host parent vessel. A non-saccular aneurysm, where the aneurysm affects the entire perimeter of the vessel wall, is referred to as a fusiform IA (FIA).

A fusiform aneurysm is defined by a circumferential dilation of the vessel's lumen [2]. While the fusiform definition is clear, the decision to classify as a fusiform is up to the clinician. The chosen FIA and SIA cases 1-3 are shown in Figure 4.1. Two neurointerventionalists were asked to define Case 1. One noted that from a radiological standpoint, a neck could be delineated with enough certainty to classify the aneurysm as saccular. However, the other noted that the entire segment was enlarged such that a clear aneurysm neck could not be defined therefore classifying it as a fusiform. For this study, mild dilation of the vessel across a portion of the circumference was considered sufficient to classify FIA 1 as fusiform, meaning all 360° of the lumen are considered to be affected for some portion of the vessel wall, see FIA Case 1 in Fig. 4.1.

According to some studies, FIAs are so infrequent that they occur in one out of every 33 IAs [2, 85]. Due to this low incidence rate, FIAs have not been the subject of many studies to date. Hemodynamics, treatment method, and the associated effect of treatment type on hemodynamic

parameters within FIAs, all need further investigation.

The endovascular therapy at the focus of this study is the flow-diverting stent, which have been thoroughly proven to reduce the rupture risk of SIAs by redirecting blood flow from entering the aneurysm and, thus, inducing reendothelialization and blood stasis leading to a stable thrombus [88]. As previously stated, the goal is to bring the intra-aneurysmal flow to stasis allowing a formation of a thrombus that can fill the aneurysm and restore the wall shear stress along the scaffolding to that of the original parent vessel prior to the pathological growth [54]. While the goal of FIA treatment is the same with flow-diverting stents (FDS) which shows promising outcomes [34] and studies showing that virtual treatments produce the desired flow-diverting effects exist [98], there are no comparative studies of FIAs and SIAs confirming that the hemodynamic effects of treatment are the same.

Computational fluid dynamics (CFD) and virtual treatment approaches provide a great opportunity to simulate blood flow and treatment effects without experimenting on individual patients in the early stages of understanding, through first-in-man or clinical trials [133]. Investigation of FIAs can be carried out without requiring any extra procedure or inconvenience to the patient. These simulations can be evaluated, and the resulting parameters analyzed to get information about the hemodynamics. Additionally, computational analysis enables for the comparison of pathological cases to their healthy counterparts, a healthy state virtually created by removing the aneurysm from the parent vessel for both the FIAs and SIAs.

Therefore, this study focuses on analyzing the hemodynamics of three different pairs of patient-specific FIAs and SIAs, paired by similarity in morphology and blood flow rate, to enhance the current understanding of the hemodynamics in FIAs and to identify differences between FIAs and SIAs in their untreated and treated states. An important part of this analysis is the effect of treatment on the hemodynamics within the different IAs. Treatment effect is analyzed by virtually deploying a single FDS in each of the six cases, with one pair of aneurysms treated with two FDS. Hemodynamics are then compared between the treated and untreated cases, and between the untreated pathological and the healthy condition.

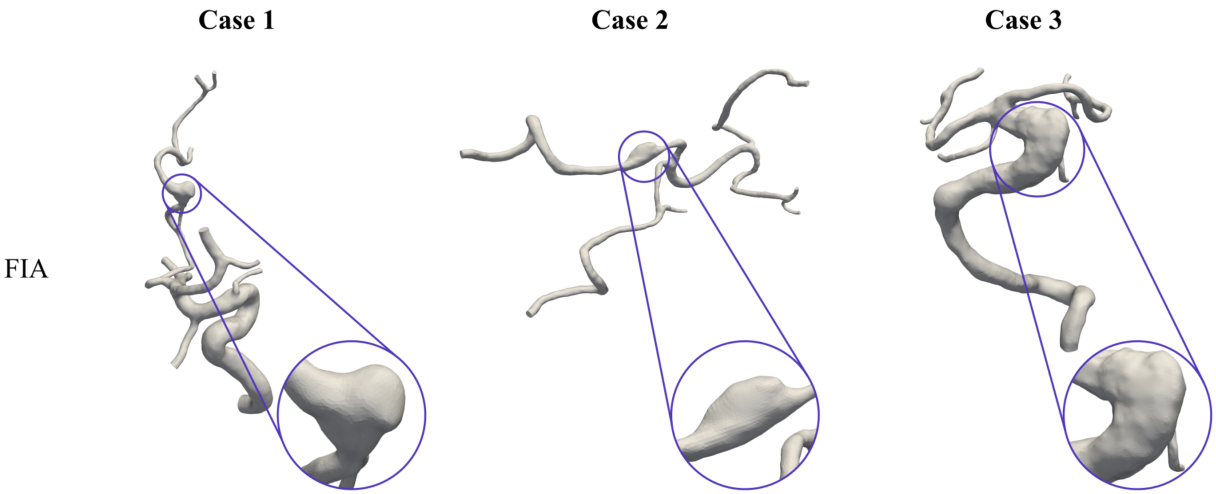

l

Figure 4.1: Visualization of the flow in every aneurysm in the cohort. First row: FIAs; Second row: SIAs. A detailed view of each IA is provided, to give an overview of the different shapes.

4.2 Methods and Materials

4.2.1 Patient Cohort and Aneurysm Imaging

Six patients in total were enrolled in this study, three cases each of FIA and SIA, all occurring in the Circle of Willis. Because FIAs are so rare, we were only able to obtain three with appropriate imaging from a database of at least 300. Even with this database, not all cases are captured with the same imaging technique. Case 1 aneurysms are located at the middle cerebral artery (MCA) and are captured with three-dimensional digital subtraction angiography (3D DSA). Case 2 aneurysms are located at the left vertebral artery (VA). Case 3 aneurysms are located on the basilar artery (BA).

While the three pairs of cases, shown in Figure 4.1, comprise different shapes and sizes, the corresponding SIA was chosen from a large repository of cases, to match the (rare) FIA as closely as possible. From the available database of 300 SIAs, the choice was made based on location within the brain (MCA, VA, BA), location on the vessel, diameter of the vessel and flow rate, and size

(aspect ratio, AR, and volume) in that order. It was impossible, however, to match exactly the fusiform cases with saccular aneurysms from this large database.

4.2.2 Creation of the Healthy Counterpart and Treated Case

To allow for an overall population comparison, as well as a comparison within each case, the hemodynamics in each IA are compared to the hemodynamics of the same patient within (1) the treated vasculature, and (2) the healthy vasculature (aneurysm virtually removed from the parent vessel). A change score, which is defined by the percent change calculated from the untreated aneurysm to the modified versions, can be used for every case and allow for a direct comparison between the response of SIAs and FIAs.

4.2.3 Vessel Reconstruction and Aneurysm Definition

To restore the parent vessel to its original anatomy, prior to aneurysm development, a healthy version of each case is created. For this ideal parent vessel case, the aneurysm sac is manually removed from the side of the parent artery, and the arterial wall is smoothed to match the surrounding parent vessel surface. This is performed in Blender by an engineer and approved by a neurointerventionalist [v2.82, Blender Foundation, Netherlands].

To perform an accurate analysis of hemodynamic parameters, the volume of the aneurysm sac and the accompanying area of the dome are defined. The reconstruction of the healthy arterial wall defines the edge of the aneurysm sac. First, the parent artery wall is expanded in all directions until it is fully intersecting the aneurysmal sac, creating an enclosed volume and clearly separating it from the parent vessel. The healthy vessel is then defined as the lumen volume that is separate from the pathological volume. Finally, if any bifurcating arteries are coming from the aneurysm, they are virtually removed and smoothed. The remaining domain, after subtracting the parent vessel defines the aneurysm sac: its volume and the neck surface that encloses the aneurysmal volume and, at the same time, overlaps with the parent vessel boundary.

4.2.4 Virtual Stenting

A fast virtual stenting approach is applied allowing different stent configurations to be simulated with short computational times. This practice allows for precise placement and position within the vessel that will affect the flow in a realistic manner. See the blue stents in Fig. 4.2 and refer to [14, 45] for more details.

Four of the six aneurysms were treated by a single neurointerventionalist. For the remaining aneurysms, the same interventionist determined the appropriate stent sizing for each case, and a researcher carried out the virtual stenting using the same process. One technique used to treat IAs endovascularly is dual stenting. To further investigate the effects on FIAs, a secondary stent was deployed in SIA/FIA 2 providing a comparison of a SIA and a FIA under different treatment conditions. The diameters of the parent vessels for SIA/FIA 2 (4.5mm/3.0mm) are typical of the internal carotid artery and middle cerebral artery, where a majority of IAs occur [53]. Case 2 was chosen for dual stenting because of these representative diameters.

4.2.5 Hemodynamic Simulation

Each case, FIA/SIA 1-3, is analyzed for the pathological (P), treated (T), and healthy (H) conditions. Overall, 18 single-stent and 2 dual-stent hemodynamic simulations are carried out within this study to analyze the intra-aneurysmal flow within FIA/SIA. For the simulations, as well as for the meshing, the fluent solver StarCCM+ (v2021.1, Siemens, Germany) is used. Walls are assumed to be rigid and blood to be Newtonian with a density of 1055 kg/m^3 and a viscosity of 0.004 $Pa \cdot s$. Boundary conditions are set at the inlets with a mass flow waveform based on the time-resolved velocity measurements captured from a healthy patient and multiplied by the patient-specific inlet cross sectional area. A flow split ratio creates the bifurcation outlet pressures, calculated with an in-house flow split method [99].

4.2.6 Analysis

Stent and morphological analysis

Stent and vessel analysis are performed using VMTK (v1.3, vmtk.org) to obtain centerlines and radii, StarCCM+ and Matlab (R2022a, MathWorks Inc) to create envelopes of the stent and vessel

volumes, and finally Matlab to process the data. The position and radius of the stent, aneurysm with parent vessel, and healthy vessel are considered. Because stent lengthening or foreshortening can be drastically dependent on vessel morphology, the stent expansion across the aneurysm is considered only. This is normalized by the nominal diameter of the stent.

Hemodynamic analysis

Blood flow within each IA is analyzed using several hemodynamic parameters for all cases (FIA SIA 1-3) under all conditions: pathological (P), treated (T), and healthy (H). We compare raw values, as well as the treatment effect (TE) which is defined as the percent change for a given metric.

$$TE = \frac{x_{post} - x_{pre}}{x_{pre}} * 100 \tag{4.1}$$

Parameter values are qualitatively and quantitatively evaluated in EnSight (2019 R3, ANSYS Inc.) and in Matlab. These metrics are separated into aneurysm dome wall parameters and volumetric hemodynamics parameters.

Concerning the wall parameters, time-averaged wall shear stress (WSS) and oscillatory shear index (OSI) are considered. These are commonly studied in IA rupture analysis[23, 126].

The WSS is the wall shear stress averaged over one cardiac cycle.

$$WSS = \int_0^T WSS\, dt \tag{4.2}$$

OSI, the fluctuation of wall shear stress over the cardiac cycle, is determined by the change in orientation of the wall shear stress vectors and their magnitudes. OSI ranges from 0 - 0.5 where an increasing value of OSI indicates a high velocity of fluctuation.

$$OSI = \frac{1}{2}(1 - \frac{\left|\int_0^T WSS\, dt\right|}{\int_0^T |WSS|\ dt}) \tag{4.3}$$

The volumetric hemodynamic parameters of interest are time-averaged velocity, time-averaged vorticity, and oscillatory velocity index (OVI); these have been defined in the literature for the analysis of intra-aneurysmal blood flow [23, 127, 114].

All hemodynamic parameters are calculated only within the aneurysm sac for FIA and SIA. The related sac definition is described in section 4.2.3. Velocity and vorticity are averaged over one cardiac cycle. OVI indicates the fluctuation of the velocity vector (V) over one cardiac cycle. Similar to OSI on the wall, the calculation of OVI within the dome is based on the change in orientation of the velocity vectors and their magnitudes.

$$OVI = \frac{1}{2}(1 - \frac{\left|\int_0^T V\, dt\right|}{\int_0^T |V|\, dt}) \tag{4.4}$$

The effect of the aneurysm formation on blood flow is analyzed using energy loss (EL). Based on the velocity, surface area, fluid density and static pressure, the energy (enthalpy) flux at the inlets and outlets is calculated for each case.

$$E = AV(\frac{1}{2}\rho V^2 + P) \tag{4.5}$$

with: V = velocity, A = surface area of inlet or outlet, ρ = fluid density, P = static pressure

EL is estimated as the difference between the proximal (inlets) and distal (outlets) fluxes in the parent vessel for each case. The resulting values of EL represents the difference in hemodynamics observed between pathological (P), treated (T), and healthy (H) cases.

$$EL = \sum E_{inlets} - \sum E_{outlets} \tag{4.6}$$

EL has been correlated with outcome of stent-treated endovascular therapies [29].

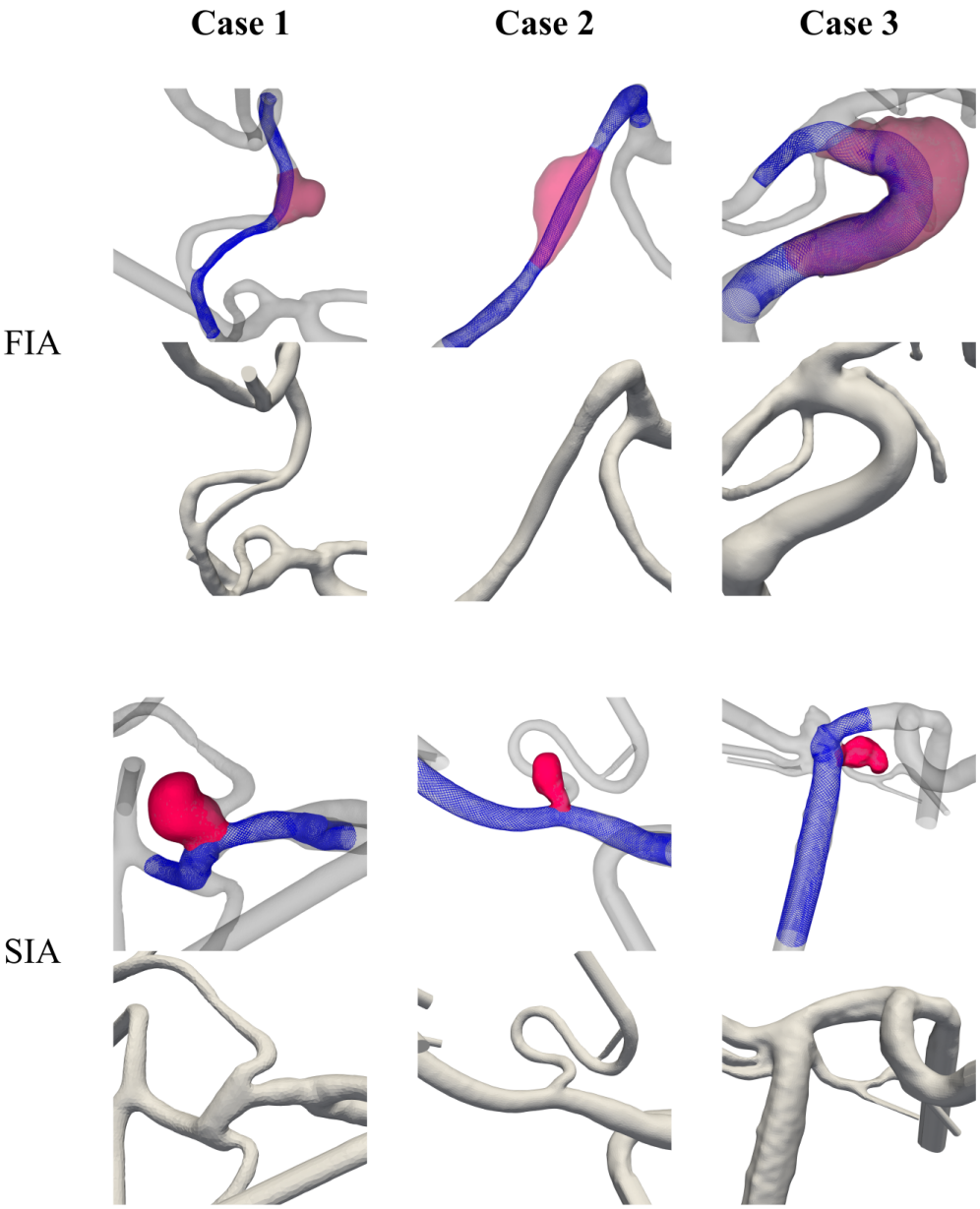

Figure 4.2: Aneurysm cohort depicting pathological aneurysm sac in red with stent treatment in blue on top rows. Lower rows show healthy vasculature. The fusiform aneurysms occupy the top two rows; saccular aneurysms are shown on the last two rows.

4.3 Fast Virtual Stenting (FVS) Software Validation

The treatment of the IAs is simulated by virtually deploying stents, using an in-house code developed by Dr.-Ing. László Daróczy, and meshed along with the vasculature [13, 14, **?**].

4.3.1 FVS Methods

A segmented surface of the parent vessel with the aneurysm is input into the fast virtual stenting (FVS) software that defines the basic topology (parent vessel and aneurysmal sac). This allows for an inlet and outlet to be defined so that, after voxelization of the domain, a centerline is created. This centerline is optimized using a cylindrical coordinate system along with the physical constraints of the vasculature and stent definition parameters (length, radius, tine radius, angle, and number of wires). The cross-section is not forced to retain its circular shape, but rather the struts are opposed onto the vessel wall independently (not all moving the same distance). (Fore)shortening is predicted using the average radius of the elliptical shape.

To test this software, 9 IA patients were enrolled to test the effects of deploying this FVS in various locations and types of aneurysms. Each patient had angiographic imaging, 3D DSA, taken after treatment with a Derivo 2 flow-diverter embolization device (DED, Acandis, Pforzheim, Germany). Five patients also had a flow phantom made of their vasculature that was subsequently treated and imaged. This provided a deployed in-vivo measurement of the stents. MeVisLab (v3.4.1, MeVis Medical Solutions AG, Bremen, Germany) allowed for segmentation of the patient geometries using pre-treatment 3D DSA and post-treatment to obtain the in-vivo stent. Pt A is shown in Fig. 4.3 with the stent deployed inside the patient's vasculature. Once segmented and enveloped, the in-vivo stent along with the FVS stent were analyzed using Matlab (R2020b, MathWorks Inc). The Acandis company also had a virtual stent deployment program, ANKYRAS, which is included in the study for comparison. Fig. 4.4 includes both the FVS deployment for Pt A and the ANKYRAS deployment of the Derivo2.

4.3.2 FVS Results

The 9 patients are designated a treatment which provides the given stent diameter and length; the actual deployed diameter and length can be determined from the in-vivo data; the FVS will also

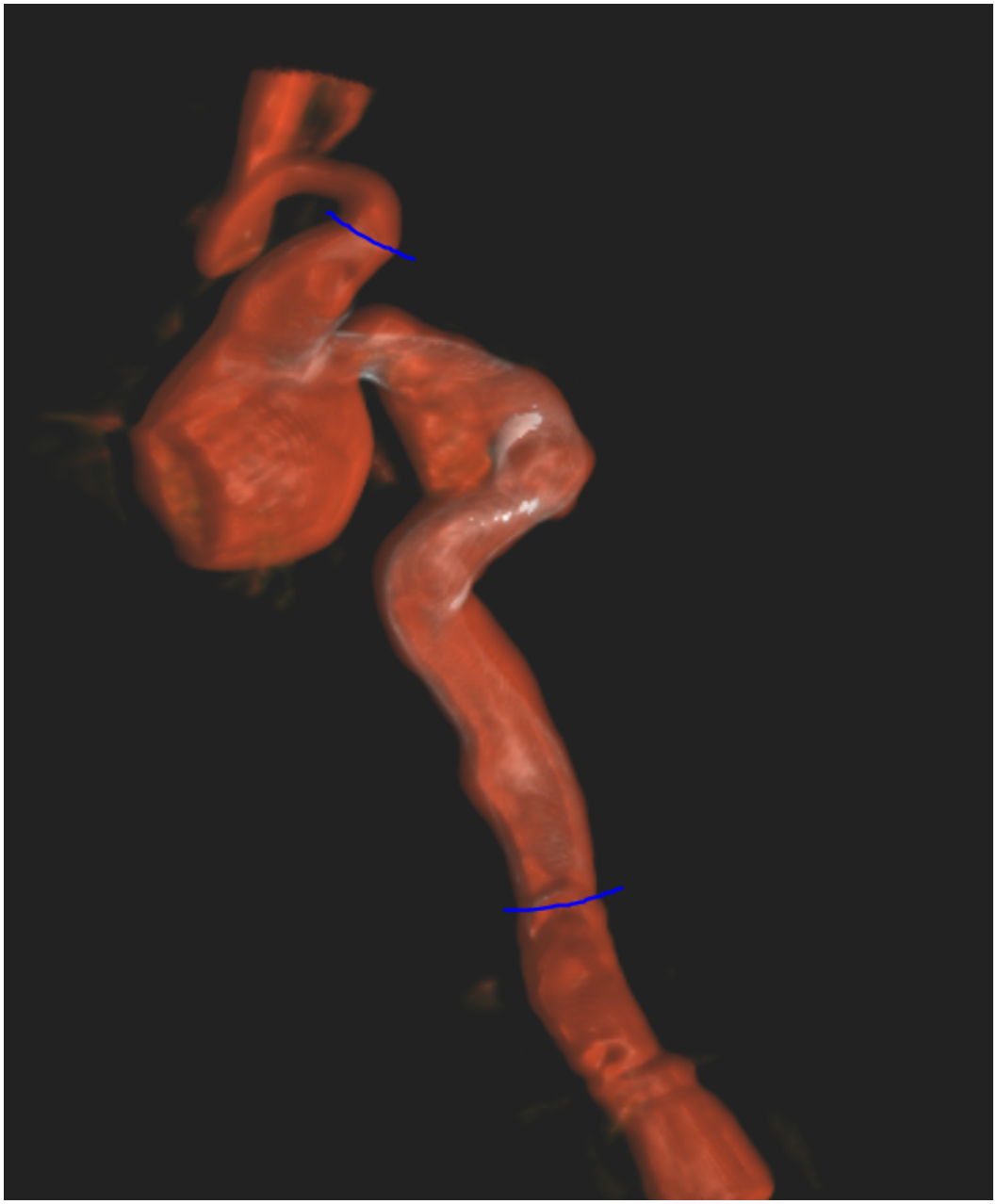

Figure 4.3: Pt A's medical imaging of the in-vivo stent that appears in silver with blue lines indicating the proximal and distal landing sites.

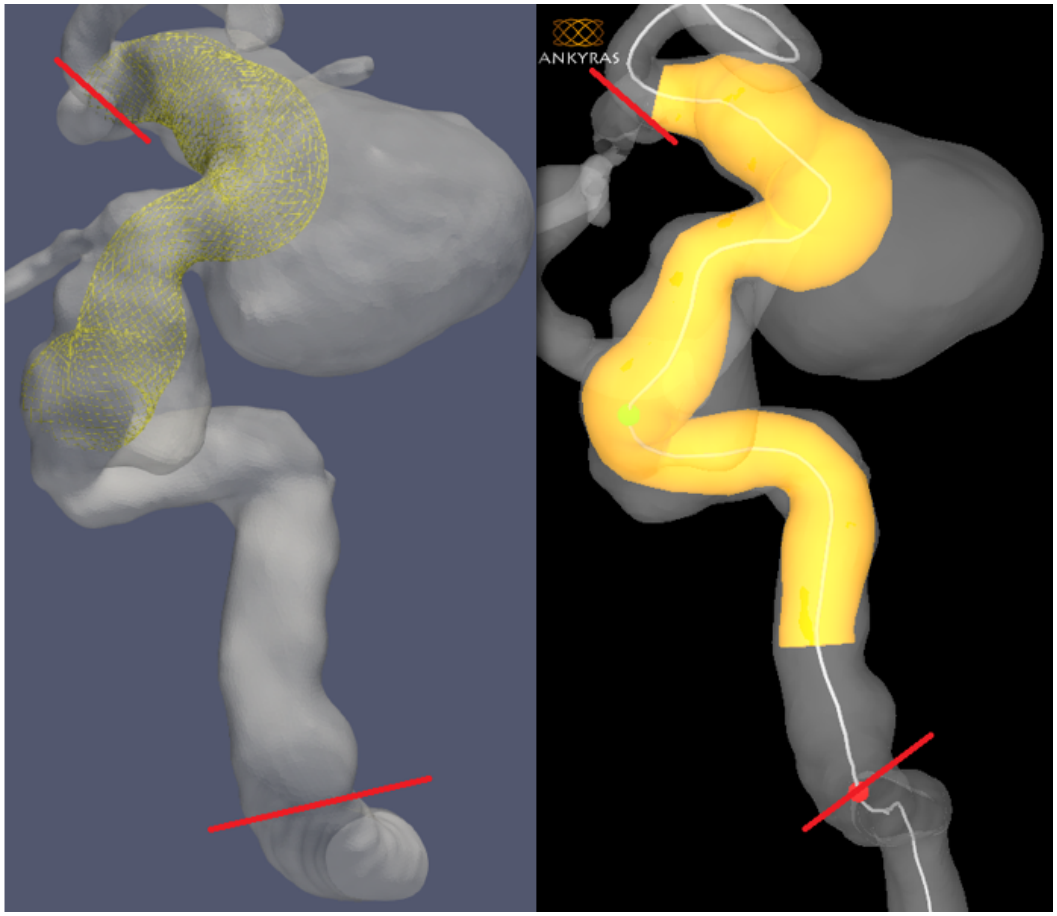

Figure 4.4: Pt A with a Derivo2 deployed using FVS (left) and ANKYRAS's software (right) with redlines demarcating the in-vivo stent landing sites.

give the diameter and length for the virtual deployment. From these lengths, an accuracy score was calculated for the FVS and Derivo deployments. These data appear in Table table:FVS. The FVS had good agreement, less than $|10\%|$ error between the computed and real stents, with only 3 cases having $\approx |20\%|$ error with the in-vivo deployment length. ANKYRAS's stent-specific software has high error $\approx -20\%$ in only one patient, and generally good agreement for the rest. The average accuracy score for the FVS is 11% while the average error for Derivo2 software is 8%.

Table 4.1: Summary of 9 patients receiving FDS treatment with in-vivo data. Predictions of stent length provided by in-house fast-virtual stenting (FVS) and manufacturer-provided FVS.

Pt	**Derivo2 Stent**	**Deployed length (mm)**	**FVS length (mm)**	**% change**	**Derivo-FVS length (mm)**	**% change**
A	5.5x30	58.6	44.59	-24%	47.08	-20%
B	5x25	38.9	38.75	0%	39.71	2%
C	5x25	34.66	37.43	8%	37.84	9%
D	5x20	37.42	38.09	2%	43.04	15%
E	5x15	30.56	33.33	9%	32.21	5%
F	4x20	29.33	29.97	2%	32.6	11%
G	4x15	22.5	20.75	-8%	23.7	5%
H	4x15	22.48	25.49	13%	24.51	9%
I	3.5x15	19.85	20.26	2%	19.66	-1%

4.3.3 FVS Discussion

The first case, Pt A, provides a challenging case to both the FVS and ANKYRAS software. This patient has a highly diseased vessel leading up to the aneurysm location, as shown in Figs. 4.3 and 4.4. One problem is that diseased vessels, such as with large dilations as seen in this patient, can lead to inaccurate segmentations. In conjunction with the question of imaging, the large oscillations in the diameter of the vessel, increasing and decreasing, was observed to cause inaccuracies in the FSV deployment. The large under-prediction of stent length in this case is probably caused by an inaccurate segmentation of the diseased vasculature, along with inaccurate compression of the stent as the vessel diameter constricts and expands. Finally, the in-vivo stent in Fig. 4.4 seems to be constricted for some reason just past the proximal landing site, not inflating to its full diameter, which increases the deployed length significantly. It is possible the segmented vessel geometry is misrepresented by inaccuracies in the reconstructions and this caused, in full or in part, the disparity between the virtual stent length and the in-vivo stent. The ANKYRAS software had similarly poor results. That software worked on the same segmentation available, and therefore the stent could

not be deployed from the correct location on the vessel, starting at the distal landing site.

Pt F had the largest stent expansion (just ahead of Pt A) with a change score of over 100% with the 15mm stent deploying to a length of roughly 30mm, and FVS predicted the largest elongation from the nominal length. This was due to a large stenosis distal to the aneurysm that is preceded by high curvature in the parent vessel. Again, a large deviation is seen for the FVS when pathologies other than the aneurysm are present. This stenosis may have been artificially enlarged by the segmentation causing some of the over-prediction. The ANKYRAS software predicted this case with better accuracy, perhaps due to a better STL or better understanding of how the specific stent responds; the Derivo2 is known to have less foreshortening than the original Derivo.

On the opposite side of the spectrum, when the imaging of the vasculature and any surrounding pathology is well captured by the segmentation, more accurate predictions of the stent deployment are obtained, as in Pt E. This patient, shown in Fig. 4.5 has high curvature in the ICA and a large stenosis proximal to the aneurysm; however, when the distal landing site is matched with the in-vivo stent, an error of only 2% was achieved in the simulated deployed length, compared to the in vivo. This is superior to ANKYRAS's prediction which used a different parent vessel segmentation, and resulted in 15% error.

4.3.4 FVS Conclusion

Correct deployment of stents is crucial for a successful endovascular treatment but can be difficult in irregular anatomies or difficult to reach locations. Unfortunately, this appears to be true for virtual deployment as well. While the goal is to have FVS software for treatment planning, and to support scientific studies to improve understanding of hemodynamics, like the one presented here, existing software is only sufficiently accurate for healthy vessels with standard curvature. Aneurysms on vessels exhibiting pathological diameter dilations or stenosis pose a problem for the deployment of virtual stents, causing over-/under-prediction of the deployed stent length, particularly when the vessel's lumen, inner-diameter, is misrepresented.

This validation study brings to the forefront yet another important reason to validate and standardize segmentation procedures. Without this, even the more evolved virtual stenting won't provide accurate results.

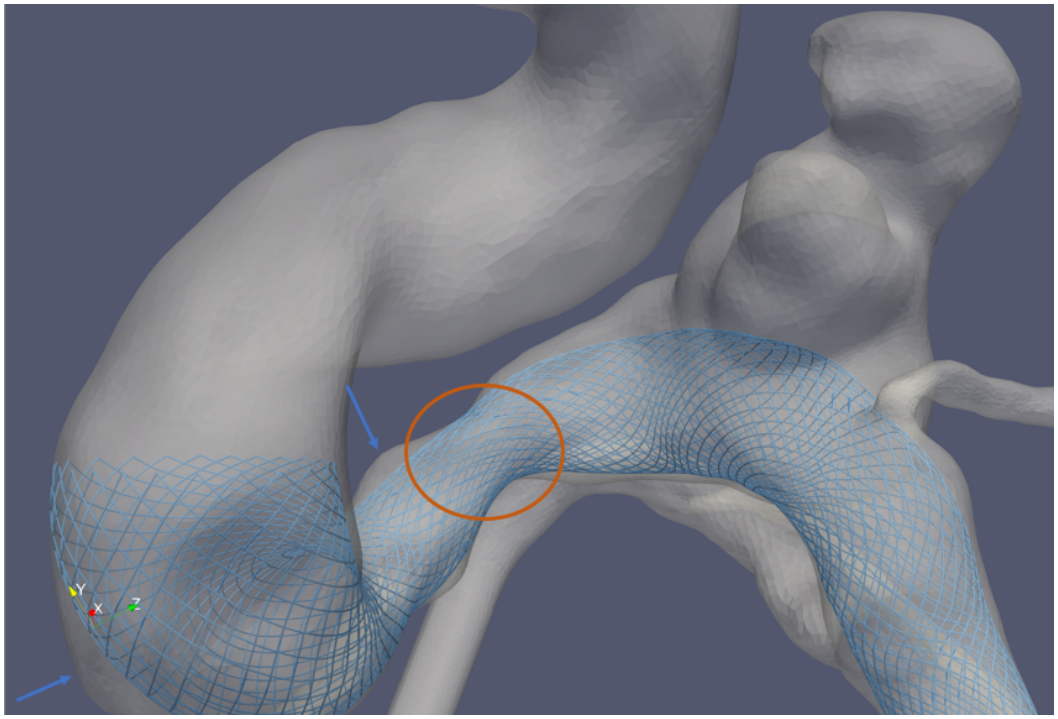

Figure 4.5: Pt E, pictured above, presents many of the challenges of Pt F but instead provides a more accurate segmentation for stent deployment such that the stenosis (brown circle) and large changes in curvature or diameter (blue arrow) do not introduce high amounts of error for the FVS software.

In conclusion, there are some certain limitations to FVS, but except for three cases (out of ten), the software did comparably well or better than Acandis's own software in the prediction of flow-diverting stents in real aneurysm cases.

4.4 Results of the Comparison of Hemodynamics between FIA and SIA

4.4.1 Morphology

Regardless of aspect ratio, SIAs typically exhibit a small neck when compared to the volume of the dome or any other length-scale of the aneurysm vasculature. However, FIAs are, by definition, circumferential meaning the neck area to aneurysm volume ratio is larger than for SIAs. This means

Table 4.2: Morphological parameters of aneurysm volume and exposed stent area to illustrate the differences between SIA and FIA

Case	Aneurysm Volume (mm^3)	Stent Area (mm^2)	Area/Volume (1/mm)
FIA1	30.4	38.6	1.3
SIA1	33.2	7.84	0.2
FIA2	159	168	1.1
SIA2	52.7	6.35	0.1
FIA3	920	656	0.7
SIA3	34.1	4.39	0.1

the flow has a better chance of filling an untreated fusiform aneurysm compared to a saccular one, where an inflow jet that impinges on the aneurysmal dome wall is not uncommon. The morphological data are presented in Table 4.2 for the cohort.

4.4.2 Hemodynamics

Aneurysm dome wall parameters

First, the wall parameters are presented. Fig. 4.6 shows the resulting WSS on the vessel surfaces for the three FIA and SIA cases. The results are shown for each condition: first, pathological (P), then treated (T), followed by healthy (H). The average WSS appears lower on the aneurysm dome after treatment for FIA and SIA. The healthy counterparts are subject to higher WSS for both FIA and SIA. The qualitative presentation of the OSI in Fig. 4.7 indicates higher temporal changes within the WSS for the pathological condition compared to the healthy condition. Only in SIA 3 does the OSI increase with treatment.

The quantitative results strengthen the conclusion drawn from Fig. 4.8. The change in WSS from pathological to treated (P to T) is negative for all cases except FIA 1. The change of OSI in each case from P to T reveals positive values for SIA 3, as previously stated, and, a minor increase in FIA 2. Remaining cases present a negative change from P to T revealing a reduction in OSI

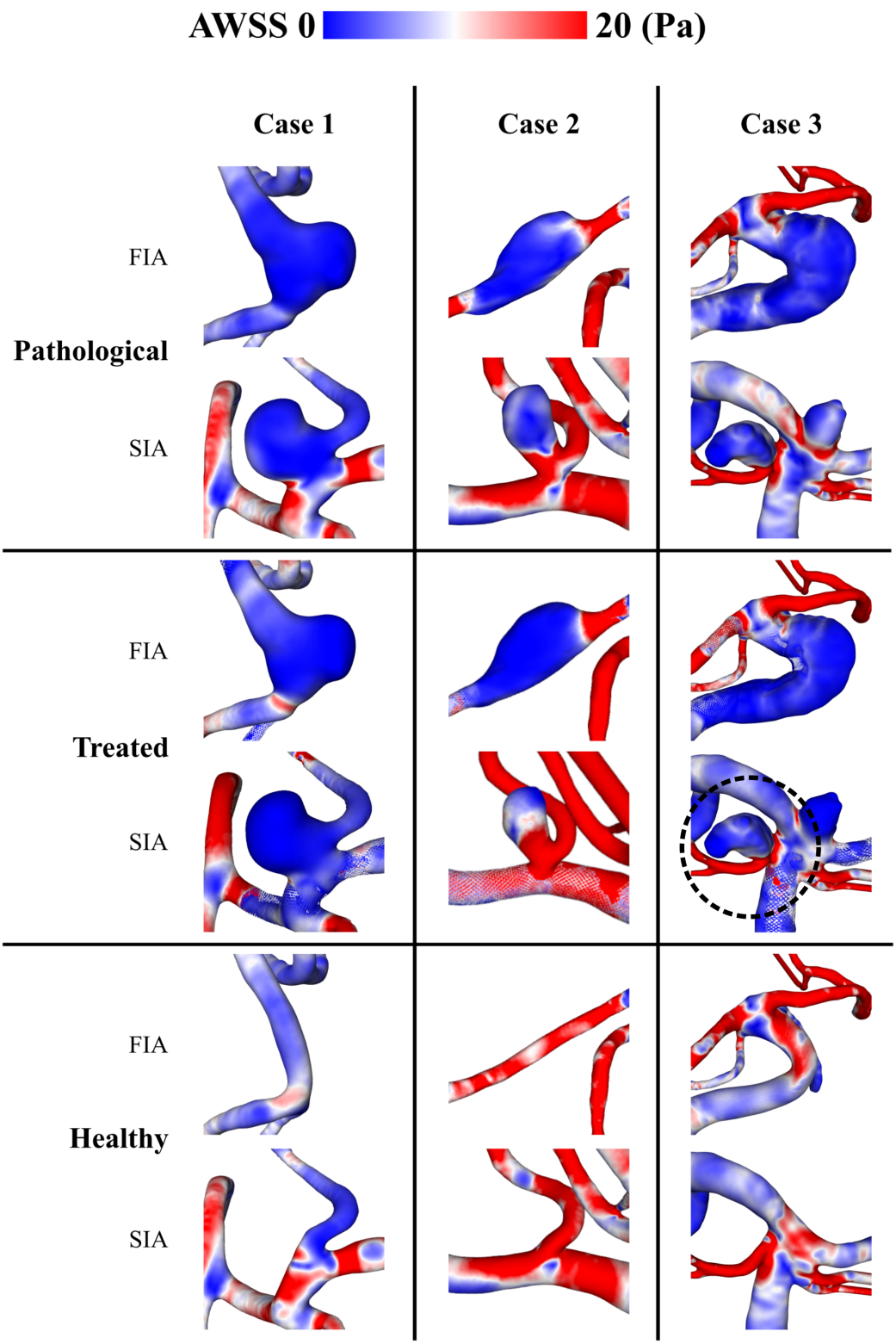

Figure 4.6: Resulting WSS on aneurysm surface for case 1 - 3 for pathological (P), treated (T) and healthy (H). Aneurysm of interest circled for SIA 3.

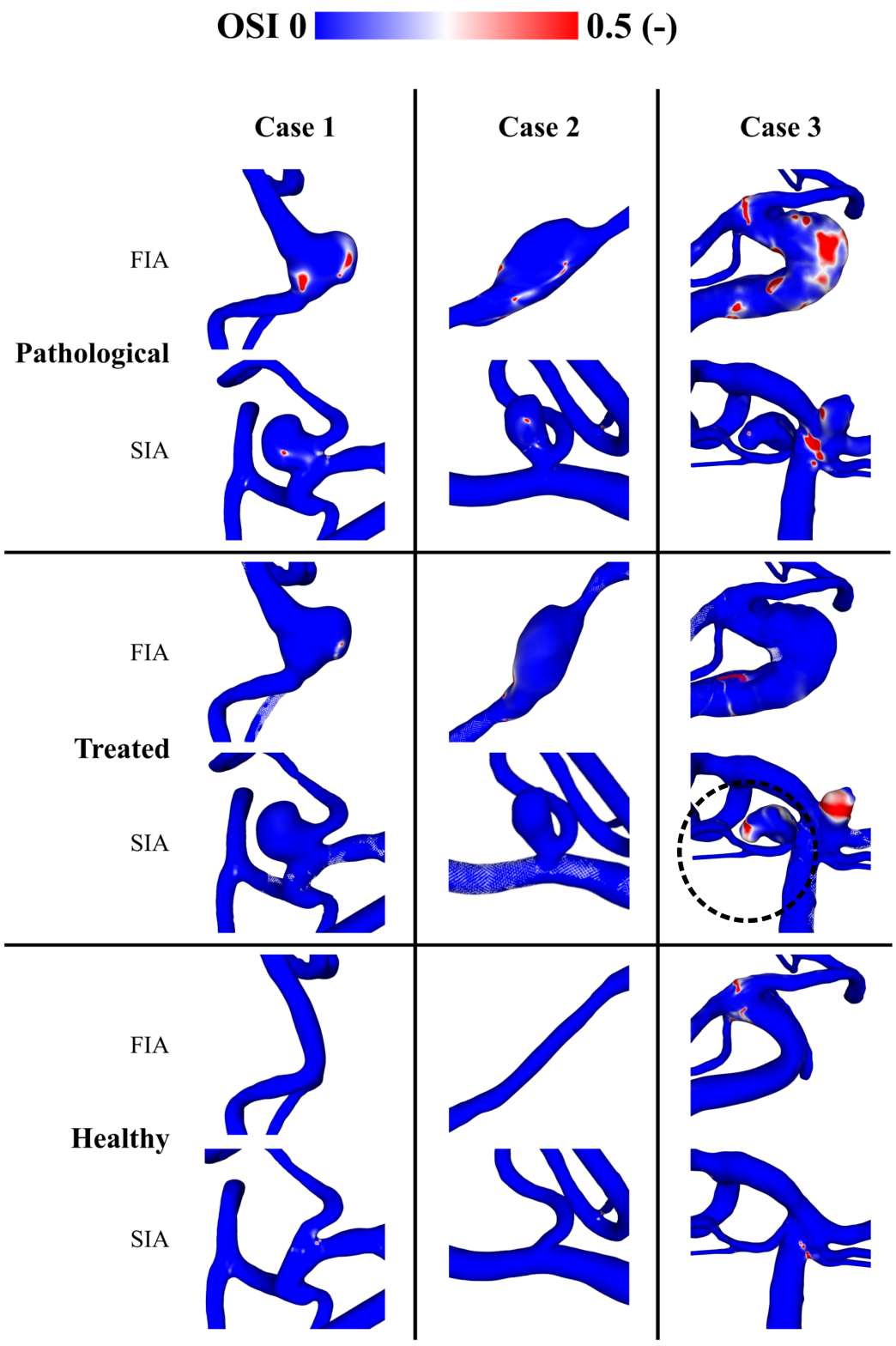

Figure 4.7: Resulting OSI on aneurysm surface for case 1 - 3 for P, T and H. Aneurysm of interest circled for SIA 3.

with treatment.

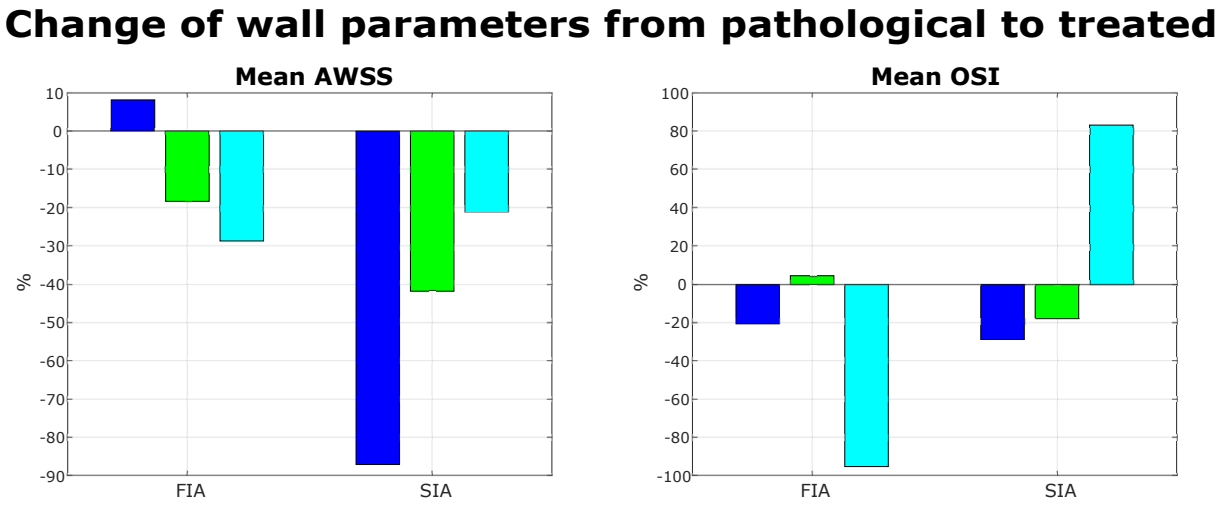

Figure 4.8: Resulting Treatment Effect (TE): The change in metrics from Pathological (P) to Treated (T) of average WSS and OSI on the aneurysm surface for cases 1 - 3

Volume-weighted Hemodynamic Parameters

Fig. 4.9 shows velocity streamlines and Fig. 4.10 the OVI distribution within all the vessel models. As directly observable for each case, the pathological condition comprises the highest OVI for all cases. This decreases with treatment and is lowest within the healthy counterparts for each case. Resulting EL for each case and condition is shown in Table 4.3. Highest EL values occur within the treated cases. For all cases besides FIA 3 the EL is slightly higher within the healthy than the pathological part.

The quantitative results of the mean values of velocity, vorticity, and OVI are shown in Fig. 4.11. Parameters are calculated in the aneurysm saccular volume, as described in section 4.2.3.

Stent Treatment

Single Stent Hemodynamics

Table 4.3: Resulting Energy Loss for each case and condition, Pathological, Treated, and Healthy, in milliWatt

Case	EL (mW)		
	P	T	H
FIA1	3.00	4.70	3.10
SIA1	4.90	9.50	5.00
FIA2	37.8	68.1	3.85
SIA2	11.0	16.5	11.2
FIA3	30.5	89.3	32.6
SIA3	4.40	5.30	0.36

The TE of velocity from P to T within the aneurysm parts is similar for SIA and FIA, being slightly higher (5 - 30 %) for SIAs. A higher vorticity reduction with treatment is found in FIAs than in SIAs, for cases 2 and 3. The OVI values are reduced with treatment for all cases except FIA 2.

Stent Expansion

An expansion was calculated based on the deployed diameter compared to the nominal diameter, using a simple percent difference as an accuracy score. The nominal diameter is the manufacturer's specification for the optimal vessel size the stent should be deployed in. The stent is chosen by the neurosurgeon based on the aneurysm location and associated vessel size. The values of the virtual expansions are summarized in Tab. 4.4 along with the given diameter. Both the mean and maximum expansion of the stent while crossing the aneurysm are considered. This is used to compare cases since only Case 1 shares the exact FDS treatment size.

Dual Stent Hemodyanmics

For every metric except vorticity, the SIA's treatment effect is larger than that of the FIA. The secondary stent shows a marked improvement in both IAs; however, the flow of the FIA is still less effected than that of the SIA as can be seen in Fig. 4.12 and Fig. 4.13. The SIAs show similar results for the saccular aneurysms treated with two stents, although the FIAs do not follow the

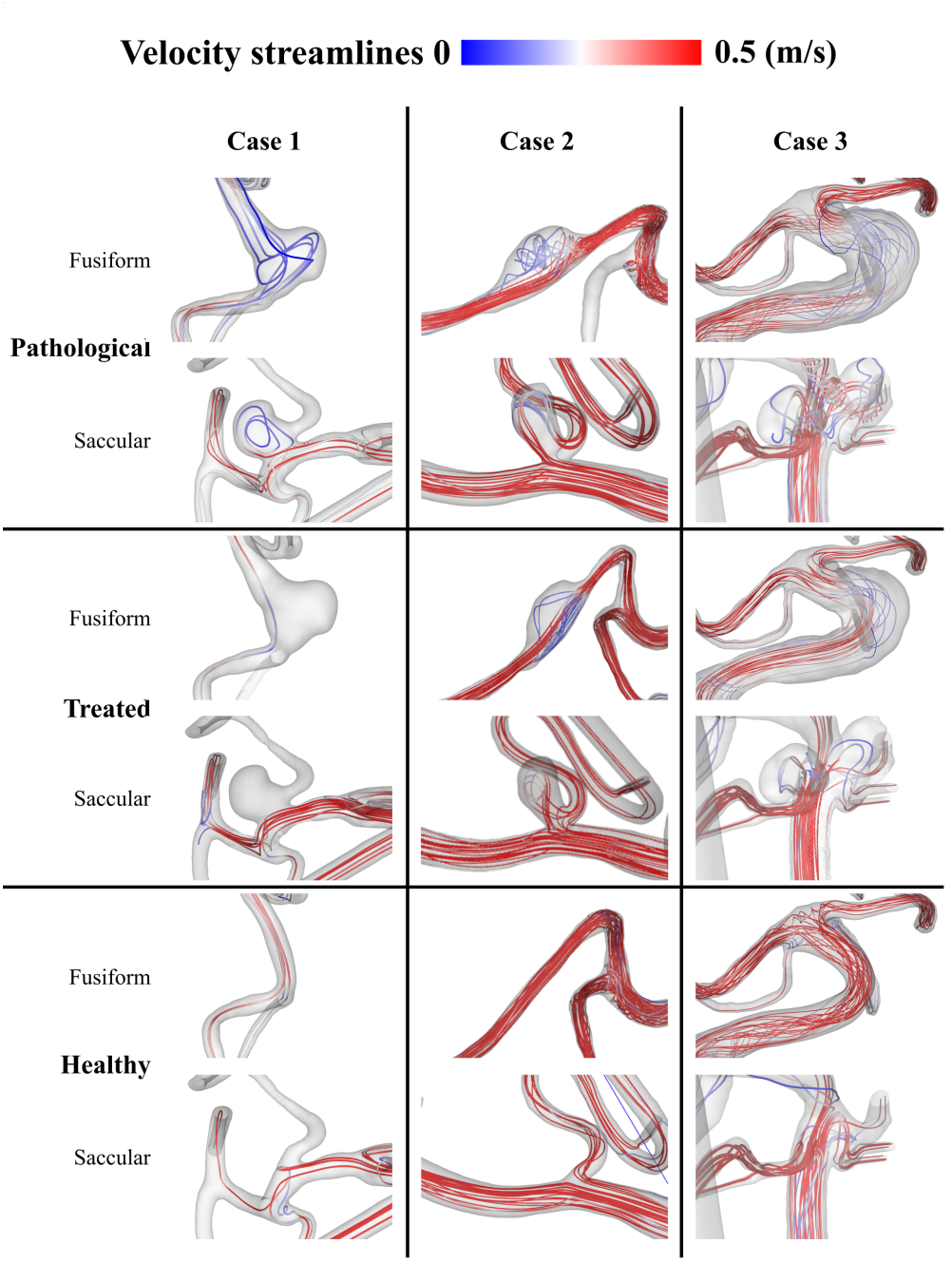

Figure 4.9: Streamlines showing average velocity within vessel models for case 1 - 3 for P, T and H.

Table 4.4: The expansion (when > 1, else contraction) of the stent's diameter past the commercially-prescribed diameter.

Case	Given Diameter (mm)	Max Expansion	Mean Expansion
FIA1	2.25	1.04	0.91
SIA1	2.25	0.91	0.82
FIA2	3.00	1.22	0.87
SIA2	4.50	1.03	0.58
FIA3	7.00	1.03	0.80
SIA3	4.00	0.83	0.72

trend seen by Chong [28].

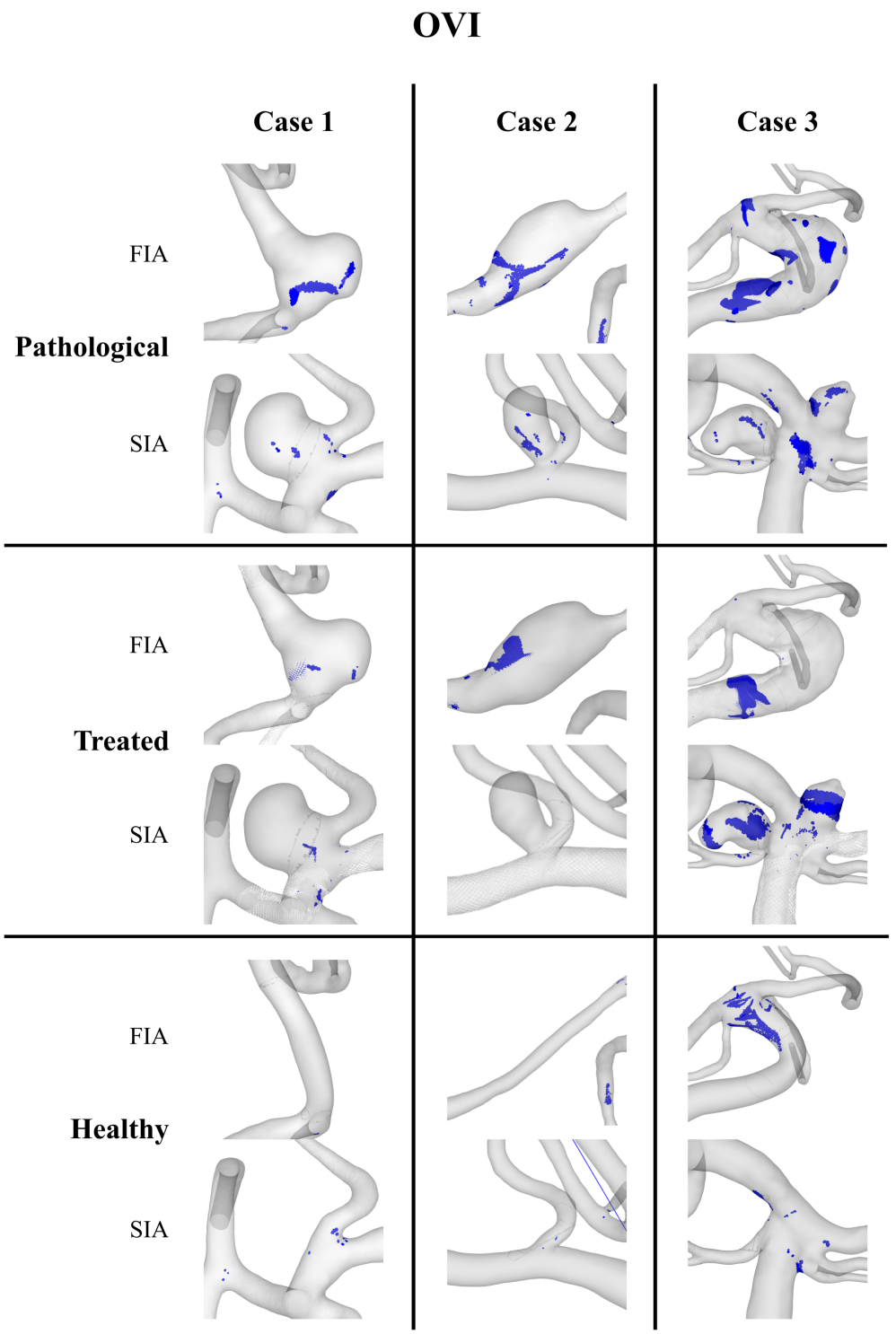

Figure 4.10: Resulting OVI > 0.1 within vessel models for case 1 - 3 for P, T and H.

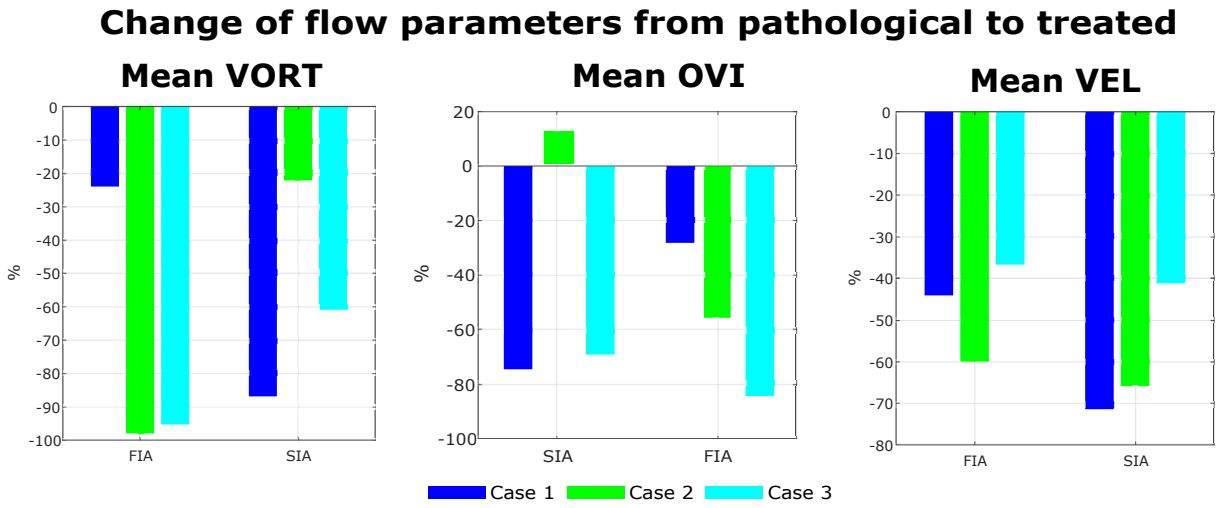

Figure 4.11: Resulting Treatment Effect (TE) from pathological (P) to treated (T) of mean vorticity, mean OVI, and mean velocity inside aneurysm for case 1 - 3

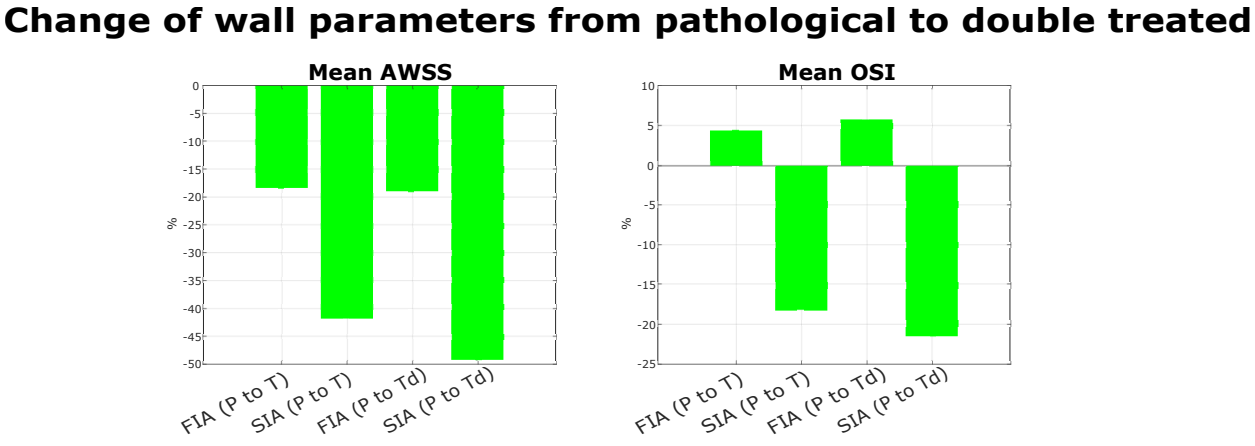

Figure 4.12: Resulting treatment effect (TE) from pathological (P) to double treated (Td) of WSS and OSI on aneurysm surface for case 2

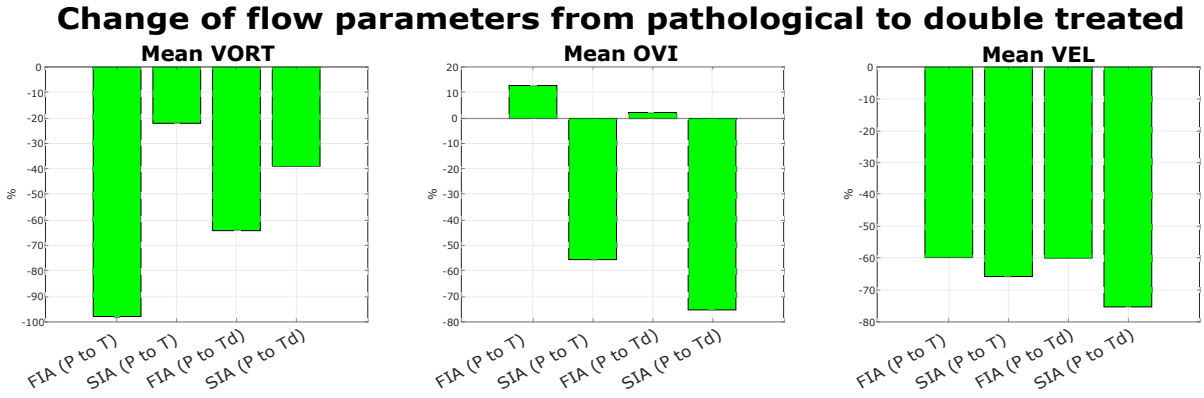

Figure 4.13: Resulting treatment effect (TE) from pathological (P) to double treated (Td) of mean velocity, mean vorticity and mean OVI inside aneurysm for case 2

4.5 Discussion

Treated IAs generally see reductions of all five hemodynamic metrics of interest studied in this work (see Section 2.3). Certain cases do not follow this trend. SIA 3 shows a strong increase of OSI which occurs at the apex of the aneurysm dome where the already low WSS may be changing direction based on minor deviations (see the streamlines in Fig. 4.9) in the flow throughout the cardiac cycle. FIA 1 has an increase of WSS which appears to be a direct result of the flow being diverted away from the treated vessel branch, and secondarily being diverted away from the aneurysmal apex, where WSS is minimum. However, because of the nature of fusiform aneurysms, this change to the treated vessel/aneurysmal sac WSS could be significant for fusiform aneurysm growth. FIA 2, like SIA 3, is subject to an increase in OSI. Again, this post-treatment increase of an oscillatory index appears in a low-velocity region and also seems to coincide with a high-OSI surface in the treated case. Interestingly, FIA 2 has one of the largest reductions in vorticity. Although when a second stent is placed, the vorticity reduction is less noticeable, and the increase in OVI is diminished, the increase in OSI is as strong with a second stent as with the first.

The treatment increases EL drastically. This indicates that due to treatment, energy flux is dissipated by small scale fluctuations in the flow. Without treatment to induce small scale velocity fluctuations that greatly contribute to dissipation, flow in the parent vessel and aneurysm dissipate very small (insignificant) amounts of energy (it is at high but not turbulent Reynolds numbers), and thus EL differences between the pathological and healthy cases are negligible. The effect of treatment on EL, however, is equally appreciable and important for FIA and SIA.

The virtual stent analysis shows an increased deployed diameter past the nominal diameter for all fusiform cases. For example, the stent for FIA 2 expands past its nominal diameter of 3mm to 3.64mm while crossing the aneurysm. Based on the presented change scores, this gives an expansion of 1.22. The analogue SIA 2's 4.5mm stent expands to the nominal diameter of 4.64mm which is considered a 1.03 expansion. The mean values follow a similar trend for all cases where the stent expansion is greater across the entire fusiform aneurysm than the saccular counterparts. The ability of the stent to freely expand circumferentially in the fusiform aneurysms lends itself to this greater maximum and mean expansion. Since the stent area and length for FIAs are substantially large (see Tab. 4.2) one outcome of over-expansion, even just within the aneurysm, is foreshortening;

however, a greater concern is that the porosity would be increased allowing more flow into the aneurysm.

While dual stenting produces greater reduction (except for OSI) in hemodynamic metrics for both types of aneurysms, FIAs seem to be affected less by the second overlapping stent than SIAs. This, paired with the expansion seen in FIAs, means the porosity, even of a dual-stent may not be sufficient in some FIA cases. Because of the large over-expansion for FIA 2 (max expansion > 1), the second stent could expand up to this size as well, giving an equally high-porosity result of the flow-diversion.

4.6 Conclusion

Many morphological differences exist between more common SIAs and rare FIAs. However, when treated with a single flow-diverting stent, there were no discernable trends in the changes in hemodynamics between these two categories of IAs. Though following treatment with a second overlapping stent, an interesting lack of response for WSS and velocity occurred for the dual-stented FIA Case 2, with an increase for vorticity and OSI (only OVI decreasing), whereas for the dual-stented SIA Case 2 showed significant decreases in all variables.

Fusiform aneurysms have no definable neck and affect the entirety of the vessel's perimeter. Because of this, close attention should be paid to stenting techniques when treating FIAs. The large expansion of the stent into the aneurysm sac, which provides a large surface to divert flow, is only helpful if the porosity is low. Since this larger surface area of the stent crossing the aneurysm neck isn't intrinsically helpful unless the stent tine surface area (porosity) increases, dual stenting or telescoping may not provide adequate treatment for increased flow diversion. Therefore, packing (a tequnique of compressing the stent to decrease the porosity) may be the most desirable advanced stenting technique for fusiform aneurysms that require greater hemodynamics effects to slow down flow and promote stable thrombus and aneurysmal healing.

Chapter 5

A NEW BILINEAR POROUS MEDIA METHOD FOR MODELING COIL EMBOLIZATION DEVICES

As described in Chapter 3, the standard porous medium approach, homogeneous and isotropic, used in the literature for the last two decades to model the effect of the coil mass, resulting from coil embolization endovascular therapy, on the hemodynamics in the aneurysmal sac does not accurately capture the effects of the treatment on the hemodynamics[27, 118]. Motivated by this deficiency of the state of the art in modeling coiled aneurysm hemodynamics, this thesis reports on an investigation into a more sophisticated model that can capture the impact of the coil mass's spatial distribution and orientation inside the aneurysmal sac. The model is derived from the detailed knowledge of the coil mass structure after deployment in the aneurysmal sac obtained from synchrotron microCT of aneurysmal silicone phantoms built to match patient-specific anatomy and treated by a neurosurgeon with the exact same coils, in type, number and order of deployment, as the patient for which the intracranial vasculature is reproduced in the phantom. This effort aims at determining the advanced coil-mass model viability in the clinical application of CFD. To provide a ground truth and elucidate the accuracy of the two coil models (standard and novel developed in the Multiphase and Cardiovascular Flows lab by former PhD student Julia Romero-Bhathal [95], coil-resolved reconstructions of the actual treated aneurysms are segmented from the microCT, placed in the aneurysmal sac by a co-registration of the segmented coil and parent vessel images, and the flow in this complex domain is simulated using very high spatial resolution mesh (typically 10-20 Million cells). The flow in the aneurysmal sac simulating coil treatment with the standard porous medium approximation is also calculated, as well as the flow in the aneurysmal sac before treatment. This wealth of simulation data allows this thesis to compare the change in hemodynamics between the treated case (represented in the simulations with any of the models described) and the baseline pretreatment. This hemodynamics alteration by the coil-mass treatment, against the pre-treatment flow, is the most meaningful metrics to discern the advantages of the two models and

their accuracy to make predictions that can then be validated clinically and added to the surgical planning workflow.

5.1 Background and Motivation

While the state-of-the-art for modeling coils deployed in an intracranial aneurysm is a isotropic, homogeneous porous medium (PM) described in detail and implemented in a higher cohort of patients in Chapters 2 and 3, the work presented in the previous chapters of this thesis has established that this PM does not predict accurately the intrasaccular hemodynamics resulting from coil treatment. Observation of MicroCT coil masses show the porosity is larger at the neck than in the core, meaning the standard porous media is averaging out this effect.

As discussed in the Introduction of this thesis, to create a CFD-based tool that achieves successful prediction of treatment outcomes and support clinical decision-making, there is a strong need for a more sophisticated model for coil embolization that captures the directionality of the coils and the inhomogeneity with which they fill the aneurysmal sac volumes. This chapter presents the implementation of a novel bilinear porous media (PM) to a large cohort of patients, and compares the results of the hemodynamics simulated with this novel model, against the changes introduced by the actual coil-resolved mass, and against those caused by the standard porous medium model.

The characteristics of the novel porous model, created by Dr. Romero-Bhathal during her PhD thesis in the Multiphase and Cardiovascular Flows lab at the University of Washington [95], only require the coil and aneurysm volumes, as well as the coil diameters to be computed. Therefore, the model can be easily implemented for patients without any knowledge of the coil structure after deployment in the aneurysmal sac. This is critical for the translation of the methodology developed, as in clinical practice, there would not be a possibility of obtaining synchrotron imaging, while the medical imaging of the patient, post treatment, is not reliable and cannot be used to reconstruct the coils as the resolution is not sufficient and beam hardening artifacts make the reconstruction of the coils, even at low resolution, highly inaccurate. Specifically, coil-resolved simulations can never be implemented in vivo, as the coil can only be resolved with micro-CT techniques that are incompatible with the radiation exposure limits imposed on humans, or even in animals. Furthermore, applying the flow resistance caused by the coils through a single equation representing a momentum sink inside the volume of the aneurysm allows for the quick simulation

of blood flow in the treated aneurysm. This is in stark contrast to the extensive computational resources needed to perform simulations with the coil-resolved reconstruction of the coil mass inside aneurysms. As barriers to carry out this research, coil-resolved simulations require many hours to set up and tens or hundreds of hours of CPU time in a large distributed memory computer to run, making them impractical in applications that aspire to be translational and have an impact on clinical workflow. While the high resolution in space and time enabled by the synchrotron micro-CT reconstruction of the coils provides the highest level of detail in the hemodynamics simulation, the segmentation, meshing, run time, and post-processing require significant resources and researcher's time, which makes extracting the key features of the coil mass from the coil-resolved simulations from a large cohort of in vitro cases very valuable for both translational and basic research approaches.

Dr. Romero Bhathal [95] created a hierarchy of porous models as part of her thesis, where the bilinear model is the simplest and still takes into account the heterogeneity and anisotropy of the coil mass by considering several "crowns" or thin ellipsoids that surround the core of the dome volume, where the coil mass has homogeneous and isotropic properties. The porosity in these crowns can be modeled as a linear function of distance from the wall (where the coil volume fraction is minimum). With the transition to the uniform porosity in the dome core region, this coil structure can be modeled, to a first approximation, as a bi-linear function of porosity that enables a simple, coil mass distribution-informed new PM model, simulation of the flow along the dome wall region (modeled by the high porosity crowns) and inside the dome core. From these crowns and core, the two parameters in a porous medium model can be defined: $\frac{1}{\alpha} = K$ and C_2.

5.2 Methodology

The development and initial implementation of the bilinear model for coiled intracranial aneurysms was presented in detail by Romero-Bhathal in her PhD thesis [95].

5.2.1 Discretizing the Aneurysm

The aneurysmal sac, defined as the volume delimited by the aneurysmal dome wall and the neck surface, is approximated by an ellipsoid to compute the major and minor axes (a1, a2/a3). Both a1 and a3 are used to calculate the volume of the ellipsoid. This estimation represents the aneurysmal

volume in calculating the properties of the bilinear model. Eight crowns, with a thickness of 0.0625mm (0.25 times the diameter of the coils), are used to represent the dome wall region in the aneurysmal volume. These crowns distinguish between the core region of the aneurysm, where the coil mass is homogenous, and the dome wall where the coils are apposed on the aneurysmal wall, resulting in only fractional filling of the near-wall volume and in a porosity that decays as a function of distance to the dome wall (with the slope of the porosity linear function controlled by the thickness and number of crowns within the model).

5.2.2 Defining the Bilinear Coefficients

The packing density, the complement of porosity $\phi = 1 - PD$, is used to select the coils used in the treatment, with a target of 25% and a maximum of 30% [46, 100, 108, 112]. This means that the global porosity is often $\geq 70\%$. The aneurysm volume is bounded by the aneurysmal dome and the surface defined by the intersection of the dome with the envelop of the coil segmented from the synchrotron microtomography.

The porosity shown in Fig 5.2.1 decreases across the crowns, from the maximum at the dome wall, and then plateaus at a minimum. This minimum porosity at the aneurysmal volume core is calculated to be fitted by the bilinear approximation, in conjunction with the porosity at each crown. The bilinear profile describes the coil mass with a porosity gradient between the high porosity crowns and the lower (constant) porosity in the core. The permeability, K, is a function of the porosity of each region,

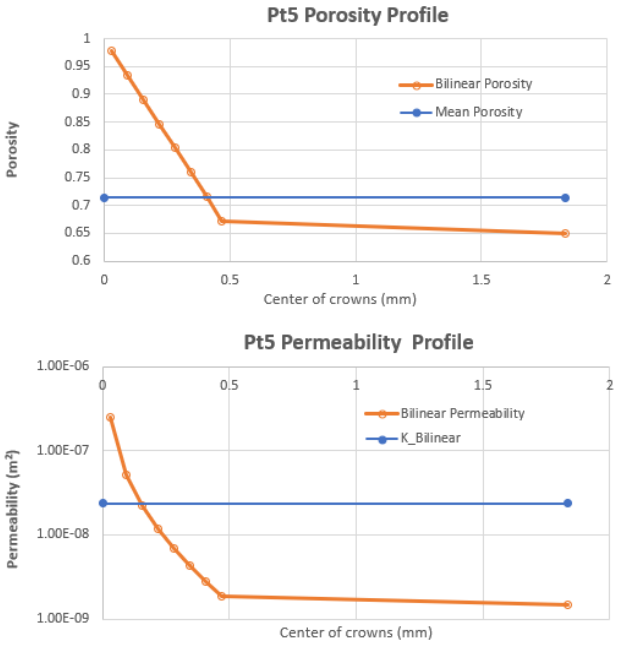

Figure 5.1: Representative porosity and permeability profile of the bilinear model with resulting permeability, K.

using the ellipsoidal approximation to the aneurysm volume model to complete the calculation. This profile can be observed in Fig. 5.2.1. K, the inverse of the viscous resistance coefficient, is defined for PM in Eq. 2.4, but for bilinear is defined as:

$$\frac{1}{K} = \frac{8(1-\phi)}{r^2}(-\ln(1-\phi) - \frac{1-(1-\phi)^2}{1+(1-\phi)^2}) \tag{5.1}$$

where r is the radius of the major axis of the ellipsoid approximation and ϕ is the porosity. This relationship, established by Boutin [16], is used to simulate the permeability to perpendicular flow through cylindrical bundles.

The inertial resistance, or form factor C_2, is calculated by the bilinear model in a similar manner, at each region and is a function of both porosity and permeability.

$$C_2 = \frac{2}{\sqrt{K(\phi)}}(3(1-\phi)^2) \tag{5.2}$$

Once K and C_2 have been calculated at each crown and in the aneurysmal volume core, the overall bilinear approximation to K and C_2 can be computed to model the effect of the coil mass deployed in the hemodynamics inside the aneurysms. To understand the capability of this novel translational model to assess the impact of the coil treatment on the hemodynamics, the novel bilinear model is implemented in Fluent using the calculated inertial and viscous factors to input into the porous medium module in the equations of motion and simulate the flow .

The porosity, K, and C_2 values are all that is prescribed in Fluent for either the PM or BL models. Rather than by physically representing several crowns and a core, each with their own K and C_2, the BL values are calculated as a summation of the crowns and core as shown in the equations below.

$$K_{BL} = \sum_{1}^{N} f_i K_i + f_c K_c \tag{5.3}$$

$$C_{2_{BL}} = (\sum_{1}^{N} \frac{f_i}{\sqrt{C_{2_i}}} + \frac{f_c}{\sqrt{C_{2_c}}})^{-2} \tag{5.4}$$

The volume fraction is denoted by f, and the i^{th} represents each crown whereas the c index represents the core or bulk of the coil mass. This is how the BL model takes into account the heterogeneity of the coil mass while still being a porous media model.

5.2.3 Patient Cohort

In this study, 5 aneurysms were studied using the standard PM model, the bilinear PM model, and the coil-resolved segmentations. Four were located on the internal carotid artery, and one was on the basilar artery. The boundary conditions used were the same as those employed in Chapter 2 and 3.

5.2.4 Analysis

Here, two Eulerian metrics are considered: average velocity within the aneurysm volume and wall shear stress on the dome surface. As Lagrangian metrics, Residence time (RT) and shear history (SH) are used; additionally, the SH:RT ratio from Chapter 3 is analyzed in this study.

Eulerian

When considering the Eulerian metrics of velocity in the sac and wall shear stress on the dome, there are many ways to compare the cases. A direct point-to-point comparison with CR simulations and other treatment models or pre-treatment simulations is not possible due to the geometry of coils reconstructed inside the original flow domain for the synchrotron coil-resolved while the coils are not reconstructed in the porous medium models. Since a full-domain point-to-point comparison is not possible, average values, computed in certain regions can be employed. Thin-crown ellipsoidal regions can be used. However, the desired goal is to have a model that can accurately predict the flow throughout the entire domain for all given metrics. Therefore, the average throughout the aneurysmal domain is used to compute the accuracy of the models, against the gold-standard CR simulations.

Lagrangian

For the Lagrangian metrics, the same combination of shear history (SH) and residence time (RT) shown in Chapter 3 is employed. In this chapter, the values of RT or SH corresponding to the 95^{th} percentile of the pre-treatment statistics are used to threshold the particle data in the post-treatment statistics. The percentage change of particle above those thresholds minus the 5% of particles above those values in the pre-treatment is the metric used to compare the cases. These

RT and SH metrics are computed accounting for particles that enter the aneurysm anytime during the 10 cardiac cycles simulated.

Considering the outliers defined by a high percentile (95%) allows the analysis to focus on the extreme behavior of platelets that will be a trigger for thrombosis. This RT or SH value is used to calculate what percentage of platelets have their residence time or shear exposure significantly increase above that physiologically meaningful value by the treatment. Therefore, if $\geq$ 5% of platelets exceed the threshold value (corresponding to the 95^{th} percentile in the pre-treatment case), indicates that the treatment has induced an increase in that Lagrangian metric (RT, SH or RT/SH), and the magnitude of that effect can be associated to the value of that percentage above the baseline (5%).

A percent change or change score is then calculated for each of the post-treatment scenarios based on the pre-treatment baselines for RT and SH. This represents the amount that the treatment has affected the Lagrangian hemodynamics, and comparing the different model predictions to the coil-resolved gold standard will shed light on the accuracy of the models for hemodynamics computations.

5.3 Results

5.3.1 Porous Media Modeling Coefficients

The porosity, used by both PM models, and the corresponding viscous and inertial factors are presented in Table 5.3.1. A range of porosities are present in the study, spanning from 0.87 and to 0.71, near the clinical target maximum. Excluding Pt4, the K values in all cases increased when using the bilinear model . However, the C_2 values had no clear trend between the standard and the novel bilinear porous medium models, increasing or decreasing throughout the cohort. These changes are caused by the consideration of the crown and core of each aneurysm for the BL model. The implementation of Eqs 5.3 and 5.4 create the differences in the K and C_2 values from the PM to the BL model.

Table 5.1: For all 5 cases, the porosity and calculated viscous, $1/K$, and inertial, C_2, factors are given for the standard porous media (PM) and bilinear (BL) PM.

		Standard PM		**Bilinear**	
Pt	**Porosity**	$1/K$	C_2	$1/K$	C_2
1	0.78	5.40E+07	337.7	1.76E+07	100.9
2	0.74	5.96E+07	396.5	4.77E+07	607.2
3	0.76	6.37E+07	357.5	3.14E+07	288.4
4	0.87	1.38E+07	199.9	1.65E+07	84.5
5	0.72	1.11E+08	428.4	4.22E+07	500.3

5.3.2 Eulerian Metrics

Two Eulerian metrics were extracted from the aneurysm dome at systole (the instant of peak flow rate value within the cardiac cycle). Aneurysm velocity was volume-averaged inside the sac, while the wall shear stress (WSS) was surface-averaged over the dome's surface. The metrics of the standard PM and of the bilinear (BL) PM are compared to the CR, providing a measure of accuracy of the two models against the gold standard hemodynamics provided by the coil-resolved simulations. Velocity data is shown in Table 5.2 and WSS data in Table 5.3.

The standard porous model overpredicts the flow dampening effect of the coils for all cases, except Pt4, as shown in the comparison of the average velocity against the CR. Similarly, reduction in WSS is consistently overpredicted by the standard PM, for all cases. This result is expected from the characteristics of the standard porous medium model, and was described in Chapter 3.

Since the Eulerian metrics of velocity and WSS, averaged throughout the aneurysmal domain, are standard for investigating flow in an aneurysm, domain-averaged metrics are presented in Tables 5.2 and 5.3, for all three coil reconstructions, along with the error between the two porous medium models and the gold-standard CR simulations. The average absolute error of the BL model is 18% for average velocity and 12% for WSS, compared to the 26% and 22% error of the standard PM model.

For the two aneurysms located at a bifurcation, patients 3 and 4, an interesting trend arises.

Table 5.2: Maximum average velocity within the aneurysm dome for the 3 virtual treatment reconstructions: standard porous media (PM), bilinear (BL) PM, and coil-resolved (CR), with the deviation from the gold-standard CR for each of the two simplified models.

Pt	PM (m/s)	PM error	BL (m/s)	BL error	CR (m/s)
1	0.042	-37%	0.080	19%	0.067
2	0.013	-15%	0.014	-9%	0.015
3	0.085	-1%	0.117	36%	0.086
4	0.133	47%	0.082	-10%	0.091
5	0.024	-30%	0.040	15%	0.034
		26%		18%	

Table 5.3: Maximum average wall shear stress (WSS) on the aneurysm dome for the 3 virtual treatment reconstructions: standard porous media (PM), bilinear (BL) PM, and coil-resolved (CR), with the deviation from the gold-standard CR for each of the two simplified models.

Pt	PM (Pa)	PM error	BL (Pa)	BL error	CR (Pa)
1	1.14	-27%	1.83	17%	1.56
2	0.28	-22%	0.34	-5%	0.36
3	2.05	-23%	2.73	2%	2.68
4	2.56	-3%	1.80	-32%	2.65
5	0.45	-34%	0.67	-2%	0.69
		22%		12%	

For Pt3, the PM predicts aneurysmal velocity better, while BL predicts WSS better. Conversely, for Pt4, the BL predicts velocity better, with PM predicts WSS better. The better model has an error of less than 10%, while the other model has an error between 32–47%. This may indicate the limitations of any porous medium model, whether PM or BL, to consistently predict Eulerian metrics for inertial-driven flows that are not primarily tangential to the neck. While there was no strong correlation with BL performance and physiological inflow, it's interesting to note that Pt3 and 4 (along with Pt1) had some of the highest flowrates with a systolic Re between 129 and 165 (the time-averaged Re is between 70 and 93). Pt2 and 5 experienced the lowest flowrates with a systolic Re of 82 and 93 respectively (time-averaged Re is 32 and 36).

5.3.3 Lagrangian Metrics

Typically, the 95^{th} percentile of RT will always increase significantly with treatment as shown for most patients in Table 5.4. However, SH may decrease with lower velocities in the aneurysm or increase due to higher small-scale gradients caused by the slowdown of flow along the regions where the coils accumulate, but not in the gaps between deployed coils, leading to a high exposure to shear stress throughout the platelet's trajectory. This inconsistent behavior can be seen in Table 5.5.

The ratio of SH to RT is a metric proposed to combine information from the two primary Lagrangian markers used in this work. Whereas in Fig. 3.4 the SH:RT is calculated as the percentage of platelets exceeding the 99.9^{th} percentile of each variable for the best visual representation, in this chapter, the 95^{th} percentile for each RT and SH are used and then the ratio is computed and shown in the plots. Furthermore, the three post-treatment simulations are considered as shown in Fig. 5.2. The ratio for pre-treatment is always 1 because the 95^{th} percentile of both SH and RT are considered, therefore the percentage of particles greater than these percentiles in the pre-treatment are both 5%. Then, the percentage of platelets with SH above the pre-treatment 95% threshold value and percentage of platelets with RT above the pre-treatment 95% threshold value are calculated, before computing the ratio and the percent change caused by the treatment.

As with the Eurlerian results, the CR provides the ground truth from which the accuracy of the two porous models can be computed. Table 5.6 shows the SH:RT percent change values of the

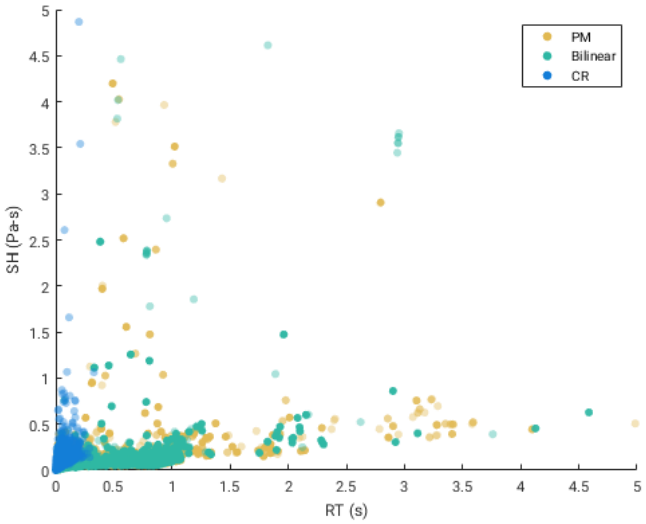

Figure 5.2: All platelets entering Patient 5 are represented in the scatter plot for the standard porous medium, the bilinear porous media, and the coil-resolved simulation.

three cases along with the error produced by the two models. While the average absolute error of the two models is almost equal, the BL model outperformed the PM in 4 out of the 5 cases. The standard PM outperformed the BL for the remaining case, which is described in detail below.

5.3.4 Improvement of the Bilinear Model

When comparing the errors produced by the PM and BL model (the lavender columns) in Tables 5.2 - 5.6, if the BL error is considered the actual error from the CR and the PM is treated as the observed/expected value, then a second calculation can be performed between the two errors using the change score from previous chapters (Eq. 2.5). This new difference between the error of the BL and error of the PM provides a way to gauge the improvement of the BL over the PM with a positive indicating an improvement and a negative being an underperformance. With every metric, the BL has at least one negative percent change. However, the average percent change for WSS was 546 which is the largest improvement of any metric. The BL also did better predicting velocity with an average score of 107. BL's average score for RT and SH were better individually at 80 and 52 respectively with the average improvement for the SH:RT metric being only 32.

Table 5.4: Residence Time (RT) is thresholded at the value for 95th percentile of the pre-treatment and compared to the post-treatment to create a change score for the 3 virtual treatment reconstructions: standard PM, bilinear (BL) PM, and coil-resolved (CR), with the deviation from the gold-standard CR for each of the two simplified models.

Pt	PM	PM error	BL	BL error	CR
1	974%	1331%	358%	426%	68%
2	21%	100%	141%	97%	4552%
3	-41%	36%	-40%	38%	-65%
4	38%	56%	61%	30%	88%
5	281%	308%	175%	153%	69%
		366%		149%	

Table 5.5: Shear history (SH) is thresholded at the value for the 95th percentile of the pre-treatment and compared to the post-treatment to create a change score for the 3 virtual treatment reconstructions: standard PM, bilinear (BL) PM, and coil-resolved (CR), with the deviation from the gold-standard CR for each of the two simplified models.

Pt	PM	PM error	BL	BL error	CR
1	-80%	5%	-54%	28%	-76%
2	20%	50%	-87%	314%	40%
3	-96%	12%	-88%	2%	-86%
4	-96%	161%	-93%	152%	-37%
5	-92%	177%	-87%	162%	-33%
		81%		132%	

Table 5.6: The SH:RT metric is built by thresholding the RT and SH at the value for the 95th percentile of the pretreatment value. It is presented here for each of the 3 virtual treatment reconstructions: standard PM, bilinear (BL) PM, and coil-resolved (CR), with the deviation from the gold-standard CR for each of the two simplified models.

Pt	PM	PM error	BL	BL error	CR
1	-98%	14%	-90%	5%	-86%
2	-1%	-98%	-94%	138%	-40%
3	-94%	57%	-80%	33%	-60%
4	-97%	46%	-95%	44%	-66%
5	-98%	62%	-95%	58%	-60%
		55%		56%	

5.3.5 Case-specific Performance

Pt1

Looking at Table 5.1, the resistance values have the largest change between the PM and the CR. This could be due to an overestimation of the aneurysm's ellipsoidal volume. Given Eq. 5.1, an exagerated ellipsoidal radius could give a drastically lower $1/K$ based on the volume increase and porosity. For C_2, recall that in the PM model, the value is calculated based on empirical evidence and is a function of $1-\phi$. Therefore, based on the $1/K$ value, the slope for the line of BL C_2 could be greater than or less than that of the PM. Following Eq. 5.2, a lower $1/K$ changes the slope of the parabola in a similar manner such that C_2 would also decrease for a given porosity. However, the decrease seen here isn't universal.

While the standard PM tends to overpredict reductions in flow and WSS, as in this case, the BL model underpredicted these reductions. The effect of treatment predicted by the two PM have the same porosity, so it follows that the flow would experience less dampening within the BL simulation since the resistance coefficients in this model are lower. This follows directly for not only velocity but also the WSS on the aneurysm dome wall. For the Lagrangian metrics, the SH:RT ratio is better predicted by the BL model as is the change in RT.

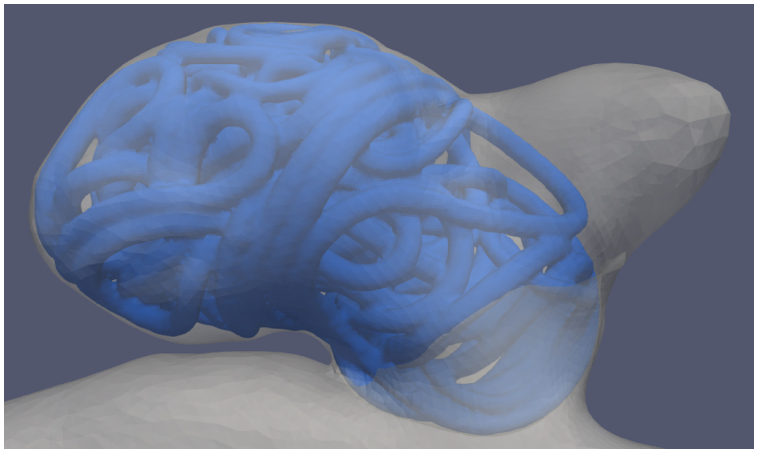

Figure 5.3: Patient 2 with the fully-resolved coil deployed.

Pt2

This case exhibited the worst ellipsoidal volume approximation, with roughly $300mm^3$ versus a true volume of $193mm^3$. The bilinear model produced an artificially low $1/K$, related to the 50% error in volume. However, the C_2 values see a drastic increase for the given porosity. Yet the overdampening caused by the standard model is still improved on, at least partially, by the BL model. This is seen by the lower error of the BL for the Eulerian metrics. However, this patient was the only case in which the BL had a higher error for the SH:RT ratio. The standard model (PM) also produced a high error, predicting almost no change in SH:RT with treatment, which is abnormal. Yet, the PM model was able to replicate the increase in SH seen on the CR ground truth, while the BL model predicted a significant decrease. Potentially, it is this overestimation of the PM coefficients, combined with the asymmetrical packing of Pt2 as shown in Fig. 5.3, that caused the poor result of the BL model for the high platelet SH. The coil is tightly packed in one region but leaves a fully clear bleb where platelets might accelerate and greatly increase shear as they enter and exit different lightly coiled regions. This asymmetric packing is not taken into account by the BL model.

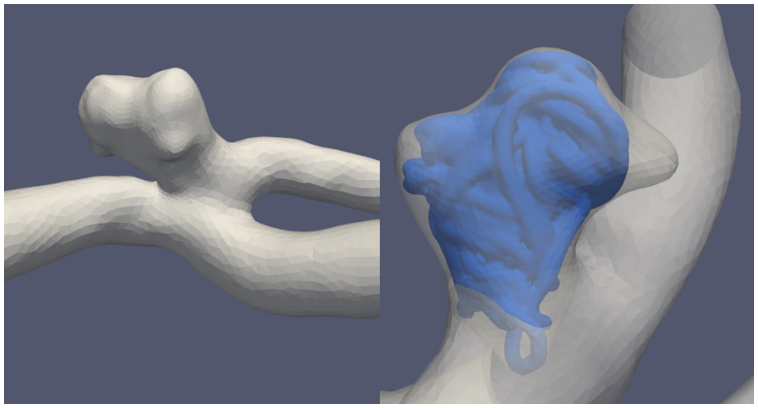

Figure 5.4: Patient 3's parent vessel (left) and aneurysm with the fully-resolved coil deployed (right).

Pt3

Patient 3's aneurysm had the smallest volume of the cohort, but the error of both models on most metrics, versus the gold-standard CR results, was almost 40%. This could be due to the fact that, like Pt2, the aneurysm exhibits blebs, shown in Fig. 5.4, that are not filled by the coils. This aneurysm is at a bifurcation which results in higher degree of impinging flow than is experienced by sidewall aneurysms. Furthermore, this case had one of the largest protrusions of a coil into the parent vessel, which created a larger, distended neck and aneurysm volume. This overlapping region where the coil impinges in the parent vessel may explain the high error of the BL in the prediction of the average velocity in the aneurysm volume.

The higher PM coefficients may have effectively dampened the inflow in this region, but the BL values were unable to slow the flow sufficiently near the parent vessel/aneurysm neck, and throughout the aneurysm volume. However, this case had the best BL prediction for dome WSS. BL also did moderately well in the prediction of Lagrangian metrics, including SH.

Pt4

This aneurysm had the largest volume, best ellipsoid prediction of the sac volume (1% error), and highest porosity of the cohort. It was located on a bifurcating branch.

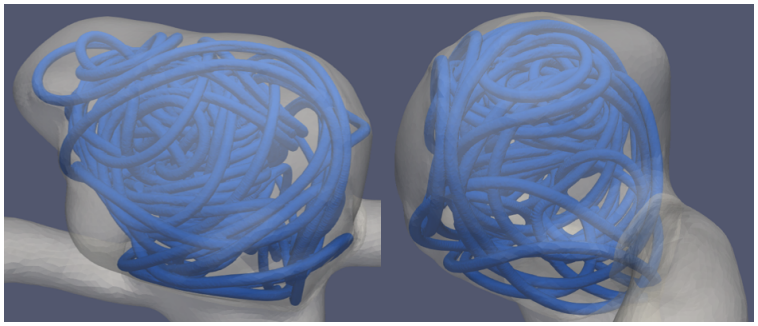

Figure 5.5: Patient 4 has a wide-necked basilar tip aneurysm (left) which is compacted primarily near the apex of the dome (right).

While BL outperformed the standard PM model in predicting velocity for this case, it was WSS that was not well predicted for this basilar tip aneurysm. As can be seen in Fig. 5.5, coils are packed mostly near the apex of the dome with high porosity near the neck region.

Since the coil structure in this patient goes against the high porosity of the outermost crowns, it explains the difficulty of the BL in predicting dome surface-averaged WSS. The BL did only marginally better at simulating the SH:RT ratio, but had much better accuracy for the standard PM for RT. Both PM models did equally poorly on the SH statistics.

Pt5

This aneurysm exhibited the smallest porosity of the cohort, $\phi = 0.715$. Similar to Pt1, the BL's K value was greatly reduced from the standard PM, again, due to an overestimation of the ellipsoidal volume. This aneurysm had the second largest ellipsoidal volume.

This large underestimation in the viscous coefficient means that slower flow within the treated aneurysm did not meet as much resistance in the BL case and contributed to the erroneously high velocities predicted by the BL, as opposed to more accurate predictions from the PM. However, the BL still outperformed the standard PM in both Eulerian metrics. Pt5 had the same trend as Pt4 for the Lagrangian metrics: the BL model was marginally better on the SH:RT, with significantly lower error for the RT metric but only marginal improvement in the SH metrics.

5.4 Discussion

The bilinear porous medium model has previously been shown to improve computation, with more accurate velocity, when compared to the standard PM [95]. This chapter further shows the improvement of the BL's model simulations, with respect to the velocity, and introduces the enhanced ability of the model to capture WSS changes due to endovascular coiling treatment, as well as the treatment effect on platelets, particularly on their RT.

The average velocity in the aneurysmal sac is helpful to quantify the volumetric effect of the coils, better captured by the BL model. The volume-averaging over the entire aneurysm domain may blur certain important features of the flow, as captured by the CR simulations. However, for comparison with the models, this metric was robust and useful. The overall good agreement of the BL with CR in terms of velocity was shown in Romero-Bhathal's seminal work with two patients [96] and eight patients [95] and is here extended to five more patients, out of which four cases outperform the PM for velocity, WSS, and SH:RT.

Similarly, WSS aids in establishing the accuracy of the two porous medium models against the CR simulations. Furthermore, WSS is an extremely common metric used in studying atherosclerosis and plaque formation due to endothelium dysfunction, and it has been extended to cerebral aneurysm growth and rupture [106]. Because the coils do not occupy any significant volume near the aneurysm dome wall in the coil-resolved simulations, WSS suffers less than velocity in terms of washing out distinct features captured in the CR simulations. However, there is still some local effects on WSS when the coils do come near the aneurysm dome wall. Velocity can be averaged throughout the entire aneurysm volume, while there is no flow on the volume occupied by the coils in the CR simulations; with WSS, the metric can be averaged over the dome wall surface, defined identically for all three simulations. The fairly consistent overprediction of the WSS reduction by the standard PM in all models confirms Chivukula's recent study of standard PM and coil-resolved simulations that also shows the artificial dampening of the flow by the PM [27], which is outperformed by the BL model in four out of the five patients.

RT has been directly associated with platelet activation, making it an exceedingly important metric in studies of thrombus initiation inside treated aneurysms, and for the prediction of treatment outcomes [27, 63]. While RT does not capture recirculation or brief stagnation, it nevertheless

gives great insights into long term stagnation in regions of the aneurysm, and its effect on platelet trajectories. Particularly, since it has been shown in Chapter 3 that the standard PM exaggerates flow dampening and therefore overestimates RT variables, it was not then surprising that the BL model outperforms the standard PM in these metrics, since the heterogeneity of the coil mass deployed inside the aneurysmal sac is now taken into account, slightly correcting the excessive dampening in the PM-predicted hemodynamics. This artificial over-dampening is similarly evident in Chivukula's study of four patients where the median and outlying RT were compared for PM and CR simulations [27].

SH is an interesting metric as it may increase or decrease from pre-treatment but is never in the range that triggers high-shear platelet activation. However, low-shear and shear-gradients have been shown to activate platelets too [78, 122], hence the shear stress accumulation is considered. While the BL outperformed the standard model in three out of five models in the calculation of SH statistics, it is clear that the PM model has trouble in certain instances to simulate flow over a complex device, and therefore computing the correct shear exposure along trajectories. The SH:RT ratio allows for the consideration of the two main Lagrangian metrics as a single Lagrangian metric, breaking the trend of the increase or decrease in SH over the increase in RT. Chivukula demonstrated this shortcoming of the standard PM [27]. In his study, one patient showed very good agreement with CR for median and outlying SH; another had good agreement, all showing decreases in the SH metrics; the other two patients, however, could not even predict the correct trend (increase vs decrease in the metric).

While any isotropic, homogeneous PM will struggle to capture the complex dynamics and perhaps even the general trend of the SH experienced by the platelets in real life, as indicated by the CR gold-standard, it remains important to determine the ability of the BL model to predict this metric, and its improvement over the standard PM model.

Because the coil envelope may protrude slightly into the aneurysm's parent vessel, the aneurysm volume may be larger than if calculated in an angiography suite or by using the automated neck detection introduced in Chapter 2. This small calculation error can result in a slightly higher porosity than real-life, but this is the most clear and unequivocal way of calculating porosity, since the exact same coil envelope surface is used to define the boundary of the porous region.

An interesting finding from this study is that of high flows tangential to the dome walls in

aneurysms located on bifurcations. There are two cases matching this description, Pt3 and Pt4, and both had the highest BL error for all the Eulerian metrics. This flow, atypical for most sidewall aneurysms, could have caused the model to produce poor predictions since the bilinear model are based on the assumption of flow entering the aneurysmal sac tangential to the coil surface, not normal as it happens in these two aneurysms. However, the BL model still achieved higher accuracy owing to the outer crowns being incorporated in the simulation, therefore taking into account the changing porosity of the coil mass. Finally, Pt2 exhibited the worst aneurysm volume estimation from the ellipsoid fitting. This yielded excessively high $1/K$ and C_2 values, which coincided with the worst error in SH at 314%. This provides a cautionary tale for aneurysms that have large blebs or distortions from the berry-like deformations, pushing them outside the boundary of an ellipsoid.

This thesis has extended the comparison of the bilinear porous model developed by Romero-Bhathal in her thesis to a cohort of 5 new aneurysms, and to the use of Lagrangian metrics. It provides strong statistical evidence that this simple model provides improvements over the standard homogeneous isotropic model commonly used in the literature. This simple model considers the structure of the coils deployed in the aneurysmal sac, with a gradient of porosity as the coils are apposed to the wall at only certain points and fill the sac at the core with an increased coil volume fraction and decreased porosity. The model considers the resistance of the flow tangential to the coils, as the coils are memory-shaped to lie tangential to the walls and the flow into the aneurysmal is predominantly tangential to the parent vessel wall, except in the most symmetric bifurcation aneurysms where the parent vessel flow may impinge normal to the neck surface and thus to the coil strands. The data shown in the Results section of this chapter clearly demonstrate that the bilinear model, while carrying a similar computational cost and requiring similar operator inputs into the simulations, provides a more accurate simulation of the hemodynamics inside aneurysms treated with coils, both in terms of Eulerian metrics, average WSS and velocity, computed here as representative of the metrics in the literature, and in terms of novel Lagrangian metrics, RT, SH and SH:RT ratio, which are computed in this thesis for the first time for coiled aneurysms to compare the standard, bilinear and coil-resolved reconstructions.

5.5 Conclusion

For all metrics, there was a case where the standard PM outperformed the BL model. In all other instances, the BL's estimation of the metrics was closer to the CR simulations, and therefore more accurate. While these data are promising, this preliminary study with only five patients cannot fully determine the accuracy of the BL model, for the Eulerian metrics, but specially on the Lagrangian platelet metrics, which are studied here for the first time. Simulations with Lagrangian tracking of platelets for the entire cohort of 24 cases studied in this thesis (Eulerian metrics) are required to assess the accuracy of the model in relation to platelet RT and SH. However, due to the bilinear model incorporating the heterogeneity of the true coil mass, it does appear to exhibit an increased ability to simulate the flow field within the aneurysm accurately. This is important particularly for the RT and SH metrics, as both provide a more in-depth description of how the thrombus formation process is affected by endovascular coil treatment. These metrics better represent the intra-aneurysmal environment that platelets are experiencing, by capturing the shear exposure and residence time under extreme behavior, which goes far beyond the surface- or volume-averaged velocities or shear stress when considering the impact on the clotting cascade and formation of a stable thrombus of the complex flow that can be seen in an aneurysm dome treated with endovascular coils.

Chapter 6

CONCLUSIONS AND RECOMMENDATIONS

6.1 Summary of Work

6.1.1 Comparison of Endovascular Therapies: FDS and Coil

The first study focused on the two primary forms of endovascular therapies: coil embolization devices and flow diverting stents (FDS). Each device has the same final objective of fully occluding the aneurysm with a stable thrombus; however, the coil resides entirely within the aneurysm dome while the FDS lies along the parent vessel. Therefore, as this study has shown, the two therapies effect the flow in fundamentally different ways. The coil affects the flow throughout the entire aneurysm, more drastically lowering the volumetric and surface metrics of the dome. Conversely, the FDS, as its name suggests, has a strong redirection of flow thus more greatly affecting the neck metrics. Interestingly because of how either the porous media for the coil is defined (or as seen in later chapters for the coil-resolved simulations) the neck metrics are often not indicative of treatment performance as they do not match the boundary of the coil/parent vessel interface. Hence, the conclusion is that coils and FDS cannot be studied in a single cohort when considering the effectiveness or outcome of endovascular therapies.

6.1.2 Incorporating Lagrangian Hemodynamic Variables into CFD

This section is a response to the lack of predictive hemodynamic metrics in the previous chapter and a lack of consensus from previous Eulerian studies. Since thrombus formation, the successful outcome of endovascular treatment, begins with platelets experiencing extreme flow behaviours resulting in increased residence times (RT). For this reason, Lagrangian tracer particles are added as a sort of platelet-surrogate since they allow for the calculation of RT and shear history (SH).

The first study focuses on a FDS-only cohort, per the results of Chapter 2. This probability of platelets activating and leading to a successful treatment is investigated using Lagrangian metrics as well as a novel metric which combines RT and SH. Since the extreme behaviours of the particles

are of primary interest, the outliers are primarily considered using the upper percentile of each metric.

The following study in this chapter explored the response of Lagrangian particles to a porous medium used to model a coil embolization device. Unlike an FDS porous jump, the treatment model for a coil affects the entire trajectory of the particle in the anuerysmal dome. The implication is that the quality of the approximation and its ability to model the device becomes more pertinent to the ability of the Lagrangian metrics to accurately characterize the change the flow sees due to the treatment. Coil resolved simulations were used as the ground truth to determine the accuracy of the porous media (PM). The PM is shown to over-predict flow reductions caused by the treatment which often correlates to an overly increased RT; furthermore, the SH of the particles are not well captured and may be greatly over or under-predicted.

6.1.3 Comparison of Fusiform and Saccular Cerebral Aneurysms Response to a FDS

Fusiform intracranial aneurysms (FIA) occur infrequently leading to significantly fewer studies and opportunities for research. Here, three FIAs are compared to a saccular intracranial aneurysm (SIA) analogue. Due to the morphology of FIAs, coil embolization devices are not possible and flow diverting stents (FDS) must be used. Simulations are performed on a pre-treatment case, stent-resolved treatment, and a reconstructed healthy vessel in Star-CCM+. There are no clear distinctions between FIAs and SIAs when comparing pre- and post-treatment of a single FDS. However, when one pair of the FIAs/SIAs were treated with two FDS, the FIA lacked the typical decrease in hemodynamic metrics from the single-stent case.

6.1.4 A New Bilinear Porous Model with Insight from Coil-Resolved Simulations and Geometries

The second study of Chapter 3 presents the problem of the standard PM employed as to model a coil embolization device: the hemodynamics, both Eulerian and Lagrangian are often not well predicted. Therefore, a new bilinear porous media (BL PM) model is compared to the standard model and again the coil resolved (CR) simulations for ground truth in an effort to find an improved approximation of the flow through coils. The BL model improves upon the previous gold-standard by taking into consideration the isotropy and heterogeneity of the coil mass without requiring

knowledge of the deployed treatment. To do this, the permeability of the homogeneous and isotropic model of several crowns are considered that exhibit decreasing porosity as it reaches the core with a given minimum porosity. This BL model again shows its ability to capture the flow effects in a more accurate manner than the standard model. BL predictions have lower error for aneurysm velocity and wall shear stress. Similarly, BL outperforms the standard model in predicting the SH:RT metric as well as for other RT metrics. This work is crucial as studies continue to move toward clinical applicability.

6.2 Recommendations for Future Work

6.2.1 Model Creation

There is a clear need for automation and standardization of the patient processing pipeline for CFD of intracranial aneurysms [15, 111]. To make research repeatable and reproducible particularly in large cohort studies, where statistical analysis is part of the contribution to reach a clinical audience, it is imperative that the results are coming from consistently created patient-specific models. The standardisation is key as we seek to bring CFD results into clinical applicability for predicting treatment outcome. The analysis of the hemodynamic variables is not useful for determining metrics of interests or thresholds unless studies maintain a consistent process.

The automation of defining the aneurysmal neck and wide-acceptance and use of this definition is crucial in moving forward. The definition of the aneurysmal neck defines not only where the neck metrics will be calculated (flow in the aneurysm and neck wall shear stress), it also defines the morphology of the aneurysm and is related to all other metrics, as it defines the boundaries of the aneurysm sac and dome.

6.2.2 Comparison of Endovascular Therapies: FDS and Coil

The outcome of this study shows that endovascularly-treated patients must be analyzed in separate cohorts of coil and FDS patients when considering the intra-aneurysmal hemodynamic changes caused by endovascular therapy. This will require further enrollment into each cohort in order to reach statistical significance before determining relationships between treatment outcome and hemodynamic parameters, Eulerian or Lagrangian. Before another large-scale study is begun, an

appropriate neck definition–and appropriate automation–should be determined for each treatment type. As shown in Chapter 2, coil patients present particular problems when using only medical imaging data and a porous media model. Furthermore, stent patients, even with solely medical imaging, can present a good idea of the neck considering the stent itself is used; however, this would prevent a priori studies unless a parent vessel reconstruction is used in place of the stent. Validated fast virtual stenting (FVS) software can be used, but again must be thoroughly verified and at best standardized.

6.2.3 Comparison of Fusiform and Saccular Cerebral Aneurysm's Response to a FDS

Further investigation is necessary to better understand the possible porosity variations in stented fusiform aneurysms. Compacting may be the best course of action for these aneurysms due to the steep drop in porosity; however, this hasn't been studied computationally due to the limited performance of the chosen fast virtual stenting (FVS) software. ‘

While studies have been done on curvature of the parent vessel and FDS-treated aneurysms [9], I recommend a study, using a FVS software as well as available pipeline Synchrotron data, to investigate the effects of porosity on curvature of the stent at the aneurysm and expansion of the stent into the aneurysm. The same porosity values for every patient are used only varying the thickness of the deployed stent (between 61-67.3 nm). Creating a function of curvature alone or curvature in addition to expansion would provide a patient-specific aspect currently absent in the modeling of the treatment.

Finally, while CFD models are unable to predict the changes in the geometry post-FDS deployment [129], there is a large set of pre- and post-treatment 3DRA images that can be used in a patient-specific image-based CFD study of 1) the morphological changes post-treatment and 2) the hemodyanmic changes caused by the stent-induced wall deformation. The hemodynamic changes without the wall deformation is already known from the study in Chapter 2 and can be used to isolate the effects of the change in vessel geometry.

6.2.4 Incorporating Lagrangian Hemodynamic Variables into CFD & A New Bilinear Porous Model with Insight from Coil-Resolved Simulations and Geometries

I also strongly recommend that the high-resolution synchrotron pipeline data be used to study the shear experienced by particles passing through the stent and compared to the porous jump. Currently, the shear seen by the particle crossing the porous jump has not been included. However, because the change and spikes in shear experienced by platelets are pertinent to activation, this may be a major blindspot in the current studies.

As the aim of research continues to be predicting endovascular therapy outcome for treatment planning and clinical support, the models used in CFD to simulate treatment must be improved. Using the recommendations presented here (standardizing and automating the aneurysm neck, focusing on dome metrics for coiled aneurysms, and using a single patient-specific waveform where possible), a large 24-patient study should be conducted to further investigate the BL model's capacity to capture the Lagrangian particle response to a coil mass. Furthermore, the ellipsoid volume approximation would benefit from an automation of the ellipse's axes.

While the BL model does see increased performance predicting Lagrangian metrics, the shear accumulated by particles will always suffer from an isotropic, homogeneous model. Therefore, I suggest investigating the pre-cursor to the BL model: discretrizing the aneurysm into several crowns of varying PM coefficients along with a homogeneous core. While this method complicates the creation of the mesh and implementation of the treatment model, the process would allow for particles to experience the varying levels of porosity seen as they enter the coil mass from the parent vessel and again as they exit.

BIBLIOGRAPHY

[1] Armin Abdehkakha, Adam L Hammond, Tatsat R Patel, Adnan H Siddiqui, Gary F Dargush, and Hui Meng. Cerebral aneurysm flow diverter modeled as a thin inhomogeneous porous medium in hemodynamic simulations. *Computers in biology and medicine*, 139:104988, 2021.

[2] M. Al-Yamany and I. B. Ross. Giant fusiform aneurysm of the middle cerebral artery: successful hunterian ligation without distal bypass. *British Journal of Neurosurgery*, 12(6):572–575, 1998.

[3] Alberto Aliseda, Venkat Keshav Chivukula, Patrick McGah, Anthony R. Prisco, Jennifer A. Beckman, Guilherme J.M. Garcia, Nahush A. Mokadam, and Claudius Mahr. LVAD Outflow Graft Angle and Thrombosis Risk. *ASAIO Journal*, 63(1):14–23, 2017.

[4] Amirhossein Arzani, Alberto M. Gambaruto, Guoning Chen, and Shawn C. Shadden. Wall shear stress exposure time: a lagrangian measure of near-wall stagnation and concentration in cardiovascular flows. *Biomech. Model. Mechanobiol.*, 16:787–803, 6 2017.

[5] L Augsburger, P Reymond, D A Rufenacht, and N Stergiopulos. Intracranial stents being modeled as a porous medium: Flow simulation in stented cerebral aneurysms. *Ann Biomed Eng*, 39(2):850–863, November 2010.

[6] M Haithem Babiker, Brian Chong, L Fernando Gonzalez, Sachmanik Cheema, and David H Frakes. Finite element modeling of embolic coil deployment: multifactor characterization of treatment effects on cerebral aneurysm hemodynamics. *Journal of biomechanics*, 46(16):2809–2816, 2013.

[7] M Haithem Babiker, L Fernando Gonzalez, Felipe Albuquerque, Daniel Collins, Arius Elvikis, and David H Frakes. Quantitative effects of coil packing density on cerebral aneurysm fluid dynamics: an in vitro steady flow study. *Annals of biomedical engineering*, 38:2293–2301, 2010.

[8] Michael Barbour. *Computational and Experimental Investigation into the Hemodynamics of Endovascularly Treated Cerebral Aneurysms*. PhD thesis, University of Washington, 2018.

[9] Michael C Barbour, Fanette Chassagne, Venkat K Chivukula, Nathanael Machicoane, Louis J Kim, Michael R Levitt, and Alberto Aliseda. The effect of dean, reynolds and womersley numbers on the flow in a spherical cavity on a curved round pipe. part 2. the haemodynamics of intracranial aneurysms treated with flow-diverting stents. *Journal of fluid mechanics*, 915:A124, 2021.

[10] Joshua B. Bederson, E. Sander Connolly, H. Hunt Batjer, Ralph G. Dacey, Jacques E. Dion, Michael N. Diringer, John E. Duldner, Robert E. Harbaugh, Aman B. Patel, and Robert H. Rosenwasser. Guidelines for the management of aneurysmal subarachnoid hemorrhage: A statement for healthcare professionals from a special writing group of the stroke council, American heart association. *Stroke*, 40(3):994–1025, 2009.

[11] E. J. Benz, M. de F. Sonati, L. Olcay, Kakali Ghoshal, and Maitree Bhattacharyya. Overview of Platelet Physiology: Its Hemostatic and Nonhemostatic Role in Disease Pathogenesis. *Sci. World J.*, pages 143–148, 2014.

[12] M Beppu, M Tsuji, F Ishida, M Shirakawa, H Suzuki, and S Yoshimura. Computational fluid dynamics using a porous media setting predicts outcome after flow-diverter treatment. *American Journal of Neuroradiology*, 41(11):2107–2113, 2020.

[13] P Berg, L Daróczy, and G Janiga. Virtual stenting for intracranial aneurysms: A risk-free, patient-specific treatment planning support for neuroradiologists and neurosurgeons. In *Computing and visualization for intravascular imaging and computer-assisted stenting*, pages 371–411. Elsevier, 2017.

[14] Philipp Berg, Sylvia Saalfeld, Gábor Janiga, Olivier Brina, Nicole M. Cancelliere, Paolo Machi, and Vitor M. Pereira. Virtual stenting of intracranial aneurysms: A pilot study for the prediction of treatment success based on hemodynamic simulations. *Int J Artif Organs*, 41(11):698–705, 2018.

[15] Philipp Berg, Sylvia Saalfeld, Samuel Voß, Oliver Beuing, and Gábor Janiga. A review on the reliability of hemodynamic modeling in intracranial aneurysms: why computational fluid dynamics alone cannot solve the equation. *Neurosurgical Focus*, 47(1):E15, 2019.

[16] Claude Boutin. Study of permeability by periodic and self-consistent homogenisation. *European Journal of Mechanics-A/Solids*, 19(4):603–632, 2000.

[17] G Canton, DI Levy, and JC Lasheras. Changes in the intraaneurysmal pressure due to HydroCoil embolization. *AMERICAN JOURNAL OF NEURORADIOLOGY*, 26(4):904–907, APR 2005.

[18] G Canton, DI Levy, and JC Lasheras. Hemodynamic changes due to stent placement in bifurcating intracranial aneurysms. *JOURNAL OF NEUROSURGERY*, 103(1):146–155, JUL 2005.

[19] G Canton, DI Levy, JC Lasheras, and PK Nelson. Flow changes caused by the sequential placement of stents across the neck of sidewall cerebral aneurysms. *JOURNAL OF NEUROSURGERY*, 103(5):891–902, NOV 2005.

[20] MA Castro, Christopher M Putman, and JR Cebral. Computational fluid dynamics modeling of intracranial aneurysms: effects of parent artery segmentation on intra-aneurysmal hemodynamics. *American Journal of Neuroradiology*, 27(8):1703–1709, 2006.

[21] Marcelo A Castro, María C Ahumada Olivares, Christopher M Putman, and Juan R Cebral. Unsteady wall shear stress analysis from image-based computational fluid dynamic aneurysm models under newtonian and casson rheological models. *Medical & biological engineering & computing*, 52:827–839, 2014.

[22] Juan R Cebral, Fernando effects of flow, Marcelo Raschi, Simona Hodis, Y-H Ding, Bradley J Erickson, Ramanathan Kadirvel, and David F Kallmes. Analysis of hemodynamics and aneurysm occlusion after flow-diverting treatment in rabbit models. *American Journal of Neuroradiology*, 35(8):1567–1573, 2014.

[23] Juan R Cebral, Fernando Mut, Jane Weir, and Christopher M Putman. Association of hemodynamic characteristics and cerebral aneurysm rupture. *American Journal of Neuroradiology*, 32(2):264–270, 2011.

[24] Fanette Chassagne, Michael C Barbour, Venkat K Chivukula, Nathanael Machicoane, Louis J Kim, Michael R Levitt, and Alberto Aliseda. The effect of dean, reynolds and womersley numbers on the flow in a spherical cavity on a curved round pipe. part 1. fluid mechanics in the cavity as a canonical flow representing intracranial aneurysms. *Journal of Fluid Mechanics*, 915:A123, 2021.

[25] Junfan Chen, Yisen Zhang, Zhongbin Tian, Wenqiang Li, Qianqian Zhang, Ying Zhang, Jian Liu, and Xinjian Yang. Relationship between haemodynamic changes and outcomes of intracranial aneurysms after implantation of the pipeline embolisation device: a single centre study. *Interventional Neuroradiology*, 25(6):671–680, 2019.

[26] Venkat Keshav Chivukula, Michael R. Levitt, Alicia Clark, Michael C. Barbour, Kurt Sansom, Luke Johnson, Cory M. Kelly, Christian Geindreau, Sabine Rolland du Roscoat, Louis J. Kim, and Alberto Aliseda. Reconstructing patient-specific cerebral aneurysm vasculature for in vitro investigations and treatment efficacy assessments. *J. Clin. Neurosci.*, 61:153–159, 2019.

[27] Venkat Keshav Chivukula, Laurel Marsh, Fanette Chassagne, Michael C Barbour, Cory M Kelly, Samuel Levy, Christian Geindreau, Sabine Rolland du Roscoat, Louis J Kim, Michael R Levitt, et al. Lagrangian trajectory simulation of platelets and synchrotron microtomography augment hemodynamic analysis of intracranial aneurysms treated with embolic coils. *Journal of Biomechanical Engineering*, 143(7), 2021.

[28] Winston Chong, Yu Zhang, Yi Qian, Leontat Lai, G Parker, and K Mitchell. Computational hemodynamics analysis of intracranial aneurysms treated with flow diverters: correlation with clinical outcomes. *American Journal of Neuroradiology*, 35(1):136–142, 2014.

[29] Winston Chong, Yu Zhang, Yi Qian, Leontat Lai, G Parker, and K Mitchell. Computational hemodynamics analysis of intracranial aneurysms treated with flow diverters: correlation with clinical outcomes. *American Journal of Neuroradiology*, 35(1):136–142, 2014.

[30] Bongjae Chung and Juan Raul Cebral. CFD for Evaluation and Treatment Planning of Aneurysms: Review of Proposed Clinical Uses and Their Challenges. *Ann Biomed Eng*, 43(1):122–138, 2014.

[31] Robert J Damiano, Ding Ma, Jianping Xiang, Adnan H Siddiqui, Kenneth V Snyder, and Hui Meng. Finite element modeling of endovascular coiling and flow diversion enables hemodynamic prediction of complex treatment strategies for intracranial aneurysm. *J Biomech*, 48(12):3332–3340, September 2015.

[32] Robert J. Damiano, Vincent M. Tutino, Nikhil Paliwal, Tatsat R. Patel, Muhammad Waqas, Elad I. Levy, Jason M. Davies, Adnan H. Siddiqui, and Hui Meng. Aneurysm characteristics, coil packing, and post-coiling hemodynamics affect long-term treatment outcome. *J. Neurointerv. Surg.*, 12(7):706–713, 2020.

[33] Daniel Ribeiro de Sousa, Carolina Vallecilla, Kamil Chodzynski, Ricardo Corredor Jerez, Orestis Malaspinas, Omer Faruk Eker, Rafik Ouared, Luc Vanhamme, Alexandre Legrand, Bastien Chopard, et al. Determination of a shear rate threshold for thrombus formation in intracranial aneurysms. *Journal of neurointerventional surgery*, 8(8):853–858, 2016.

[34] R D G Silva R H M L Gaspar J F M Araújo M W F Neves J L B de Aquino T A Barba Belsuzarri E A Barletta, R L Ricci. Fusiform aneurysms: A review from its pathogenesis to treatment options. *Surg Neurol Int.*, 189(9), 2018.

[35] J. E. Florman and B. H. Kopell. Neurosurgery for cerebral aneurysm, November 2021.

[36] George N Foutrakis, Howard Yonas, and Robert J Sclabassi. Saccular aneurysm formation in curved and bifurcating arteries. *American Journal of Neuroradiology*, 20(7):1309–1317, 1999.

[37] Soichiro Fujimura, Hiroyuki Takao, Takashi Suzuki, Chihebeddine Dahmani, Toshihiro Ishibashi, Hiroya Mamori, Makoto Yamamoto, and Yuichi Murayama. A new combined parameter predicts re-Treatment for coil-embolized aneurysms: A computational fluid dynamics multivariable analysis study. *J. Neurointerv. Surg.*, 10(8):791–796, 2018.

[38] Alberto M Gambaruto, Joao Janela, Alexandra Moura, and Adélia Sequeira. Sensitivity of hemodynamics in a patient specific cerebral aneurysm to vascular geometry and blood rheology. *Mathematical biosciences and engineering*, 8(2):409–423, 2011.

[39] Christoph Groden, Jochen Laudan, Scott Gatchell, and Herrmann Zeumer. Three-dimensional pulsatile flow simulation before and after endovascular coil embolization of a terminal cerebral aneurysm. *Journal of Cerebral Blood Flow & Metabolism*, 21(12):1464–1471, 2001.

[40] S Hadad, F Mut, R Kadirvel, Y-H Ding, D Kallmes, and JR Cebral. Evaluation of outcome prediction of flow diversion for intracranial aneurysms. *American Journal of Neuroradiology*, 42(11):1973–1978, 2021.

[41] James J. Hathcock. Flow effects on coagulation and thrombosis. *Arteriosclerosis, Thrombosis, and Vascular Biology*, 26(8):1729–1737, 2006.

[42] JD Hellums, DM Peterson, NA Stathopoulos, JL Moake, and TD Giorgio. Studies on the mechanisms of shear-induced platelet activation. In *Cerebral ischemia and hemorheology*, pages 80–89. Springer, 1987.

[43] Qinghai Huang, Jinyu Xu, Jiyong Cheng, Shengzhang Wang, Kuizhong Wang, and Jian Min Liu. Hemodynamic changes by flow diverters in rabbit aneurysm models: A computational fluid dynamic study based on micro-computed tomography reconstruction. *Stroke*, 44(7):1936–1941, 2013.

[44] Fujimaro Ishida, Masanori Tsuji, Satoru Tanioka, Katsuhiro Tanaka, Shinichi Yoshimura, and Hidenori Suzuki. Computational fluid dynamics for cerebral aneurysms in clinical settings. *Trends in Cerebrovascular Surgery and Interventions*, pages 27–32, 2021.

[45] Gábor Janiga, László Daróczy, Philipp Berg, Dominique Thévenin, Martin Skalej, and Oliver Beuing. An automatic cfd-based flow diverter optimization principle for patient-specific intracranial aneurysms. *J Biomech*, 48(14):3846–3852, Nov 2015.

[46] Hae Woong Jeong and Sung-Chul Jin. Practical feasibility and packing density of endovascular coiling using target® nano™ coils in small cerebral aneurysms. *J Cerebrovasc Endovasc Neurosurg*, 17(4):295–300, 2015.

[47] Woowon Jeong and Kyehan Rhee. Hemodynamics of cerebral aneurysms: computational analyses of aneurysm progress and treatment. *Computational and mathematical methods in medicine*, 2012, 2012.

[48] Jolyon Jesty, Wei Yin, Peter Perrotta, and Danny Bluestein. Platelet activation in a circulating flow loop: combined effects of shear stress and exposure time. *Platelets*, 14:143–149, 1 2003.

[49] Yeqing Jiang, Liang Ge, Ruoyu Di, Gang Lu, Lei Huang, Gaohui Li, Xiaochang Leng, Sufang Zhang, Hailin Wan, Daoying Geng, et al. Differences in hemodynamic characteristics under high packing density between the porous media model and finite element analysis in computational fluid dynamics of intracranial aneurysm virtual treatment. *Journal of neurointerventional surgery*, 11(8):853–858, 2019.

[50] Juan R Cebral and Xinjie Duan and Piyusha Gade and Bong Jae Chung and Fernando effects and Khaled Aziz and Anne M. Robertson. Regional Mapping of Flow and Wall Characteristics of Intracranial Aneurysms. *Ann Biomed Eng*, 44(12):3553–3567, 2016.

[51] N M P Kakalis, A P Mitsos, J V Byrne, and Y Ventikos. The haemodynamics of endovascular aneurysm treatment: A computational modelling approach for estimating the influence of multiple coil deployment. *IEEE Trans Med Imaging*, 27(6):814–824.

[52] David F. Kallmes, Yong Hong Ding, Daying Dai, Ramanathan Kadirvel, Debra A. Lewis, and Harry J. Cloft. A new endoluminal, flow-disrupting device for treatment of saccular aneurysms. *Stroke*, 38:2346–2352, 8 2007.

[53] Alexander Keedy. An overview of intracranial aneurysms. *McGill Journal of Medicine*, 9(2), 2020.

[54] Junhyung Kim, Gyojun Hwang, Bum-Tae Kim, Sukh Que Park, Jae Sang Oh, Seung Pil Ban, and O-Ki Kwon. Safety and efficacy of flow diverter therapy for unruptured intracranial aneurysm compared to traditional endovascular strategy: A multi-center, randomized, open-label trial. 2022.

[55] J Kozeny. Üeber kapillare leitung des wassers im boden. *Wiener Akad*, 136:271–306, 1927.

[56] Trung B Le, Daniel R Troolin, Devesh Amatya, Ellen K Longmire, and Fotis Sotiropoulos. Vortex phenomena in sidewall aneurysm hemodynamics: experiment and numerical simulation. *Annals of biomedical engineering*, 41:2157–2170, 2013.

[57] Sang-Wook Lee, Luca Antiga, and David A Steinman. Correlations among indicators of disturbed flow at the normal carotid bifurcation. *J. Biomech. Eng.*, 131:061013, 6 2009.

[58] Xiaochang Leng, Yang Wang, Jing Xu, Yeqing Jiang, Xiaolong Zhang, and Jianping Xiang. Numerical simulation of patient-specific endovascular stenting and coiling for intracranial aneurysm surgical planning. *Journal of translational medicine*, 16(1):1–10, 2018.

[59] Michael R. Levitt, Michael C. Barbour, Sabine Rolland Du Roscoat, Christian Geindreau, Venkat K. Chivukula, Patrick M. McGah, John D. Nerva, Ryan P. Morton, Louis J. Kim, and Alberto Aliseda. Computational fluid dynamics of cerebral aneurysm coiling using high-resolution and high-energy synchrotron X-ray microtomography: Comparison with the homogeneous porous medium approach. *J. Neurointerv. Surg.*, 9(8):777–782, 2017.

[60] Chuanhui Li, Shengzhang Wang, Jialiang Chen, Hongyu Yu, Ying Zhang, Fan Jiang, Shiqing Mu, Haiyun Li, and Xinjian Yang. Influence of hemodynamics on recanalization of totally occluded intracranial aneurysms: a patient-specific computational fluid dynamic simulation study. *J Neurosurg*, 117(2):276–283, August 2012.

[61] Jian Liu, Linkai Jing, Chao Wang, Nikhil Paliwal, Shengzhang Wang, Ying Zhang, Jianping Xiang, Adnan H Siddiqui, Hui Meng, and Xinjian Yang. Effect of hemodynamics on outcome of subtotally occluded paraclinoid aneurysms after stent-assisted coil embolization. *J. Neurointerv. Surg.*, 8(11):1140–1147, November 2016.

[62] Samar A Mahrous, Nor Azwadi Che Sidik, and Khalid M Saqr. Newtonian and non-newtonian cfd models of intracranial aneurysm: a review. *CFD Letters*, 12(1):62–86, 2020.

[63] Laurel M M Marsh, Michael C Barbour, Venkat Keshav Chivukula, Fanette Chassagne, Cory M Kelly, Samuel H Levy, Louis J Kim, Michael R Levitt, and Alberto Aliseda. Platelet dynamics and hemodynamics of cerebral aneurysms treated with flow-diverting stents. *Annals of biomedical engineering*, 48(1):490–501, 2020.

[64] Mhairi J. Maxwell, Erik Westein, Warwick S. Nesbitt, Simon Giuliano, Sacha M. Dopheide, and Shaun P. Jackson. Identification of a 2-stage platelet aggregation process mediating shear-dependent thrombus formation. *Blood*, 109(2):566–576, 2007.

[65] Patrick M McGah, D. Leotta, K. Beach, and Alberto Aliseda. Effects of wall distensibility in hemodynamic simulations of an arteriovenous fistula. *Biomech Model Mechanobiol*, 13:679–695, 2013.

[66] Patrick M McGah, D. Leotta, K. Beach, J.J. Riley, and Alberto Aliseda. The impact of flow stresses on remodeling of peripheral artery bypass graft: intimal hyperplasia at the stenosis and vessel wall dilatation in the post-stenotic region. *J Vascular Surg*, 56(2):403–409, 2012.

[67] Patrick M McGah, Michael R Levitt, Michael C Barbour, Ryan P Morton, John D Nerva, Pierre D Mourad, Basavaraj V Ghodke, Danial K Hallam, Laligam N Sekhar, Louis J Kim, and Alberto Aliseda. Accuracy of Computational Cerebral Aneurysm Hemodynamics Using Patient-Specific Endovascular Measurements. *Ann Biomed Eng*, 42(3):503–514, October 2013.

[68] Patrick M McGah, J D Nerva, R P Morton, M C Barbour, M R Levitt, P D Mourad, L J Kim, and A Aliseda. In vitro validation of endovascular Doppler-derived flow rates in models of the cerebral circulation. *Physiological Measurement*, 36(11):2301–2317, October 2015.

[69] Alan Michelson. *Platelets*. Elsevier, 3rd edition, 2013.

[70] Aristotelis P Mitsos, Nikolaos MP Kakalis, Yiannis P Ventikos, and James V Byrne. Haemodynamic simulation of aneurysm coiling in an anatomically accurate computational fluid dynamics model. *Neuroradiology*, 50:341–347, 2008.

[71] AM Moerman, S Korteland, K Dilba, K van Gaalen, DHJ Poot, A van Der Lugt, HJM Verhagen, JJ Wentzel, AFW van Der Steen, FJH Gijsen, et al. The correlation between wall shear stress and plaque composition in advanced human carotid atherosclerosis. *Frontiers in Bioengineering and Biotechnology*, 9:1499, 2022.

[72] Andrew J Molyneux, Richard SC Kerr, Ly-Mee Yu, Mike Clarke, Mary Sneade, Julia A Yarnold, and Peter Sandercock. International subarachnoid aneurysm trial (isat) of neurosurgical clipping versus endovascular coiling in 2143 patients with ruptured intracranial aneurysms: a randomised comparison of effects on survival, dependency, seizures, rebleeding, subgroups, and aneurysm occlusion. *The Lancet*, 366:809–817, 9 2005.

[73] Hernán G Morales, Ignacio Larrabide, Arjan J Geers, Martha L Aguilar, and Alejandro F Frangi. Newtonian and non-newtonian blood flow in coiled cerebral aneurysms. *Journal of biomechanics*, 46(13):2158–2164, 2013.

[74] Yuichi Murayama, Soichiro Fujimura, Tomoaki Suzuki, and Hiroyuki Takao. Computational fluid dynamics as a risk assessment tool for aneurysm rupture. *Neurosurgical Focus FOC*, 47(1):E12, 2019.

[75] Andrea D Muschenborn, Jason M Ortega, Jason M Szafron, David J Szafron, and Duncan J Maitland. Porous media properties of reticulated shape memory polymer foams and mock embolic coils for aneurysm treatment. *BioMedical Eng OnLine*, 12(1):1, October 2013.

[76] F Mut and JR Cebral. Effects of flow-diverting device oversizing on hemodynamics alteration in cerebral aneurysms. *American journal of neuroradiology*, 33(10):2010–2016, 2012.

[77] Fernando Mut, Danny Ruijters, Drazenko Babic, Carlos Bleise, Pedro Lylyk, and Juan R Cebral. Effects of changing physiologic conditions on the in vivo quantification of hemodynamic variables in cerebral aneurysms treated with flow diverting devices. *International Journal for Numerical Methods in Biomedical Engineering*, 30(1):135–142, 2014.

[78] Warwick S Nesbitt, Erik Westein, Francisco Javier Tovar-Lopez, Elham Tolouei, Arnan Mitchell, Jia Fu, Josie Carberry, Andreas Fouras, and Shaun P Jackson. A shear gradient–dependent platelet aggregation mechanism drives thrombus formation. *Nature medicine*, 15(6):665–673, 2009.

[79] Malebogo N. Ngoepe, Alejandro F. Frangi, James V. Byrne, and Yiannis Ventikos. Thrombosis in cerebral aneurysms and the computational modeling thereof: A review. *Front. Physiol.*, 9(APR):1–22, 2018.

[80] Matteo Nobili, Jawaad Sheriff, Umberto Morbiducci, Alberto Redaelli, and Danny Bluestein. Platelet activation due to hemodynamic shear stresses: damage accumulation model and comparison to in vitro measurements. *ASAIO journal (American Society for Artificial Internal Organs: 1992)*, 54(1):64, 2008.

[81] Andres F. Osorio, Ruben Osorio, Andres Ceballos, Reginald Tran, William Clark, Eduardo A. Divo, I. Ricardo Argueta-Morales, Alain J. Kassab, and William M. DeCampli. Computational fluid dynamics analysis of surgical adjustment of left ventricular assist device implantation to minimise stroke risk. *Comput Methods Biomech Biomed Engin*, 16:622–638, 6 2013.

[82] Rafik Ouared, Bastien Chopard, Bernd Stahl, Daniel A Rüfenacht, Hasan Yilmaz, and Guy Courbebaisse. Thrombosis modeling in intracranial aneurysms: a lattice boltzmann numerical algorithm. *Computer Physics Communications*, 179(1-3):128–131, 2008.

[83] Nikhil Paliwal, Robert J Damiano, Jason M Davies, Adnan H Siddiqui, and Hui Meng. Association between hemodynamic modifications and clinical outcome of intracranial aneurysms treated using flow diverters. In Robert J Webster and Baowei Fei, editors, *SPIE Medical Imaging*, page 101352F. SPIE, March 2017.

[84] Nikhil Paliwal, Prakhar Jaiswal, Vincent M Tutino, Hussain Shallwani, Jason M Davies, Adnan H Siddiqui, Rahul Rai, and Hui Meng. Outcome prediction of intracranial aneurysm treatment by flow diverters using machine learning. *Neurosurgical focus*, 45(5):E7, 2018.

[85] Seong-Ho Park, Man-Bin Yim, Chang-Young Lee, Ealmaan Kim, and Eun-Ik Son. Intracranial fusiform aneurysms: it's pathogenesis, clinical characteristics and managements. *Journal of Korean Neurosurgical Society*, 44(3):116, 2008.

[86] Wonhyoung Park, Yunsun Song, Kye Jin Park, Hae-Won Koo, Kuhyun Yang, and Dae Chul Suh. Hemodynamic characteristics regarding recanalization of completely coiled aneurysms: computational fluid dynamic analysis using virtual models comparison. *Neurointervention*, 11(1):30–36, 2016.

[87] phenox GmbH. phenox — p64 — flow modulation device.

[88] Laurent Pierot and Ajay K. Wakhloo. Endovascular treatment of intracranial aneurysms. *STROKE*, 44(7), 2013.

[89] M Raschi, F Mut, R Löhner, and J R Cebral. Strategy for modeling flow diverters in cerebral aneurysms as a porous medium. *Int J Numer Methods in Biomed Eng*, 30(9):909–925, March 2014.

[90] Krishnan Ravindran, Amanda M Casabella, Juan Cebral, Waleed Brinjikji, David F Kallmes, and Ram Kadirvel. Mechanism of action and biology of flow diverters in the treatment of intracranial aneurysms. *Neurosurgery*, 86(Suppl 1):S13, 2020.

[91] V. L. Rayz, L. Boussel, L. Ge, J. R. Leach, A. J. Martin, M. T. Lawton, C. McCulloch, and D. Saloner. Flow residence time and regions of intraluminal thrombus deposition in intracranial aneurysms. *Ann Biomed Eng*, 38(10):3058–3069, 2010.

[92] Vitaliy L Rayz, Loic Boussel, Gabriel Acevedo-Bolton, Alastair J Martin, William L Young, Michael T Lawton, Randall Higashida, and David Saloner. Numerical simulations of flow in cerebral aneurysms: comparison of cfd results and in vivo mri measurements. *Journal of biomechanical engineering*, 130(5), 2008.

[93] Kyehan Rhee, Moon Hee Han, and Sang Hoon Cha. Changes of flow characteristics by stenting in aneurysm models: influence of aneurysm geometry and stent porosity. *Annals of biomedical engineering*, 30:894–904, 2002.

[94] Andrew J Ringer, Rafael Rodriguez-Mercado, Erol Veznedaroglu, Elad I Levy, Ricardo A Hanel, Robert A Mericle, Demetrius K Lopes, Giuseppe Lanzino, and Alan S Boulos. Defining The Risk Of Retreatment For Aneurysm Recurrence Or Residual After Initial Treatment By Endovascular Coiling. *Neurosurgery*, 65(2):311–315, Aug 2009.

[95] Julia Romero Bhathal. *Experimental and numerical study of blood flow in cerebral aneurysms treated with endovascular coils*. PhD thesis, Université Grenoble Alpes, 2022.

[96] Julia Romero Bhathal, Fanette Chassagne, Laurel Marsh, Michael R Levitt, Christian Geindreau, and Alberto Aliseda. Modeling flow in cerebral aneurysm after coils embolization treatment: A realistic patient-specific porous model approach. *Cardiovascular Engineering and Technology*, pages 1–14, 2022.

[97] Sylvia Saalfeld, Philipp Berg, Annika Niemann, Maria Luz, Bernhard Preim, and Oliver Beuing. Semiautomatic neck curve reconstruction for intracranial aneurysm rupture risk assessment based on morphological parameters. *Int. J. Comput. Assist. Radiol. Surg.*, 13(11):1781–1793, 2018.

[98] Sylvia Saalfeld, Janneck Stahl, Jana Korte, Laurel Morgan Miller Marsh, Bernhard Preim, Oliver Beuing, Yurii Cherednychenko, Daniel Behme, and Philipp Berg. Can endovascular treatment of fusiform intracranial aneurysms restore the healthy hemodynamic environment?–a virtual pilot study. *Frontiers in Neurology*, 12:2454, 2022.

[99] Sylvia Saalfeld, Samuel Voß, Oliver Beuing, Bernhard Preim, and Philipp Berg. Flow-splitting-based computation of outlet boundary conditions for improved cerebrovascular simulation in multiple intracranial aneurysms. *International journal of computer assisted radiology and surgery*, 14(10):1805–1813, 2019.

[100] Akiyo Sadato, Motoharu Hayakawa, Kazuhide Adachi, Ichiro Nakahara, and Yuichi Hirose. Large Residual Volume, Not Low Packing Density, Is the Most Influential Risk Factor for Recanalization after Coil Embolization of Cerebral Aneurysms. *PLoS ONE*, 39(2), May 2010.

[101] Khalid M Saqr, Sherif Rashad, Simon Tupin, Kuniyasu Niizuma, Tamer Hassan, Teiji Tominaga, and Makoto Ohta. What does computational fluid dynamics tell us about intracranial aneurysms? a meta-analysis and critical review. *Journal of Cerebral Blood Flow & Metabolism*, 40(5):1021–1039, 2020.

[102] Ali Sarrami-Foroushani, Toni Lassila, and Alejandro F Frangi. Virtual endovascular treatment of intracranial aneurysms: models and uncertainty. *Wiley Interdisciplinary Reviews: Systems Biology and Medicine*, 9(4):e1385, 2017.

[103] Jonas Schollenberger, Nicholas Harold Osborne, Luis Hernandez-Garcia, and C Alberto Figueroa. A combined computational fluid dynamics and mri arterial spin labeling modeling strategy to quantify patient-specific cerebral hemodynamics in cerebrovascular occlusive disease. *bioRxiv*, pages 2021–01, 2021.

[104] Daniel M Sforza, Christopher M Putman, and Juan R Cebral. Computational fluid dynamics in brain aneurysms. *International journal for numerical methods in biomedical engineering*, 28(6-7):801–808, 2012.

[105] Bahador Sharifzadeh, Rasool Kalbasi, and Mehdi Jahangiri. The effect of turbulence model on predicting the development and progression of coronary artery atherosclerosis. *Journal of Computational & Applied Research in Mechanical Engineering (JCARME)*, 10(1):183–199, 2020.

[106] Al Amin Sheikh, Anis Suhaila Shuib, and Mohd Hardie Hidayat Mohyi. A review of hemodynamic parameters in cerebral aneurysm. *Interdisciplinary Neurosurgery*, 22:100716, 2020.

[107] Elena Sinauridze, Dmitry Kireev, Nadezhda Popenko, Aleksei Pichugin, Mikhail Panteleev, Olga Krymskaya, and Fazoil Ataullakhanov. Platelet microparticle membranes have 50- to 100-fold higher specific procoagulant activity than activated platelets. *J. Thromb. Haemost.*, 97:425–434, 11 2007.

[108] Menno Sluzewski, Willem Jan van Rooij, Marian J Slob, Javier Oliván Bescós, Cornelis H Slump, and Douwe Wijnalda. Relation between aneurysm volume, packing, and compaction in 145 cerebral aneurysms treated with coils. *Radiology*, 231(3):653–658, 2004.

[109] David A Steinman. Image-based computational fluid dynamics modeling in realistic arterial geometries. *Annals of biomedical engineering*, 30:483–497, 2002.

[110] David A Steinman, Jaques S Milner, Chris J Norley, Stephen P Lownie, and David W Holdsworth. Image-based computational simulation of flow dynamics in a giant intracranial aneurysm. *American Journal of Neuroradiology*, 24(4):559–566, 2003.

[111] Gordan R. Stuhne and David A. Steinman. Finite-element modeling of the hemodynamics of stented aneurysms. *J. Biomech. Eng.*, 126(3):382–387, 2004.

[112] Shinichi Tamatani, Yasushi Ito, Hiroshi Abe, Tetsuo Koike, Shigekazu Takeuchi, and Ryuichi Tanaka. Evaluation of the stability of aneurysms after embolization using detachable coils: correlation between stability of aneurysms and embolized volume of aneurysms. *American Journal of Neuroradiology*, 23(5):762–767, 2002.

[113] Abraham Yik-Sau Tang, Siu-Kai Lai, Kar-Ming Leung, Gilberto Ka-Kit Leung, and Kwok-Wing Chow. Influence of the aspect ratio on the endovascular treatment of intracranial aneurysms: A computational investigation. 2012.

[114] Satoru Tanioka, Fujimaro Ishida, Tomoyuki Kishimoto, Masanori Tsuji, Katsuhiro Tanaka, Shinichi Shimosaka, Mitsuru Toyoda, Nobuhisa Kashiwagi, Takanori Sano, and Hidenori Suzuki. Quantification of hemodynamic irregularity using oscillatory velocity index in the associations with the rupture status of cerebral aneurysms. *Journal of NeuroInterventional Surgery*, 11(6):614–617, 2019.

[115] Maurizio Tomaiuolo, Lawrence F Brass, and Timothy J Stalker. Regulation of platelet activation and coagulation and its role in vascular injury and arterial thrombosis. *Interventional cardiology clinics*, 6(1):1, 2017.

[116] Masanori Tsuji, Fujimaro Ishida, Tomoyuki Kishimoto, Kazuhiro Furukawa, Yoichi Miura, Masato Shiba, Takanori Sano, Keiji Fukazawa, Katsuhiro Tanaka, Hiroshi Tanemura, et al. Double porous media modeling in computational fluid dynamics for hemodynamics of stent-assisted coiling of intracranial aneurysms: A technical case report. *Brain Hemorrhages*, 1(1):85–88, 2020.

[117] Nikhil Tulshibagwale and Stephen P Gent. Simulating coil embolization treatments of intracranial aneurysms using computational fluid dynamics. In *Frontiers in Biomedical Devices*, volume 41037, page V001T07A002. American Society of Mechanical Engineers, 2019.

[118] Yasuyuki Umeda, Fujimaro Ishida, Masanori Tsuji, Kazuhiro Furukawa, Masato Shiba, Ryuta Yasuda, Naoki Toma, Hiroshi Sakaida, and Hidenori Suzuki. Computational fluid dynamics (cfd) using porous media modeling predicts recurrence after coiling of cerebral aneurysms. *PloS one*, 12(12):e0190222, 2017.

[119] Koohyar Vahidkhah, Scott L. Diamond, and Prosenjit Bagchi. Platelet dynamics in three-dimensional simulation of whole blood. *Biophys. J.*, 106(11):2529–2540, 2014.

[120] Ajay K. Wakhloo, M. J. Gounis, J. S. Sandhu, N. Akkawi, A. E. Schenck, and I. Linfante. Complex-shaped platinum coils for brain aneurysms: Higher packing density, improved biomechanical stability, and midterm angiographic outcome. *Am. J. Neuroradiol.*, 28(7):1395–1400, 2007.

[121] Chao Wang, Zhongbin Tian, Jian Liu, Linkai Jing, Nikhil Paliwal, Shengzhang Wang, Ying Zhang, Jianping Xiang, Adnan H Siddiqui, Hui Meng, et al. Flow diverter effect of lvis stent on cerebral aneurysm hemodynamics: a comparison with enterprise stents and the pipeline device. *Journal of translational medicine*, 14:1–10, 2016.

[122] Erik Westein, Andries D van der Meer, Marijke JE Kuijpers, Jean-Philippe Frimat, Albert van den Berg, and Johan WM Heemskerk. Atherosclerotic geometries exacerbate pathological thrombus formation poststenosis in a von willebrand factor-dependent manner. *Proceedings of the National Academy of Sciences*, 110(4):1357–1362, 2013.

[123] Karol Wiśniewski, Bartłomiej Tomasik, Zbigniew Tyfa, Piotr Reorowicz, Ernest J Bobeff, Ludomir Stefańczyk, Bartłomiej J Posmyk, Krzysztof Jóźwik, and Dariusz J Jaskólski. Porous media computational fluid dynamics and the role of the first coil in the embolization of ruptured intracranial aneurysms. *Journal of Clinical Medicine*, 10(7):1348, 2021.

[124] J R Womersley. Method for the calculation of velocity, rate of flow and viscous drag in arteries when the pressure gradient is known. *J. Physiol.*, 127:553–63, 3 1955.

[125] George KC Wong and WS Poon. Current status of computational fluid dynamics for cerebral aneurysms: the clinician's perspective. *Journal of Clinical Neuroscience*, 18(10):1285–1288, 2011.

[126] J Xiang, VM Tutino, KV Snyder, and H Meng. Cfd: computational fluid dynamics or confounding factor dissemination? the role of hemodynamics in intracranial aneurysm rupture risk assessment. *American Journal of Neuroradiology*, 35(10):1849–1857, 2014.

[127] Jianping Xiang, Sabareesh K Natarajan, Markus Tremmel, Ding Ma, J Mocco, L Nelson Hopkins, Adnan H Siddiqui, Elad I Levy, and Hui Meng. Hemodynamic–morphologic discriminants for intracranial aneurysm rupture. *Stroke*, 42(1):144–152, 2011.

[128] Jinyu Xu, Zhichen Wu, Ying Yu, Nan Lv, Shengzhang Wang, Christof Karmonik, Jian-Min Liu, and Qinghai Huang. Combined effects of flow diverting strategies and parent artery curvature on aneurysmal hemodynamics: a cfd study. *PloS one*, 10(9):e0138648, 2015.

[129] Lijian Xu, Bing Zhao, Xiaosheng Liu, and Fuyou Liang. Computational methods applied to analyze the hemodynamic effects of flow-diverter devices in the treatment of cerebral aneurysms: Current status and future directions. *Medicine in Novel Technology and Devices*, 3:100018, 2019.

[130] Hooman Yadollahi-Farsani, Marcus Herrmann, David Frakes, and Brian Chong. A new method for simulating embolic coils as heterogeneous porous media. *Cardiovascular engineering and technology*, 10:32–45, 2019.

[131] Wei Yin, Saravan Kumar Shanmugavelayudam, and David A Rubenstein. The effect of physiologically relevant dynamic shear stress on platelet and endothelial cell activation. *Thrombosis Research*, 127:235–241, 2011.

[132] Yu Zhang, Winston Chong, and Yi Qian. Investigation of intracranial aneurysm hemodynamics following flow diverter stent treatment. *Medical engineering & physics*, 35(5):608–615, 2013.

[133] Liang Zhong, Jun-Mei Zhang, Boyang Su, Ru San Tan, John C Allen, and Ghassan S Kassab. Application of patient-specific computational fluid dynamics in coronary and intra-cardiac flow simulations: Challenges and opportunities. *Frontiers in physiology*, 9:742, 2018.